INFORMATION TO USERS

This manuscript has been reproduced from the microfilm master. UMI films the text directly from the original or copy submitted. Thus, some thesis and dissertation copies are in typewriter face, while others may be from any type of computer printer.

The quality of this reproduction is dependent upon the quality of the copy submitted. Broken or indistinct print, colored or poor quality illustrations and photographs, print bleedthrough, substandard margins, and improper alignment can adversely affect reproduction.

In the unlikely event that the author did not send UMI a complete manuscript and there are missing pages, these will be noted. Also, if unauthorized copyright material had to be removed, a note will indicate the deletion.

Oversize materials (e.g., maps, drawings, charts) are reproduced by sectioning the original, beginning at the upper left-hand corner and continuing from left to right in equal sections with small overlaps. Each original is also photographed in one exposure and is included in reduced form at the back of the book.

Photographs included in the original manuscript have been reproduced xerographically in this copy. Higher quality 6" x 9" black and white photographic prints are available for any photographs or illustrations appearing in this copy for an additional charge. Contact UMI directly to order.

UMI

A Bell & Howell Information Company
300 North Zeeb Road, Ann Arbor MI 48106-1346 USA
313/761-4700 800/521-0600

SPUTTER SYNTHESIZED AND PULSED LASER DEPOSITED SOFT AND HARD FERRIMAGNETIC COMPOUNDS

by

PUBUDU SAMARASEKARA

A dissertation submitted to the graduate faculty in Physics in partial fulfillment of the requirement for the degree of doctor of philosophy, The City University of NewYork.

1996

This manuscript has been read and accepted for the graduate faculty in Physics in satisfaction of the dissertation requirement for the degree of Doctor of philosophy.

Dec. 15, 1995
Date

Fred J. Cadieu
Chairman of Examining Committee

Dec 21, 1995
Date

Joseph B. Kruger
Executive Officer

Fred J. Cadieu
Professor F. J. Cadieu

Professor A. Lisyansky

M. G. Miksic
Professor M. Miksic

Professor E .Chudnovsky

Doctor S. Hegde

Supervisory committee

THE CITY UNIVERSITY OF NEWYORK

ABSTRACT

SPUTTER SYNTHESIZED AND PULSED LASER DEPOSITED SOFT AND HARD FERRIMAGNETIC COMPOUNDS

by

Pubudu Samarasekara

Adviser: Professor F.J. Cadieu

We have deposited soft and hard ferrimagnetic compounds using Nd:YAG pulsed laser deposition and rf sputtering techniques. Soft ferrimagnetic material materials are useful in microwave and millimeter wave monolithic integrated circuits such as isolators, circulators, and phase shifters, magneto-optic recording media. The hard ferrimagnetic compounds are also useful in magnetic recording and microwave devices. We have deposited cubic (or soft) magnetic materials such as $NiFe_2O_4$ and (Li,Ti,Mn,Zn) Fe_5O_8, and hexagonal (or hard) ferrimagnetic compounds such as $SrFe_{12}O_{19}$. For the first time we have deposited non-epitaxial Sr ferrite films with strong (110) texture on Al_2O_3 polycrystalline substrates using rf sputtering at deposition temperatures as low as 500 ^{0}C in 100 mTorr of Ar gas. The coercivity of films drastically increases from 0.5 kOe to 3.8 kOe with annealing in oxygen of 500 Torr. We have synthesized Ni ferrite films with complete (111) texture without any content of other crystallites on C-plane sapphire substrates at 930 ^{0}C using pulsed laser deposition in 200 mTorr of oxygen. Also we have laser ablated (400) textured Ni ferrite films on R-plane sapphire substrates at 910 ^{0}C. Any other oriented Ni ferrite film depositions have not been reported before this work. In addition to these, the highly (111) textured

(Li,Ti,Mn,Zn) mixed ferrite films have been fabricated on C-plane sapphire at 930 ^{0}C using laser ablation. The other elements have been added to Li ferrite to lower the saturation magnetization, to make them more useful in microwave applications. In all these cases, the texture of film remarkably depends on the substrate temperature.

ACKNOWLEDGEMENTS

I specially thank to Professor F. J. Cadieu for his generous support, supervision, and encouragement throughout this thesis works. I also like to thank and appreciate all the supports from Professor S.A. Shaheen, Dr. H. Hedge, Dr. K. Chen, Dr. R. Rani, Dr. A. Navarathna, Mr. Kieran Tracy, Mr. W. Mendoza, and Mr. B. Peng.

I am grateful to my dissertation committee members Professor A. Lisyansky, Professor M. Miksic, Professor E. Chudnovsky, Doctor S. Hegde. In addition to this, I like to thank all the faculty and staff members in Physics Department of Queens College in NewYork and all the faculty and staff including Professor L. R. Testardi and Mr. J. Smathers in MARTECH Florida.

The Kikuchi backscattered electron diffraction was performed by Dr. H. Garmestani and his group at National High Magnetic Field Laboratory at Tallahassee in Florida.

I also like to thank my wife Prabha Kumari for her patience and support during this thesis works, and my daughter Nelum.

This thesis works have been partly supported by grants to Professor F. J. Cadieu from the Air Force Office of Scientific Research.

Pubudu Samarasekara

CONTENTS

LIST OF TABLES

LIST OF FIGURES

CHAPTER 1

INTRODUCTION

Since the 1940s, the ferrimagnetic compounds have developed as an important commercial field because of their strong magnetic coupling, high electrical resistivity, low loss characteristics, low cost, chemical stability against environmental corrosion, and mechanical hardness. Most of the research works have been limited to the bulk ferrites until the late 1970s. The bulk ferrimagnetic compounds, which are sintered by mixing the powder of oxides or carbonates of the constituent at about $1000\,^{0}C$, are useful in inductors, high frequency transductors, wide band transformers, pulse transformers, power transformers, ferrite antennas, motors, generators, band pass filters, wave guides, gyrators, circulators, modulators, isolators, phase shifters - - etc. Their higher electrical resistivity makes ferrites suitable for use in high frequency (microwave) ac fields without giving rise to eddy current losses. The Faraday rotation is observed at microwave frequencies, i.e., the plane of polarization of the wave is rotated as it travels through an axially magnetized ferrite pencil in a circular waveguide. This effect can be utilized to build a whole class of non-reciprocal devices such as Unilines, gyrators, differential phase shifters, etc.

With the developments of computers, other memory devices, camcorders, cellular phones, satellite communication equipments,...etc, a new era of ferrites began. The magnetic

thin films of ferrite type compounds have received wide attention since the late 1970s, because of their potential applications in magnetic recording media, microwave and millimeter wavedevices such as tunable filters , delay lines, and oscillators, also in magneto optical devices, and magnetic bubble memories. Bulk ferrite devices are too costly and heavy in some applications. If thick films (about 100 microns) of ferrites with suitable magnetic properties (extremely low conductivity, narrow resonance linewidth) were available, they could lower the cost and offer the possibility for integrating these important functions into compact microwave monolithic integrated circuitry (MMIC). Magnetic losses of microwave devices are caused largely by the ferrimagnetic resonance (FMR). If the ferrimagnetic resonance linewidth is higher, the resonance becomes broader and resonance losses can manifest themselves in the operating frequency range of microwave devices such as circulators, isolators or filters. Nearly single crystal or epitaxial thick films (several microns) are useful in microwave applications. Polycrystalline thin films (about 1000Å) with small grain sizes are prime candidates for magnetic recording media. Commercially available circulators are based on polycrystalline cores because they are not biased at the ferromagnetic resonance field. Under these conditions the microwave loss does not depend on the microstructure (two magnon process correlated to microstructure contribute only to resonance linewidth). Therefore high performances can be achieved with polycrystals.

Ferrimagnetic compounds can be divided into three main categories depending on their crystal structures as following.

(1) Hexagonal or magnetoplumbite type ferrite

(2) Cubic type ferrites (spinel or inverse spinel)

(3) Garnet (rare earth) type ferrites

These ferrite types will be explained in detail in next chapter. Magnetoplumbite type ferrites with hexagonal structure are important among other ferrites because of their magnetocrystalline uniaxial anisotropy. Easy axis of these ferrites align along the C-axis of hexagonal lattice. The large crystalline anisotropy field of hexaferrite is favorable in resisting both recording and self demagnetization, and therefore, reducing the demagnetization loss in the short wavelength region [20]. All other ferrites are not magnetically uniaxial, and easy axis of cubic ferrites lies along one of the cubic edges or the body diagonal of cubic lattice. Ba ferrite and Sr ferrite are the two prime candidates in first category.

Some other researchers have been able to synthesis Barium ferrite thin films, which belongs to first category, on ZnO [18] and sapphire Al_2O_3 [1][19] substrates epitaxially, on amorphous Si/SiO_2 [2][4][6] (thermally oxidized silicon) and fused quartz [3][5], using rf [1][2][6], dc [1][3], target facing sputtering [4][18], laser ablation deposition(LAD) [19], and arc discharge evaporation [5]. Most of these films have been grown epitaxially by matching hexagonal close packed oxygen planes in substrate with that of hexagonal ferrite [1], or self epitaxially on spinel layer (111) of ferrite grown on substrate [2][4][6].

Although these ferrite compounds have a resistivity as high as 10^6 ohm-cm at room temperature, researchers have been able to deposit them using dc sputtering [1][3] and arc discharge evaporation [5] because ferrite is semiconductive and its resistivity decreases rapidly

with temperature. Most of these films have been deposited at low pressures [1][2][4][6] (less than 10 mTorr) of oxygen and argon gas combination using Ba enriched targets [2][3][6], and directly crystallized at high temperatures [2][3][4] or crystallized subsequently after annealing in oxygen or in air at higher temperatures (above 800 ^{0}C) [1][5][6]. Due to bombardment by massive 0^{-2} ions in sputtering gas, Ba concentration of films decreases, and film growth is disrupted at higher pressure [2], higher oxygen partial pressure [2], and smaller distance between target and substrate [2] [4]. Sometimes some other phases such as spinel and corundum can be formed due to lack of oxygen and Barium in the film at higher substrate temperatures [3] as well as at small substrate temperatures [4]. On the other hand at lower oxygen partial pressure, all ferric ions (Fe^{+3}) transform into ferrous (Fe^{+2}) ions, because of lack of oxygen atoms. Because ferrous ions easily transform to ferric ions by releasing an electron, electrical conductivity of the film increases in this case[2].

The C-axis orientation and texture of ferrite films strongly depends on the substrate temperature and the crystal structure or type of the substrate [3] [4]. Some researchers have been able to show that the roughness of films depends on the total pressure of the chamber during sputtering [2]. At higher pressure (>20 mTorr), the kinetic energy of sputtered atoms decreases due to collision with other atoms or ions, before they arrive at the substrate. Therefore they can not diffuse for a longer time or longer distance in growing film, and which causes a higher number of nucleation centers in the growing film. Sometimes some nonmagnetic phases also from in the film which decreases the magnetization of film compared to that of bulk [1].

Through the control of sputtering parameters, quality films of Barium ferrite with easy axis in plane [1] and perpendicular to the plane of film have been fabricated [2][3][4]. The deposition rate of ferrite films synthesized using sputtering methods (10-17 Å /min) is lower compared to that of other rare earth and transition metal films. To obtain a higher deposition rate with sputtering, most of the researchers have used a larger targets of about 8.5 cm diameter [2] [10]. Also the arc discharge evaporation has been used to obtain a higher deposition rate of about 4000 Å /min [5][11][12]. Because the particles are evaporated from arc cathode spots at very high temperatures above 30,000 ^{0}K, this method can deposit particles with proper energy and activity on the plasma free substrate. Sometimes the target facing type sputtering has been helpful to reduce the bombardment of massive oxygen ions and gamma electrons on the growing film [4] [18]. Because of this reason, the target facing type sputtering offers a higher deposition rate (0.15 microns per hour) and smooth stoichiometric films among other sputtering methods [4].

By substituting some other elements such as (In^{+3} for Fe^{+3}), the coercivity of hexagonal ferrite can be reduced to 1 kOe from 2 kOe for some applications because recorded bits are not erased satisfactorily by means of a conventional ring head at higher coercivities [18]. Although the perpendicular recording was predicted to be able to achieve higher recording density than longitudinal recording, current Winchester technology still favors magnetic easy axis in plane oriented media [13]. The wavelength responses for all the nonoriented , perpendicular oriented and longitudinally oriented hexaferrite particulate tapes show higher signal output at shorter wavelengths than the typical high band 8-mm metal

particulate tapes [14].

A model for Barium ferrite film grain growth has been discussed in terms of platelet shaped grain with C-axis oriented perpendicular to plane of film and acicular grains with C-axis in the plane of film [6]. Because the platlets occupy a larger volume than the acicular grain in the film, there has been a preferential C-axis orientation perpendicular to the film plane. Using microdiffraction pattern (TEM or SEM), it has been shown that the C-axis of Barium hexaferrite is perpendicular to the long axis of grain inside each grain. Also the orientation of C-axis of films mostly depends on the C-axis orientation of initial nucleus. If the C-axis oriented perpendicular to the film, then the basal plane of hexaferrite is parallel to the plane and it can grow fast laterally without any restriction. Because of this reason, the deposition rate of films with C-axis perpendicular to the film plane is higher compared to that with C-axis in plane films [8].

Strontium and Barium ferrite have nearly identical properties, although crystal anisotropy constant, K_1, of Strontium ferrite (3.57×10^6 erg/cc) is somewhat larger than that of Barium ferrite (3.25×10^6 erg/cc), because of higher anisotropy field of Strontium ferrite compared to Ba ferrite [7]. Magnetic and crystal properties of Strontium ferrite and Barium ferrite are given in table 1, for comparison. But interest of Strontium ferrite thin films has been developed recently (at the end of 1993). We have been able to fabricate strontium hexaferrite films non-epitaxially with C-axis in the plane of film on Al_2O_3 polycrystalline substrate for the first time [9]. During this same time frame, Some other researchers deposited

Strontium ferrite films with C-axis perpendicular to the plane of film onto Si(111) substrates [15], and C-axis in plane film onto fused quartz [16] and Si(111) [15] substrates using rf sputtering by controlling the temperature and rf input power, similar to the Ba ferrite films mentioned earlier. As the rf input power is increased, the deposition rate of film increases and the film C-axis orientation of growing crystallites changes from perpendicular to in plane [15]. Prior to this, the difficulties of synthesizing a textured hexaferrite film onto Al_2O_3 have been shown by some other researchers [17]. They have been able to deposit textured hexaferrite films onto SiO_2, GGG, and ZnO substrates, but not on Al_2O_3 substrates [17].

The texture of our Strontium hexaferrite films depends on the deposition temperature. Films were fabricated using commercially available Strontium enriched targets with rf sputtering system at much lower temperature of 500 ^{0}C. Films deposited at 500 ^{0}C show a strong (110) texture. As temperature is increased, X-ray pattern of films becomes more random and finally it is similar to the powder pattern of Strontium ferrite. Films were crystallized and magnetic as deposited above the deposition temperatures of 450 ^{0}C. After annealing the films at temperatures ranging from 500 ^{0}C to 625 ^{0}C in oxygen atmosphere of 500 Torr, the coercivity of films increases drastically from 0.5 kOe to 3.8 kOe and x-ray patterns do not show any noticeable change. The properties of films did not depend on the total pressure of the chamber in the range from 20 to 100 mTorr, the distance from target to substrate or, rf power. A secondary phase was crystallized at higher oxygen partial pressures. Oxygen content of target was sufficient to form hexaferrite phase. All these will be explained in detail in chapter 4.

Most of works related to ferrite films have been confined to films of hexaferrite materials, and only a little works have been done on the cubic type ferrite films. Cubic type ferrites except Co ferrite have soft magnetic properties compared to most of other magnetic materials such as rare earth- transition metal magnetic material, and hexaferrite. Previously some other researchers have prepared polycrystalline Co ferrite on substrates of organic compounds (polyethylene terephthalte, polymethyl methacrylate, polycarbonate, Teflon), stainless steel and polyester fiber using electroless plating technique [21], also Co ferrite on ZnO under layer deposited on thermal oxidized Si wafer substrates using target facing sputtering [22], Co ferrite with different Co concentrations on glass substrates using rf sputtering [23], magnetite or Fe_3O_4 on MgO and C sapphire using pulsed laser deposition [24], Li ferrite on (0001) Al_2O_3 using pulsed laser deposition [25], polycrystalline Ni-Zn ferrite on glass slides Si wafers with Cr/Au surface, GaAs wafers with a layer of Cr/Au using spin-spray plating process [26], Mn-Zn ferrite on SiO_2/Si substrates using ion beam sputtering [27], Ni-Zn ferrite onto glass substrates using ferrite plating technique [28].

Some of research works on garnet type compounds can be summarized as following ; Bi substituted garnet ($\{BiDy\}_3\{FeGa\}_5O_{12}$) deposited onto GGG(111), fused quartz, glass substrates using rf magnetron sputtering [29], also Bi substituted gadolinium iron garnet synthesized on GGG substrates using laser ablation [30], praseodymium substituted iron garnet films fabricated on GGG substrates using liquid phase epitaxy [31], highly Ce substituted garnet films grown on GGG, and NGG substrates using rf sputtering [32], polycrystalline YIG deposited on Al_2O_3 using laser ablation [33], Bi substituted garnet films on

glass substrates using rf diode sputtering [34].

We have been able to fabricate single crystal Ni ferrite films with complete (111) texture on C-plane sapphire and polycryatalline films with strong (400) texture on R-plane sapphire using Nd:YAG laser ablation system. We have also synthesized Ni ferrite films on fused silica, A-plane sapphire and Al_2O_3 polycrystalline substrates using pulsed laser ablation. Also Ni ferrite films have been deposited on polycrystalline Al_2O_3 using rf sputtering. Films synthesized on A-plane sapphire, fused silica, and polycrystalline Al_2O_3 do not show any strong orientation of easy axis. Only difference between ferrite films deposited on Al_2O_3 polycrystalline substrates using rf sputtering and pulsed laser ablation was the deposition rate. Pulsed laser deposition give a remarkably higher deposition rate. Eay axis oriented films on C-plane sapphire and R-plane sapphire were observed at high temperatures above 900 ^{0}C. In addition to steady input power of rf, pulsed rf sputtering has been introduced to obtain a higher deposition rate. Details are given in in chapter 5 and chapter 6.

We also synthesized (Li,Mn,Ti,Zn) ferrite films on polycrystalline Al_2O_3 substrates using rf sputtering, also on C-plane, R-plane, A-plane sapphire, fused silica and polycrystalline Al_2O_3 substrates using Nd:YAG pulsed laser deposition. Most of these films, except films deposited on C-plane sapphire, do not show any preferential orientation of easy axis of magnetization. Again the films deposited on C-plane sapphire substrates indicate strong (111) texture at deposition temperature of 930 ^{0}C. These will be explained in detail in chapter 7.

CHAPTER 2

THEORETICAL ASPECTS

2.1 HYSTERISIS BEHAVIOR

All magnetic materials show a fair amount of change in magnetization in an external applied magnetic field. This magnetization change takes place due to the spin rotation and domain wall motion in the magnetic material. This phenomena can be described by hysterisis or magnetic loop. As magnetic field increases, the magnetization increases and finally the magnetization reaches the saturation value, denoted by M_S, beyond this point magnetization can not be significantly increased. A typical hysterisis loop is given in figure 1. If, on reaching the point C, the field strength is decreased, the curve will follow the upper limb of the open loop. A reason for this lag in the change of flux density is the irreversible movement of the domain walls. At the beginning (in the region OA), the magnetization is almost reversible and, magnetization come to zero after removing external field. The slope

of this part of the curve is called the initial susceptibility. After this point the process of magnetization is not reversible. If the field is removed now, the magnetization comes back to point D. The magnetization at this point D is called remanence or denoted by M_r. Further increased of the magnetic field in negative direction results a continues decrease of the intensity of magnetization , which finally becomes zero. The field at this point is called coercive force H_c. This part of the magnetization curve is called demagnetizing curve. If magnetic field is further increased in the negative direction , then finally it comes to saturation value in the opposite direction. The area of the loop is equal to $\oint HdM$, which is referred to as hysterisis loss or heat dissipation of material. If the magnetic field is reversed before it reaches the saturation, then a non symmetrical minor loop is traced.

Depending on the coercivity, anisotropy field (or anisotropy energy), and hysterisis loss, magnetic material can be divided into two parts which are called soft and hard magnetic materials. Soft magnetic materials have smaller coercivity, hysterisis loss, and anisotropy field. The shape of the loop is related to the anisotropy of magnetic material, and to the direction of applied magnetic field. It is easier to saturate the magnetization in one direction (or it is saturated at smaller applied field) for anisotropy materials. This direction is called the easy direction of magnetization. Because of interactions between individual atomic magnetic moments and their neighbors in the crystal, there is an energetically preferred or easy direction for magnetization relative to the crystal axis. A direction perpendicular to this direction is called the hard direction. By measuring the loops in two perpendicular directions, the anisotropy of material can be determined.

Free magnetic poles induced at the ends of magnetized material create a magnetic field in the opposite direction of magnetization, which is referred to as demagnetizing field. The demagnetizing field is equal to N_dM. Here N_d is called the self-demagnetizing factor, which is related to the shape of magnet. If the magnetic body of irregular shape is magnetized, even a uniform distribution of magnetization gives rise to a nonuniform demagnetization field, which results in an irregular distribution of magnetization. In this case demagnetization factor can not be defined, and it becomes uniform for uniform distribution of magnetization only in the case of an ellipsoid. The addition of demagnetization factors in the direction of three principle axis of an ellipsoid is equal to 4π in CGS units, although the expression of each one of these is in a complicated form. For a thin film these can be defined in following form approximately for sample with area of 4mm x 4mm [8].

$$N_{d\text{-}in}=0$$

$$N_{d\text{-}out}=4\pi \qquad (2.1)$$

This is related to the fact that the demagnetization field or demagnetization factor becomes weaker at a larger separation of induced free magnetic poles. Film thickness is much smaller compared to the length of one side of the film sample. So the internal field can be given as following.

$$H_{internal\text{-}in}= H_{applied}$$

$$H_{internal\text{-}out}=H_{applied}-4\pi M \qquad (2.2)$$

The maximum energy product of film , denoted by $(BH)_{max}$ is equal to $(4\pi M_s)^2/4$ in CGS system. This is a measurement of maximum magnetic energy which can be stored in a unit volume of material.

The anisotropy of thin films can be described mostly by

(a) Magnetocystalline anisotropy

(b) Exchange anistropy

(c) Shape anisotropy

(e) Stress induced anisotropy

Only two of above anisotropies will be explained in detail in this thesis. Magnetic anisotropy is the dependence of internal energy in the direction of spontaneous magnetization. Sometimes the crystal symmetry of the material contributes to the magnetic anisotropy. This is called magnetocrystalline anisotropy. For hexagonal materials which shows uniaxial anisotropy, the anisotropy energy can be expressed in following form,

$$E_a = K_{u1} \sin^2(\phi) + K_{u2} \sin^4(\phi) + \text{- - - -} \qquad (2.3)$$

Here ϕ is the angle between the C-axis of crystal and the internal magnetization. For cubic materials, this energy can be given in terms of direction cosines (α_1, α_2, α_3) of domain magnetization in following form,

$$E_a = K_1(\alpha_1^2\alpha_2^2+\alpha_2^2\alpha_3^2+\alpha_3^2\alpha_1^2) + K_2 (\alpha_1^2\alpha_2^2\alpha_3^2) + \text{- - - -} \qquad (2.4)$$

Easy direction of magnetization is related to the minimum of E_a, which depends on signs of K_1, K_2 for cubic material. Easy direction of magnetization always aligns in the direction of C-axis for hexagonal type materials. The stress induced anisotropy will be explained in detail in section 2.4.

2.2 MAGNETIC AND STRUCTURAL PROPERTIES OF CUBIC FERRITES

Ferrimagnetism of materials arises due to the interaction between the spin (magnetic moment) and internal magnetic field of material by surrounded spins (magnetic moments) similar to the other magnetism in materials. The exchange energy between two magnetic moments is given by

$$E_{ex} = -2JS_1.S_2\cos(\phi) \qquad (2.5)$$

Here S_1 and S_2 are spins of two electrons. ϕ is the angle between two spin vectors. J is called exchange integral, and given by

$$J = \int \psi_a(1)\, \psi_b(2)\, \psi_a(2)\, \psi_b(1)[(1/a)-(1/a_2)-(1/a_1)+(1/r_{12})]dt \qquad (2.6)$$

Here a, a_1, a_2, r_{12} represent lattice separation, distance between atom 1 and electron 2, distance between atom 2 and electron 1, and distance between electrons respectively.

Because J is negative for ferrimagnetic materials, exchange energy becomes positive. So antiparallel spin alignment is favorable to minimize the exchange energy in

ferrite. Also the mechanism of ferrite such as oxide materials can be explained in terms of indirect (or superexchange) interaction. If one magnetization in antiparallel alignment is stronger than the other, the difference between two magnetization will give rise to a strong magnetism in material.

The general formula for cubic type ferrites is $MO{:}Fe_2O_3$, here M can be any divalent metal ion such as Mn^{+2}, Fe^{+2}, Co^{+2}, Ni^{+2}, Cu^{+2}, Zn^{+2}, Mg^{+2}, Cd^{+2}. Sometimes the divalent metal ion can also be replaced by a mixture of trivalent and monovalent metal ions. $Li_{0.5}Fe_{2.5}O_4$ with $(1/2)Li^{+1} + (1/2)Fe^{+3}$ is one well known example for this. The simplest ferrite Fe_3O_4 is named as magnetite. The intensity of intrinsic magnetization mostly depends on the type of divalent metal ion. By mixing more than one metal ion, mixed ferrites, which show some interesting magnetic properties, can be obtained. $(Mn,Ti.Li)_{0.5}Fe_{2.5}O_4$ used in this thesis work belongs to this category of mixed ferrite. Ferrites with spinel type structure is shown in figure 2. A unit cell of cubic ferrite contains eight formula units of $MO{:}Fe_2O_3$. The black and hatch circles show the metal ions with radius of 0.6 to 0.8 Å, and white circles represent the oxygen ions with radius of about 1.32 Å. Because oxygen ions are larger in size compared to metal ions, they touch each other and make a close packed face centered cubic lattice. The metal ions occupy interstial sites in this oxygen lattice. If metal ion is surrounded by four oxygen ions as shown by hatched circles, then the site is called tetrahedral or 8a site. If it is surrounded by 6 oxygen ions as shown by black circles, then the site is called octahedral or 16d sites. Because number of oxygen ions surrounded 8a and 16d in the ratio of 2:3, divalent metal (M^{+2}) ions occupy 8a and trivalent Fe^{+3} ions occupy 16d sites. This is

called normal spinel structure. Sometimes half of iron ions and all metal ions occupy 16d, and other half of Fe^{+2} ions occupy 8a. This is named as inverse spinel structure. The distribution of metal ions in 8a and 16d sites depends on the radius of metal ions, the electrostatic energy of lattice, and the matching of electronic configuration of metal ions to surrounding oxygen ions.

The spins align antiparallel to each other in 8a and 16d sites due to the strong negative indirect or superexchange interaction between spins in 8a and 16d sites through oxygen ions. The superexchange interaction can be explained as following for two metal ions separated by an oxygen ion [36] [37]. Because two unpaired electrons in p orbit of O^{-2} are moving on a stretched dumbbell like path, they can pass through both metal ions at some certain angle between the lines adjoining the each metal ion and oxygen ion. One of the unpaired electrons in p orbit can be excited and transferred to the one of metal ions. So the exchange interaction tends to direct the spin of transferred electron in a direction such that the ion has maximum magnetic moment according to Hund's rules. Meantime the other unpaired electron in p orbit of oxygen transfers to the second metal ion. According to Pauli exclusive principle for fermions, two electrons in p orbit have opposite spins. So the spins of two metal ions point in opposite directions. Because the angles 8a-0-16d, 8a-0-8a, 16d-0-16d are equal to 125, 80, 90 degrees respectively, the negative superexchange interaction is stronger between 8a and 16d sites in inverse spinel structure. Only ferrites belong to the normal spinel category are Zn ferrite and Cd ferrite. Only the magnetic moments of metal ions contribute to the net magnetic moment of inverse spinel ferrite, which is equal to

8x(magnetic moment of M^{+2}) per unit cell. The magnetic moment per molecule or formula unit is equal to one eigth of above total magnetic moment per unit cell. Calculated and observed magnetic moments of ferrites are given in table 2.

The magnetic moment of inverse spinel ferrite can be increased by adding some normal spinel such as Zn ferrite. In this case, Zn^{+2} ions occupy 8a sites and force the same number of Fe^{+3} ions to 16d from 8a. This will cause to increase the magnetic moment of 16d sites. If a fraction x of Zn ferrite is added to fraction (1-x) of inverse spinel ferrite, then the net magnetization can be expressed in terms of number of Bohr magneton in M^{+2} (say n) as following [38].

$$M=\{5(1+x)+n(1-x)-5(1-x)\}\mu_b$$

$$M=\{n+(10-n)x\}\mu_b \qquad (2.7)$$

Also the orientation of easy axis of cubic ferrites can be explained in terms of magnetocrystalline anisotropy energy as following. When $K_1>0$ the first terms of $E_a=K_1(\alpha_1^2\alpha_2^2+\alpha_2^2\alpha_3^2+\alpha_3^2\alpha_1^2)$ $+K_2(\alpha_1^2\alpha_2^2\alpha_3^2)$ + - - - is minimum at the [100], [010], [001] directions. So easy axis of magnetization alings along one of the cubic edges for ferrites in this category such as magnetite, Co ferrite. If $K_1<0$, E_a becomes minimum at any of [111] directions. So easy axis of magnetization orients in any of body diagonal of ferrites in this category such as Ni ferrite, Li ferrite, - -etc. Because any of these cubic ferrites have more than one easy directions for magnetization, they are called nonuniaxial magnetic materials.

2.3 MAGNETIC AND STRUCTURAL PROPERTIES OF HEXAFERRITE

The general form of hexagonal type ferrites can be given as $MO:6(Fe_2O_3)$. Here M can be replaced from large divalent ions such as Ba, Sr and Pb with ionic radii 1.43, 1.27, 1.32 Å respectively. Because of low crystal symmetry of hexagonal compounds compared to cubic material, hexaferrites have large magnetocrystalline anisotropy. The hexagonal unit cell of ferrite is large containing two molecules or 2x32=64 atoms. As illustrated in figure 3, the unit cell is elongated in magnetically active C direction. The C and A axis are 23.2 Å, 5.88 Å respectively. Since Strontium(Sr^{+2}) and oxygen(O^{-2}) ions are larger compared to Fe^{+3} and about same size, they make a close-packed lattice. The smaller Fe^{+2} ions occupy interstial sites in the lattice. The unit cell contains 10 layers of close packed oxygen and strontium ions with four ions per layer. Only two of these contain one Sr ion in each. In each hexagonal block a Sr ion substitutes for an oxygen ion in the center of the three layers. So this unit of 10 layers can be considered as a stack of four blocks with alternating hexagonal and cubic stacked sequences. Fe ions occupy tetrahedral, octahedral, and hexahedral sites, depending on the number of surrounding oxygen ions. Eighteen of the 24 Fe ions occupy octahedral sites, four occupy tetrahedral sites, and two occupy hexahedral sites. A complex structure of hexaferrite is given in figure 4(a) and 4(b) from two different views. More details are available in Wijn and Smit ,1959.

Only the Fe^{+3} ions with magnetic moment 5(Bohr magnetron) contribute toward the magnetization in hexaferrite. Because there are no unpaired electrons in Sr^{+2} ions, they

do not create any magnetic moment. Due to the negative superexchange interaction as described in previous section, the magnetic moment of each Fe^{+2} ion is perpendicular to the plane of oxygen ions, and parallel and antiparallel to the C-axis or <0001> direction. Finally the magnetic moment of 16 Fe^{+3} ions point along one direction of C-axis, and 8 ions in the opposite direction. Finally the net or resultant magnetic moment is equal to (16-8)5(Bohr magneton)=40(Bohr magneton) per unit cell [35]. Because each unit cell contains two molecules, the total magnetic moment is 20(Bohr magneton) per molecule. This is equal to 100 emu/g or 530 emu/cc at 0 ^{0}K. Also the orientation of easy axis of magnetization can be explained in terms of magnetocrystalline anisotropy energy. When the angle ϕ is equal to zero,

$$E_a = K_{u1} \sin^2(\phi) + K_{u2} \sin^4(\phi) = 0$$

This means that energetically favorable direction of magnetization is along C-axis, when there is no external forces such as magnetic field, stress (compression, or tensile)- - etc.

2.4 INDUCED ANISOTROPY OF FILMS

Stress induced anisotropy, roll magnetic anisotropy, and anisotropy induced at crystal transition point can be given as examples. Because stress induced anisotropy is the only topic related to this work, it will be explained in detail here. A stress σ (either tensile or compressive) applied to a magnetic body can change the direction of domain magnetization through the magnetostriction. Starting from the expression of magnetostatic energy and strain

tensor, the equation of tensile stress induced anisotropy for a cubic lattice can be proven.

$$E_s = -(3/2)\lambda_{100}\sigma (\alpha_1^2\gamma_1^2+\alpha_2^2\gamma_2^2+\alpha_3^2\gamma_3^2)-3\lambda_{111}\sigma (\alpha_1\alpha_2\gamma_1\gamma_2+\alpha_2\alpha_3\gamma_2\gamma_3+\alpha_3\alpha_1\gamma_3\gamma_1) \qquad (2.8)$$

This energy depends on the direction of domain magnetization ($\alpha_1,\alpha_2,\alpha_3$) and direction of applied stress ($\gamma_1,\gamma_2,\gamma_3$) [38]. The isotropic magnetostriction constant of cubic material can be given for a polycrystalline material as [38]

$$\lambda_s=(2/5)\ \lambda_{100}+(3/5)\lambda_{111} \qquad (2.9)$$

The stress of a thin film is induced due to the difference between thermal expansion coefficient of film (α_f) and substrate (α_s), when the film temperature is decreased from the deposition temperature to room temperature (or during annealing). The stress induced anisotropy of a polycrystalline film is approximately given by following equation [39] [44], using above equation of energy E_s.

$$K_u= -3\lambda_s\sigma /2 \qquad (2.10)$$

$$\text{But } \sigma = E(\alpha_f - \alpha_s)\ \Delta T/(1- \nu) \qquad (2.11)$$

$$\text{Therefore } K_u= -3\lambda_s E\Delta T(\alpha_f-\alpha_s)/2(1-\nu) \qquad (2.12)$$

Here λ_s is the magnetostriction constant of polycrystalline film, E is Young's modules, ν is the Poisson ratio, ΔT is the difference between deposition (or annealing) temperature, and room temperature.

The stress induced anisotropy is small compared to the magnetocrystalline

anisotropy for most of hard magnetic material. So it can be neglected for most of hard magnetic material films. But it plays an important role in soft magnetic materials such as cubic ferrites. The stress induced anisotropy has been calculated for bulk ferrites [40], garnet films [34], and iron oxides [41][42]. Because the stress induced anisotropy is directly related to the temperature difference ΔT, it is possible to determine the origin of anisotropy whether it is due to stress or any other reason. For most of cubic ferrites, isotropic magnetostriction constant is negative. Therefore sign of K_u depends on sign of stress (σ). If $\alpha_f > \alpha_s$, then stress is positive and it is called tension. If $\alpha_f < \alpha_s$, then stress is negative and it is called compression.

Furthermore, the coercivity also depends on the stress as following [43].

Increment of coercivity = $\Delta H_c = 3 (\lambda \Delta \sigma)/M_s$ (2.13)

This implies that the coercivity of film also increases with deposition (or annealing) temperature as well as anisotropy. The numerical estimations based on actual experimental data will be given in chapter 6 and 7.

CHAPTER 3

EXPERIMENTAL PROCEDURE

3.1 FABRICATION OF FILMS

3.1.1 RF SPUTTERING

Although the rf sputtering is widely used to synthesize metal films with different compositions such as rare earth and transition metal, recently it has been useful in deposition of oxide films such as ferrites. Some of our Strontium ferrite, Ni ferrite, and Li mixed ferrite films have been deposited in a stainless steel chamber using rf sputtering. Prior to the sputtering, chamber was pumped down to pressure of about 10^{-8} Torr range to avoid contamination due to atmospheric gasses. In this vacuum process, the chamber was first pumped down to about 20 mTorr using mechanical pump, then to about 10^{-6} Torr using cryopump, finally to about 10^{-8} Torr using ion pump. The chamber was heated using conductive heater bands running around the chamber or using high wattage lamps to outgas

the chamber before rf power was turned on. A high quality film can be deposited through the control of sputtering parameters such as deposition temperature, pressure, type of sputtering gas, rf input power, distance between target and substrate, bias voltage, - - etc.

Customarily made Strontium enriched bar targets with Sr:Fe=1:4, and commercially available stoichiometric Ni ferrite, and Li mixed ferrite targets were helpful to synthesize Sr ferrite, Ni ferrite, Li mixed ferrite respectively. All these bar targets showed a fairly uniform composition all over the bar target. Films deposited with commercially available stoichiometric Sr ferrite targets found to be extremely deficient in Sr. By mixing $Sr(CO_3)$ and Fe_2O_3 in a desired composition and heating it to excessive 1200 ^{0}C, Sr ferrite bar targets were manufactured. Similar production methods are applicable for Ni ferrite and Li mixed ferrite targets.

All of these films deposited using rf sputtering synthesized on polycrystalline Al_2O_3 substrates non-epitaxialy. Films were deposited using dynamic rf sputtering with an oxygen gas flow circulating through the chamber which was controlled by a gas flow controller to maintain a constat pressure in the chamber. The substrate was heated using quartz lamps in voltage range 0-80 V and current range 0-7A. The substrate temperature was varied from plasma (74 ^{0}C) temperature to 700 ^{0}C, which was measured using a K type thermocouple attached to the substrate. Higher temperatures can be obtained by adding more lamps. Also a cylindrical shaped metal sheet, which was placed behind the lamp to focus heat radiation right onto the substrate, was helpful to obtain a higher substrate temperature.

The distance between target and substrate was changed between 3 cm and 8 cm to obtain a higher deposition rate and stoichiometric films. Pure Ar gas to a mixture of Ar/O_2 at total pressure of 10-120 mTorr were used as sputtering gas in the chamber. By controlling the Ar and O_2 flow rates coming to the chamber, different combinations of Ar/O_2 gas mixture have been obtained. Rf input power was varied from 100 to 250W. The reflected power was minimized using a tuner box with capacitors and inductors, attached to rf power supply [45]. Deposition rate of films was about 0.1 microns per hour. Film thickness was approximately 1-3 microns. After deposition some of the films were annealed in situ at higher temperatures up to 800 ^{0}C, at 300-500 Torr of oxygen for 30 minutes.

3.1.2 RF PULSE SPUTTERING

Using a programmable rf power supply (rf plasma products RF-10) with automatic tuner, rf input power can be changed in between two different power levels. If a large rf power above 250 W is dumped into the target for a longer time, that will break targets due to the high heat. This method has been introduced to obtain a higher deposition rate without destroying bar targets. Rf lower power level and upper power level were varied between 150W and 350W, with pulse time of 30 seconds. Because rf power does not stay in upper rf input power level more than 30 seconds, it can be cooled down during next 30 seconds while it remains in lower rf power level. Bias voltage as well as reflection power changed during this cycle of 1 minute. Ni ferrite films have been deposited on Al_2O_3 polycrystalline substrates using stoichiometric bar targets at temperature and pressure ranges described in previous section. Targets were glued to the target holder using conducting silver epoxy bonding to obtain a reliable thermal contact. Some of them were annealed in a similar method mentioned earlier.

3.1.3 PULSED LASER ABLATION

The pulsed laser deposition method, which was developed since 1960s, is very useful to obtain a higher deposition rate of insulator type oxide films such as superconductors and ferrites. Also films with very reliable stoichiometry can be deposited using multicomponent material targets. The deposition rate of ferrite films synthesized using laser ablation method is several times (about 15 -20 times in our case) higher than that of films deposited using sputtering techniques. The pulsed laser deposition technique and its recent developments are given in detail in some latest text book [46].

The laser systems can be mainly divided into two parts as following.

(a) Excimer laser (or gas laser)

(b) Solid state laser

We used a Nd:YAG solid state laser equipment with three different available wavelengths 1064 nm, 530 nm, 355 nm. Here fundamental wavelength is 1064 nm, and other two wavelengths can be obtained using harmonic generator attached to laser. The fundamental wavelength interacts with a crystal and polarize in two different directions to produce the half wavelength. By mixing this again with fundamental, the 355 nm can be obtained. In this Nd:YAG laser, electrons jump between energy levels $F_{3/2}$ and $I_{11/2}$ in Nd^{+3} and emit a laser with small peak energy and large time width. The electrons in Nd^{+3} absorbs energy of optical photons emitted by four flash lamps, and jumps to upper energy level. Because the upper level of transition has a longer life time, a large population of excited

neodymium ions can build up in the YAG rod. If oscillation can be prevented while the population inversion builds, and if the stored energy can be released, the laser will emit a short pulse of high intensity light. This is the main reason for high output energy of laser system about 2j /pulse. An electro-optic Q-switch with high reflector, quarter wave plate , pockels cell and polarizer introduces high cavity loss to prevent oscillation. The output power of laser measured with a photocell is 1.7 W /cm^2 in this case. This power depends on the setting of amplifier and oscillator with two YAG rods. The setting of amplifier and oscillator are 35 J/pulse and 40 J/pulse respectively in this case. Normally amplifier power should be less than oscillator power. Also the laser was set to 30 pps in this case. All relevant parameters are given in table 3.

Finally laser beam comes to the chamber after reflecting from two mirrors and moving through a lens. By moving the lens, laser can be focused with maximum intensity to one spot on the target. The diagram of our laser set up was given in figure 5 in detail. Also the laser beam was moved on the target using some actuators attached to a mirror, which were controlled by NewPort programmable handhold controller. The program written to move the laser beam and the path of laser beam on the target were given in figure 6. This motion of laser beam on target was helpful to obtain a uniform film.

Total pressure of chamber was 75-500 mTorr during ablation with oxygen flow circulating through the chamber, which was controlled by a needle valve. The substrate was heated using a tungsten stripe filament connected to a power supply of 0-130 Amp current.

The substrate temperature in the range up to about 1100 ^{0}C was measured using a optical pyrometer. The laser was purged using dry N_2 gas during ablation as well as 20 min prior to it and 20 min after it. Some Ni ferrite, and Li mixed ferrite films have been deposited on polycrystalline Al_2O_3, sapphire A-axis, C-axis and R-axis oriented Al_2O_3 substrates, and fused silica substrates using this technique.

3.2 MEASUREMENTS OF FILMS

The crystal structure, texture of the film, and a and c lattice parameters were determined using a X-ray diffractrometer with Cu K_α, attached to a Si-Li semiconductor detector cooled with liquid N_2 to avoid thermal excitation of electrons and thermal diffusion of Li^{+2}. In this case Cu K_β radiation was filtered using a Ni filter. A multi channel analyzer (MCA) were used to measure the counts at different angles.

The magnetic measurements were performed using Princeton Applied Research Model 155 vibrational sample magnetometer (VSM), with fields up to 18 kOe provided by an Iron core electromagnet at room temperature. In this apparatus, the sample vibrates vertically with a constant amplitude and frequency, and a current is induced in the material which is proportional to magnetic moment. This current is read by two pick up coils mounted at pole pieces of magnets. The vibration modes keep constant using capacitors. The measured magnetic moments of samples vary from 10^{-1} emu to 10^{-3} emu range. The substrate and sample holder together contribute some diamagnetic properties to measurements of films. So we have measured sample holder and substrate itself at room temperature, and corrected our hysterisis loops. As an example, the diamagnetic contribution from Al_2O_3 polycrystalline substrate was 10^{-6} emu/gm.

The composition of different metal elements, thickness of film and the microstructure in terms of shape and size of grains were determined using scanning electron

microscope (SEM) together with a pulse height analyzer (PHA). In this equipment, an electron beam bombards on sample, then the sample emit X-rays that is characteristic of element. This X-ray beam goes to Si-Li detector attached to a PHA. Intensity of line of energy dispersive curve is related to the abundance of element, and energy is related to the type of element in sample. The resolution of our SEM 50 Å was good enough to observe grain sizes of film. By observing the cross section of one edge of the film, thickness of film can be measured. The thickness of film was useful to determine the deposition rate and the magnetization of film (magnetic moment in a unit volume).

CHAPTER 4

SPUTTER SYNTHESIS NONEPITAXIAL Sr HEXAFERRITE FILMS

4.1 INTRODUCTION

The hexaferrite type compounds are important among other ferrites, because of their magnetocrystalline uniaxial anisotropy with easy axis oriented along the C-axis of hexagonal lattice. All these structural and magnetic properties were explained in detail in chapter 2. Also some of important standard values related to magnetic properties of bulk Sr ferrite are given in table 1. Thin film of hexaferrites have many applications in microwave devices and in recording media. The epitaxial growth of hexferrites by matching close packed oxygen planes in film and substrate have been reported in many publications [1-7]. In most of these cases, highly textured films have been obtained at higher deposition or annealing temperatures in excess of 800 ^{0}C.

We have synthesized $SrO.6(Fe_2O_3)$ nonepitaxially on polycrystalline Al_2O_3 substrates using rf sputtering at temperatures as low as 500 ^0C [9]. The deposition temperature dependence of texture of Sr ferrite is emphasized in this chapter. Also the properties of Sr ferrite films depends on annealing condition, and oxygen partial pressure. In plane coercivities as high as 3.8 kOe were achieved after annealing in oxygen. The stress induced anisotropy is very small compared to the large magnetocrystalline anistropy of hexaferrites. The anisotropy of our synthesized films are very close to that of bulk Sr ferrite.

4.2 EXPERIMENTS

All films were deposited through planar diode sputtering with target to substrate distance from 3 cm to about 6 cm. The Al_2O_3 substrate was heated using quartz lamps connected to a dc power supply. The current and voltage were changed up to 80V and 6.4A to obtain higher temperatures up to 700 ^{0}C. The substrate temperature was measured using a thermocouple. Sometimes two lamps and a reflector placed behind lamp were helpful to obtain a higher temperature. The strontium hexaferrite phase could not be crystallized using commercially available stoichiometric targets, due to the deficiency of Sr. With 100 mTorr of pure Ar gas at deposition temperature of 500 ^{0}C, the Sr to Fe ratio was about 30% of stoichiometric value. Due to the energetic bombardment by O^{-2} ions, the Sr content of film dropped gradually with increasing substrate temperature and oxygen partial pressure in the chamber. This indicates that there was a large preferential resputtering of Sr due to the bombardment by O^{-2} ions on growing film.

To compensate this Sr deficiency in film, custom-made Sr enriched targets with Sr:Fe:O=1:4:7 were used. The size of bar target was approximately 1cm x 4cm. The oxygen content of targets was good enough to directly crystallize hexaferrite phase. The total pressure of chamber was varied from 20 to 100 mTorr. The oxygen and Ar gas flow to the chamber was controlled using a flow controller during this dynamic process. Also the oxygen partial pressure of chamber was controlled by controlling the ratio of oxygen flow rate to the

Ar flow rate. In this case, the oxygen partial pressure was changed up to 10% of total pressure. The rf forward power also varied from about 100 W to 200 W. The reflection power of rf and bias voltage of target at rf forward power of 150 W were about 4 W and 1200 V respectively. Also the rf reflection power and bias voltage change in between 3 W-15 W and 1200 V-1380 V respectively in this range of rf forward power. Some of films were annealed in situ in same temperature range at 300 to 500 Torr of oxygen for about 30 minutes, using same quartz lamps.

4.3 RESULTS AND DISCUSSION

All these hexaferrite films given in detail in this thesis deposited at 100 mTorr total pressure, and deposition temperature from 500 ^{0}C to 650 ^{0}C with target to substrate distance of 6 cm and rf forward power of 150 W. The properties of our films do not depend on target to substrate distance, rf input power, or total pressure of chamber. These films could be directly crystallized as deposited. Some of them were annealed at about 550 ^{0}C at 500 Torr of oxygen for 30 minutes to improve magnetic properties. Only the films deposited at or above substrate temperature of 500 ^{0}C formed in the basic hexaferrite structure as determined from X ray traces. Below this deposition temperature films did not show any magnetic properties, and they were found to be amorphous according to X ray data. So the ferrites also have a minimum crystallized temperature similar to rare earth -transition metal compounds (RE-TM) [8].

The deposition rate and thickness of films were approximately 0.1 microns per hour and 2-3 microns in this small range of temperatures from 500 ^{0}C to 625 ^{0}C. The deposition rate of our Sr hexaferrite films slightly increases with temperature. Normally films with inplane texture of hexaferrite gives a lower deposition rate compared to films with perpendicular texture [6]. Because C-axis of hexaferrite is longer, the surface mobility of atoms can disrupt the growth of films with C-axis in plane easily [6][8]. Because of this reason, the deposition rate of C-axis inplane films become smaller. So our results well agree with the model described in terms of acicular and platelets grains [6].

The Cu-K_α X-ray diffraction patterns of films deposited at 500^{0}C, 550^{0}C, 625^{0}C are given in figures 7(a), 7(b), 7(c) respectively. Also the powder diffraction pattern of Strontium ferrite is given in table 4 for comparison. The dominant texture at 500 ^{0}C was in plane with (110) as in figure 7(a). But it shows both (110), and (114) reflections at 550 ^{0}C as shown in figure 7(b). The diffraction pattern of films at deposition temperatures exceeding 600 ^{0}C resemble the powder pattern of Sr ferrite. All the peaks indicated through arrows are substrate peaks. This can be explained in terms of stacking parameter [8]. The a,c values of Sr ferrite hexagonal lattice are 5.88Å, 23.12Å respectively. At higher deposition temperatures, both deposition rate and surface mobility of atoms become higher. All these parameters disrupt the film growth with C-axis (long axis) in plane of the film. So more grains without C-axis in plane are to be expected at higher deposition temperatures.

The film easy axis orientation, as dictated by the average c-axis orientation of hexaferrite crystallites in the film was found to be strongly dependent on the deposition temperature. To estimate the degree of anisotropy in the film, we define a function R given by,

$$R=N \sum_i \cos(\theta_i)^* (I_i / I_{oi})$$

Here $N= [\sum_i (I_i/I_{oi})]^{-1}$

and θ_i is the angle between the c axis of particular grain and the normal to the film plane, I_i are the intensities of X-ray diffraction lines of film, I_{oi} are the corresponding powder pattern

intensities. This R function gives a measure of the average of C axis orientation with respect to the film plane. Function R is zero for (hk0) textures, unity for pure perpendicular texture, and 0.5 for powder diffraction pattern. R changes from zero to 0.5 for our films. The R value for patterns in figure 7(a), 7(b), 7(c) are approximately zero, 0.38, 0.45 respectively. These R values corresponds to average C-axis orientations away from the film normal of 90^0, 68^0, 63^0 respectively. For the intermediate temperatures, the films exhibited mixed texture crystallites. The dependence of R factor on deposition temperature is given in figure 8.

The magnetic hysterisis loops measured using VSM parallel and perpendicular to the plane of film deposited at 525 ^{0}C are shown in figure 9. The perpendicular loop is given without any demagnetization correction. The diffraction trace of the film showed predominant (110) with (114) reflections. The R value estimated to be around 0.15, corresponding to C axis orientation of 9 ^{0} with respect to film plane. The remanent to saturation magnetic moment ratio of this film was 0.62 in plane, and 0.31 perpendicular to the film plane. This means that there could be some crystallites with easy axis oriented perpendicular to the film plane because aniostropy constants of grains with easy axis in plane and perpendicular to the plane have opposite signs. The magnetic measurements also implies that the C-axis orients randomly in the plane of film at lower deposition temperatures. The anisotropy field in plane to out of plane textured films is same as that of bulk Sr ferrite (16 kOe). Also the magnetic moment does not increase significantly above 16 kOe. The $4\pi M_s$ of film calculated using the thickness measured with SEM was found to be 4.6 kG, with corresponding value of 366 emu/cc saturation magnetization. This is slightly less than the

saturation magnetization of Sr ferrite 380 emu/cc. Reason could be the formation of small fraction of amorphous nonmagnetic secondary phase or nonmagnetic phase crystallized at grain boundaries. Also X ray diffraction patterns do not suppose to show the formation of previously explained nonmagnetic phase. This could be also a reason for the slight change of remanent to saturation magnetic moment ratio in film plane (0.62) from the theoretical value (0.637).

As shown in figure 10, the hysterisis loops of films deposited at higher temperatures above 625 ^{0}C show a remanent to saturation flux density ratio of 0.5 for both in plane and perpendicular to the film plane as shown in figure 10. This ratio gradually changes with deposition temperature. This means that orientation of magnetic easy axis gradually rotates with deposition temperature. So all of our X-ray data agree with magnetic measurements of films.

The coercivities of films drastically increased on annealing the films in an oxygen atmosphere of 500 Torr at temperature of 550 ^{0}C about 30 minutes. The inplane loop of films deposited at 550 ^{0}C temperature, before and after annealing, are given in figure 11. The in plane coercivity increased from about 0.5 to 3.8 kOe during annealing in oxygen. No change of grain size or X-ray patterns was noticeable as a result of postdeposition annealing. The coercivity increases as oxygen atoms fill in the Sr ferrite unit cell. The oxygen introduced at high temperature can be retained in unit cell at room temperature by quenching. On the otherhand, the microstress of film can be released with annealing at a higher temperature. If

the usual hindrance to wall motion such as microstress and inclusions decreases with annealing, then that can effect on pinning sites of domain wall motion. This will also cause to increase the coercivity, but it does not change X- ray diffraction patterns.

The typical grain size in the polycrystalline films determined from SEM was about 2500 Å at 550 ^{0}C deposition temperature as shown in figure 12. Each division of the scale given corresponds to 1500 Å. The elongated (acicular) grains in SEM micrograph again indicates the random orientation of C -axis in the plane of film, similar to results obtained by some other researchers for Ba ferrite [6]. Previously some other researchers have been able to show that the C-axis of hexaferrite is perpendicular to the long axis of these elongated grain [6].

As oxygen partial pressure increases, a secondary non magnetic phase begins to crystallize. The X- ray diffraction traces of films at pure Ar, 5% of O_2, 10% of O_2 are given in figure 13. At higher oxygen partial pressure (10% of O_2), nonmagnetic phase completely crystallized and X-ray does not show any line of hexaferrite. These films were deposited at 600 ^{0}C at total pressure of 100 mTorr of Ar/O_2 mixture, and annealed in oxygen of 500 Torr at 550 ^{0}C for 30 minutes. The peaks indicated through arrows are substrate peaks. This nonmagnetic phase was identified to be $SrFe_2O_4$ using standered powder diffraction patterns. Because the magnetic moment of Sr^{+2} is zero due to the lack of unpaired electrons, the total magnetic moment of spinel $SrFe_2O_4$ is zero. Also the saturation magnetization of film decreases with oxygen partial pressure due to the formation of nonmagnetic phase.

CHAPTER 5

EPITAXIAL AND NON-EPITAXIAL Ni FERRITE FILMS SYNTHESIZED USING PULSED LASER DEPOSITION

5.1 INTRODUCTION AND EXPERIMENT

The thin films of $NiFe_2O_4$ are useful in monolithic microwave integrated circuits, and in some other microwave applications. The domain wall oscillation and spin precession take place at smaller and higher frequency respectively in microwave frequency range. Because saturation magnetization of ferrite is directly related to the frequency of domain wall resonance, domain wall oscillation can be avoided using ferrites with small saturation magnetization. In other words, domain wall oscillation happens at very small frequencies below microwave frequency range for ferrites with small magnetization. Also because these are soft magnetic materials, they can be magnetized to saturation magnetization by applying

a smaller field, and domain walls can be swept. The domain wall oscillation can be avoided in this way too.

The structural and magnetic properties of these type of cubic inverse spinel ferrites were given in detail in chapter 2. The calculated and measured values of magnetic moments of Ni ions are 2 and 2.3 Bohr magnetons respectively, which are equal to the magnetic moment of pure Ni ferrite per molecule unit because the magnetic moments of iron ions cancel each other. This slight difference of magnetic moments takes place due to the unquenched orbital moments and incomplete inverse spinel structure. Easy direction of magnetization is oriented along one of four body diagonal for Ni ferrite type compounds. Because only 8 out of 64 tetrahedral sites and 16 out of 32 octahedral sites are occupied by metal and iron ions in the cubic unit cell, there is good possibility of forming some other phases in addition to Ni ferrite phase. If there is more iron or Ni in the compound compared to stoichiometric of Ni ferrite, they can occupy these vacant sites and that will cause to change the magnetic moment without changing the structure of the compound. Also because the size of Fe^{+3} and Ni^{+2} are almost same and 0.65 Å and 0.72 Å in terms of radius respectively, they can occupy any vacant octahedral or tetrahedral site in lattice. This can also cause to form some other phases.

We have been able to synthesize Ni ferrite films on C-plane, R-plane, A-plane Al_2O_3 sapphire substrates, polycrystalline Al_2O_3 substrates and fused silica substrates using pulsed laser deposition (PLD) [48]. Nd:YAG laser with 1064 nm fundamental wavelength and 30 pps was used to ablate these films. All these films could be crystallized as deposited above

some minimum deposition temperature similar to previously reported RE-TM, and Sr ferrite films. We obtained quality films without any post deposition annealing, similar to some ZnO films deposited using PLD by some other researchers [49]. Sputtered films usually needs a post deposition annealing to form ferrite films with (111) texture [50]. The highly textured films could be deposited at higher temperatures above 830 ^{0}C. The substrates were heated using a tungsten filament, and laser beam was moving on the target as explained in chapter 3. Previously Ni ferrite films have been synthesized on some other substrates using PLD by some other researchers [52]. A flowing oxygen gas pressure of 200 mTorr was used during the deposition of all these films. At lower oxygen partial pressure, some other phases crystallized. Target to substrate distance was fixed to about 1.5 cm approximately. The incoming laser beam makes angle of 20 degrees with vertical line. Our films were deposited with deposition rate of about 5Å/s for 2 hours. The total number of pulses used to make a film were approximately 2.16 X 10^5 in this case.

In addition to this, Ni ferrite films growth on (111) MgO substrates at deposition temperatures around 900 ^{0}C using liquid phase epitaxy (LPE) was reported by some other researchers. Also the effect of stress on the film magnetic and structural properties has been given in detail in several early reports[39].

5.2 Ni FERRITE FILMS ON C-PLANE SAPPHIRE SUBSTRATES

The texture of films deposited on C-plane (006) sapphire strongly depends on the deposition temperature. Films could be crystallized only above deposition temperature of 550 ^{0}C. Below this temperature, films were amorphous and nonmagnetic according to Cu-K_α X-ray and VSM data respectively. The intensity, d-space, and angle of standard powder pattern of Ni ferrite are given in table 5. At 625 ^{0}C, X-Ray diffraction pattern of film is similar to powder pattern of Ni ferrite as shown in figure 14(a). As temperature increases, it gradually changes to (111) texture. At 930 ^{0}C, films show complete (hhh) texture with (111), (222), (333) lines as shown in figure 15. This means that cubic body diagonal of Ni ferrite is perpendicular to the plane of film. At deposition temperature of 675 ^{0}C, the (222) reflection was still enhanced but the (311) reflection of the X ray diffraction pattern dominated as shown in figure 14(b). The (222) reflection starts to dominate above 770 ^{0}C. The substrate line is indicated with "S" in X-ray patterns.

A 10,000 times magnified SEM micrograph of (111) textured film is given in figure 16. The picture indicates some triangular or pyramidal shape grains with a little content of cubic shape grains, which implies that film is highly textured. The average length of side of triangular shaped grains is about 1μm according to the length scale given in picture. Also the size of different grains are different and it changes between 0.4 μm and 2 μm. Again the shape of grains confirms that (111) direction of cubic unit cell is perpendicular to film plane.

Also the film was found to be uniform, and no defects nor voids were observed.

The magnetic hysterisis loops measured at room temperature for (111) orientad single crystal Ni ferrite films in plane and perpendicular to film plane are given in figure 17. The coercivities in plane and perpendicular to the plane of this film are 120 Oe, and 95 Oe respectively. The saturation flux density, $4\pi M_S$, was 1.9 kG as deduced from the approach to saturation of the perpendicular magnetization using the demagnetization factor for perpendicular to the film plane measurements which is very close to $Nd=4\pi$. The thickness of this (111) oriented single crystal film was approximately about 3.5 microns. One of the solid curves indicates the perpendicular to the plane hysterisis loop after demagnetization correction for internal magnetic field.

The hysterisis loop of bulk Ni ferrite measured in one direction with VSM is given in figure 18. There was no significant difference among loops measured in other directions. This implies that target shows isotropic properties. The coercivity and saturation magnetic field of bulk Ni ferrite are about 5 Oe and 2500 Oe according to this loop. The coercivity and anisotropy of films are larger compared to those of bulk, due to stress induced anisotropy in the film [34][39][41][42]. The stress arises due to the difference between thermal expansion in film and substrate.

Using the equation 2.12 given in section 2.4, the stress induced anisotropy K_u for this (111) oriented single crystal Ni ferrite film can be estimated as following. The thermal

expansion coefficients are about 5.6 X 10^{-6} K^{-1} perpendicular to the plane of substrate (or parallel to the C-axis of substrate), and 1 X 10^{-5} K^{-1} for Ni ferrite. The difference between room temperature and deposition temperature is about 900 ^{0}C. Young's modulus and Poisson ratio of Ni ferrite are about 1.68 X 10^{12} dyne/cm^2 and 0.32 respectively [53]. The magnetostriction constant of Ni ferrite in (111) direction is -22 X 10^{-6}. The estimated value of stress induced anisotropy for this sample was found to be 3.23 X 10^5 erg/cm^3 perpendicular to the plane of film, which is comparable to the stress anisotropy calculated by some other researchers [39]. The crystal anisotropy constant K_1, K_2 for cubic Ni ferrite are -6.7 X 10^4 and 0.26 x 10^4 erg/cm^3 respectively [38]. So stress induced anisotropy of Ni ferrite film is significant and that can effect both on coercivity and anisotropy field. For anisotropic (or textured) magnetic materials, the magnetostriction constant (or elongation) and stress (σ) are different in different directions even in the same sample. Therefore the stress induced anisotropy and change of coercivity will be different in different directions.

In addition to this, (111) textured film was found to be epitaxial and single crystal using Kikuchi backscattered electron diffraction method. For $NiFe_2O_4$, d_{111} exceeds the "a" lattice parameter of Al_2O_3 by 1.18%. The origin of epitaxy is generally the matching of lattice planes in film and substrate. The epitaxy of this film may arise by matching (110) plane of C-plane substrate with (222) in Ni ferrite. Both these planes are perpendicular to the film plane in this special case, and d spacing of (110) of substrate and (222) of Ni ferrite are 2.380 and 2.408Å respectively at room temperature. The orientation of each sapphire substrate itself is given in table 8. We have not done any experiment to verify matching of these certain planes,

above prediction is just one possibility. Also the resonance line width of our (111) oriented Ni ferrite films were measured to be 1000 Oe, which is larger compared to that of bulk target (434 Oe). The measured value of $4\pi M_S$ of films was in between 1600-1900 G.

5.3 Ni FERRITE FILMS ON R-PLANE SAPPHIRE SUBSTRATES

Similar to the films deposited on C-plane sapphire, the texture of films deposited on R- plane (012) strongly depends on the deposition temperature. All these films deposited at pressure of 200 mTorr of oxygen flowing through chamber. At lower temperature of 650 ^{0}C, the X-ray diffraction pattern shows the reflection of all lines in powder pattern of Ni ferrite as shown in figure 19. This means that the easy axis of film is not oriented in any proper direction. As the deposition temperature is increased, the orientation of easy axis gradually changes. Finally the film shows strong (400) texture at deposition temperature of 910 ^{0}C, as shown in figure 20. The intensity ratio I(400)/I(311) is equal to 6.15 at this temperature 910 ^{0}C. The peaks indicated with "S" belong to substrate.

The graph between magnetization versus applied field as measured with SQUID magnetometer located at MARTECH is given in figure 21. The coercivities inplane and perpendicular to the plane of film are about 280 Oe, and 530 Oe. The coercivity and

anisotropy of film are larger compared to that of bulk Ni ferrite again due to stress induced anisotropy. The saturation flux density calculated using the thickness and volume of film was 2.2 kG. This shows that X-ray data well agree with magnetic data. Using same parameters given in previous section except magnetostriction constant and thermal expansion coefficient of substrate, the stress induced anisotropy can be estimated as following. The magnetostriction constant of Ni ferrite in (100) direction is -45.9×10^{-6}. The estimated value of stress induced anisotropy was found to be 7.65×10^{5} erg/cm^3 perpendicular to the film plane approximately, which is significant compared to crystal anisotropy again.

The films deposited at higher temperatures were chemically and mechanically stable and molecules were sticked very well to the film. Only few atomic layers of film could be removed after it was kept in strong HF acid for about 1 hour. But films deposited at temperatures below 650 ^{0}C could be removed completely without any difficulties. At higher temperatures particles have a higher mobility and they can move on film surface until they find energetically favorable sites in film, and that will make films more stable at higher deposition temperatures. These (400) textured films were found to be polycrystalline using Kikuchi backscattered electron diffraction indicating that the films consisted of oriented crystallites with a diameter of less than 1 μm.

5.4 Ni FERRITE FILMS ON SOME OTHER SUBSTRATES

In addition to above substrates, the Ni ferrite films were deposited on Al_2O_3 polycrystalline substrates, amorphous fused silica and sapphire A-plane Al_2O_3 substrates using PLD. Although the temperature and pressure were controlled in a wide range, a textured films of $NiFe_2O_4$ could not be synthesized on these substrates. But single phase of Ni ferrite can be crystallized on these substrates as well as on C-plane and R-plane sapphire substrates without any other impurity phases. Sometimes the texture of epitaxial films depends on deposition rate and oxygen partial pressure too. But X-ray diffractions of our films were not sensitive to the pressure of oxygen flow in the range of 75 to 500 mTorr. The crystallite orientation strongly depends on the deposition temperature as shown by X -ray patterns.

The X-ray diffraction pattern of film deposited on A-plane sapphire at 650 ^{0}C is given in figure 22. The (311) reflection is strong at this low temperature similar to the powder diffraction of Ni ferrite. The X-ray pattern of film deposited at 910 ^{0}C shows strong (400) reflection as shown in figure 23. The intensity ratio I(400)/I(311) is equal to 1.18 at higher deposition temperature. This means that it is possible to obtain a strong (400) texture at deposition temperatures higher than 930 ^{0}C, which is above maximum obtained temperature of our system.

The X-ray traces of Ni ferrite deposited on amorphous fused silica at deposition

temperature of 650 ^{0}C is shown in figure 24. It shows the random orientation of crystallites at this temperature with a strong (311) reflection. In this case the background has an amorphous hump near 22 degrees from the substrate. However the film shows strong (220), (440) reflections at lower deposition temperature of 550 ^{0}C as shown in figure 25. Slightly below this temperature, X-ray diffraction patterns did not show any peaks at all, indicating a poor crystallization of the phase. Also the X-ray patterns did not change with oxygen pressure at this fixed low temperature. Sometimes it will be possible to obtain a complete in plane (110) texture at very low deposition temperatures by means of fine controlling of deposition conditions.

The films deposited on polycrystalline Al_2O_3 substrates exhibited broadened diffraction lines which could only be sharpened to a certain extent by subsequent heat treatments of films. The (311) reflection is still strong in this case similar to films gown by rf sputtering, which will be explained in detail with X-ray traces in chapter 6. In this case the diffraction lines from polycrystalline Al_2O_3 substrate dominate the pattern and, some impurity phases are present. This also indicates that crystallization of Ni ferrite phase is not complete, and a large fraction of film is amorphous.

CHAPTER 6

POLYCRYSTALLINE Ni FERRITE DEPOSITED USING RF SPUTTERING

6.1 INTRODUCTION

A memory device in digital computers must have following properties (a) square loop (b) fast magnetic reversal (about 1 ns) and (c) low coercive force. Because soft ferrites such as Ni ferrite have low coercivities, the area surrounded by magnetic hysterisis loop is smaller and the heat loss becomes minimum. Because of this reason, soft ferrites are important candidates in theses type of applications. But they have higher demagnetization factors due to free pole at pores, and this may reduce the squareness of loop. So making ferrites without porosity is a biggest task for these type of applications. By increasing the

sintering temperature, ferrites with larger grain sizes can be sintered, and this will decrease the porosity. Also on the other hand, the coercivity increases at higher sintering temperatures due to stress induced anisotropy. The effect of stress on coercivity as well as on anisotropy will be explained in detail in this chapter. Also the polycrystalline films are more useful compared to single crystal or epitaxial films, in some applications such as magnetic recording and in commercially available circulators as described in chapter 1. The line width ΔH at 3 dB, Lande' g-factor, $4\pi M_S$, and dielectric constant of our bulk Ni ferrite targets are 460 Oe, 2.13, 2097G, and 12.6 respectively.

The polycrystalline Ni ferrite films deposited on polycrystalline Al_2O_3 substrates using following two different rf sputtering methods will be explained in detail in this chapter.

(a) rf sputtering with steady forward power and,

(b) pulse rf sputtering

The variation of properties of films with deposition temperature, total pressure, oxygen partial pressure, annealing conditions, deposition rate were studied in detail. The X-ray diffraction patterns of our Ni ferrite films were sensitive only to the deposition temperature. The magnetic properties such as coercivity and anisotropy mostly depend on the deposition temperature, annealing conditions, and oxygen partial pressure during sputtering. The pulse rf sputtering was introduced to increase the deposition rate.

6.2 EXPERIMENT

The films were deposited on heated Al_2O_3 substrates at deposition temperature range from 60 ^{0}C to 600 ^{0}C and in ambient plasma temperature 57 ^{0}C, in total pressure range from 20 mTorr to 70 mTorr. The substrates were heated using quartz lamps, and temperature was measured using a thermocouple attached to substrate. A mixture of oxygen and Ar gas were used during sputtering as well as pure Ar gas. The oxygen partial pressure of chamber were varied up to 10% of total pressure. Some of the films deposited at low temperatures were annealed at 300-500 mTorr of oxygen at temperatures of 270 ^{0}C to 600 ^{0}C, for 30 minutes to 4 hours in the same chamber, to crystallize the Ni ferrite phase. Commercially available Ni ferrite bar targets could form stoichiometric films as measured by SEM. The deposition rate of these films were approximately 0.1 microns/hour, and thickness of films were approximately 1.4 microns as measured by SEM. The steady rf forward power were varied in a range from 150 W to 200 W, the corresponding bias voltage and rf reflection were in range 900 to 1700 V and 0 to 20 W respectively. In addition to these, some Ni ferrite films were deposited on Al, and Ta buffer layers sputtered on Al_2O_3 substrates using rf sputtering.

The deposition rate of films synthesized using steady rf sputtering (0.1 micron/hour) was very low compared to films deposited using pulsed laser deposition (5 Å/s). The pulsed rf sputtering were helpful to overcome this problem. The maximum deposition rate of films fabricated using pulse sputtering was about 0.42 micron /hour. The shape of

pulse wave resembles to a square wave with a period of 1 minute as shown in figure 26. The upper and lower rf forward power used to obtain this maximum deposition rate were 250 and 350 W. Also the change of deposition rate, with different rf upper and lower forward power range from 150 to 350 W, has been investigated.

6.3 RESULTS AND DISCUSSION

6.3.1 FILMS SYNTHESIZED BY STEADY RF SPUTTERING

As pressure was increased from 20 mTorr to 70 mTorr of pure Ar, all magnetic properties and X-ray diffraction patterns remain same. But if a mixture of Ar/O_2 gas was used during sputtering, then the deposition rate can be decreased with pressure. Since it is possible to obtain quality smooth films at low pressure as described in chapter 1, we deposited most of films explained in this chapter at 20 mTorr of pure Ar and 30 mTorr of Ar/O_2 mixture. The Ni ferrite phase could be crystallized only above deposition temperature of 223 ^{0}C, if there is no oxygen gas in the chamber. Below this minimum crystallization temperature, the films deposited without oxygen gas were found to be amorphous and nonmagnetic. Also the films synthesized at lower temperatures did not show any X-ray lines before annealing. The X-ray lines of these films were visible after annealing film in a higher oxygen pressure.

The coercivity at the deposition temperature of 223 ^{0}C was 70 Oe, and coercivity increases with deposition temperature. The anisotropy and coercivity of films are higher compared to that of bulk. The in plane magnetic hysterisis loops of two films synthesized at different deposition temperatures, measured using VSM, are given in figure 27. Both theses films were deposited at 20 mTorr of Ar, and annealed at 604 ^{0}C in 400 Torr of oxygen for 1

hour. The film with larger coercivity was deposited at 417 ^{0}C, and other one was deposited at 404 ^{0}C. Because the coercivity and anisotropy increases with deposition temperature, this anisotropy would be introduced due to the stress as described in chapter 2, section 2.4. Using the equation 2.13, the change of coercivity can be estimated in this case as following.

The stress induced anisotopy can be estimated using the same equation 2.12 given in chapter 2, similar to calculation in chapter 5. We can use the same parameters given in chapter 5 for Ni ferrite except magnetostriction constant, substrate temperature and thermal expansion coefficient of substrate. The magnetostriction constant for a polycrystalline sample can be calculated using equation 2.9 given in chapter 2, and it was found to be approximately 3.14 X 10^{-5} [40]. Also the thermal expansion coefficient of polycrystalline Al_2O_3 is about 8.8 X 10^{-6} K^{-1}. If we estimate the stress induced anisotropy at a lowest deposition temperature of 430 ^{0}C, it will be equal to 1.25 X 10^4 erg/cm^3. Although this value is smaller compared to that of films deposited on sapphire substrates, it is still comparable to crystal anisotropy constants of Ni ferrite. Also the stress induced anisotropy will be larger than this value at higher deposition temperatures. The change of in plane coercivity estimated using equation 2.13 was found to be 375 Oe, as deposition temperature was increased from 223 ^{0}C to 400 ^{0}C without annealing. The saturation magnetization was equal to 151 erg/cc for this Ni ferrite film. This calculation well agree with our experimental data. The magnetostriction constant is same in all directions for isotropic magnetic materials. But the stress can be different in different directions. So again the stress induced anisotropy and change of coercivity will be different in different directions in the same film.

The hysterisis loops in plane and perpendicular to the plane of film deposited at a lower deposition temperature of 310 ^{0}C are given in figure 28. According to these loops, the film shows some isotropic properties corresponding to random orientation of C-axis at smaller deposition temperatures. The in plane and perpendicular to the plane of films deposited at higher deposition temperature of 600 ^{0}C are given in figure 29. These loops indicate some anisotropic properties. All these loops were measured using VSM at room temperature. Also the saturation flux density and corresponding magnetic field of these loops are 1.9 kG and about 5 kOe respectively after substrate corrections. The saturation magnetization is slightly less than that of bulk. All these loops perpendicular to film plane are given without any demagnetization correction.

Also the coercivity increases with oxygen partial pressure in the chamber during sputtering as shown in figure 30. Both theses films deposited at ambient plasma temperature of 70 ^{0}C, at total pressure of 30 mTorr without annealing. The film with larger and smaller in plane coercivities were deposited at oxygen partial pressures of 80%, and 20% respectively. The in plane coercivity gradually increases with oxygen partial pressure in between these two oxygen partial pressures as given in table 6. The coercivity measured in a direction perpendicular to the plane of film also shows the same variation. Also the films can be crystallized at lower deposition temperatures, if there is some oxygen in the chamber during sputtering. Similar to results obtained for Sr ferrite, the change of coercivity may be due to the filling of oxygen in cubic ferrite unit cell.

A SEM micrograph of a Ni ferrite film deposited at 310 ^{0}C is given in figure 31. No crystallites were observed in this case because deposition temperature was not high enough to crystallize grains. The magnetic properties of films depend on annealing conditions as well as on deposition conditions during sputtering. The coercivity of films increases with annealing temperature and annealing time interval. In addition to these, we deposited some Ni ferrite films on Al buffer layer sputtered on Al_2O_3. The coercivity of these films also increases with deposition temperature in this case too. Also some films were deposited on Ta buffer layer sputtered on Al_2O_3 substrate. All theses films have same properties as films deposited on Al_2O_3 substrates without any buffer layer.

The X-ray diffraction patterns show strong (311) reflection at lowest deposition temperature of 310 ^{0}C as shown in figure 32. As temperature was increased, other lines also become evidence and it becomes closer to the random (or powder) pattern of Ni ferriteas at 600 ^{0}C as given in figure 33. The substrate lines of Al_2O_3 are indicated with "S" in these X-ray patterns. Some reflection such as (222) do not appear in these X-ray patterns of films. Also the deposition rate increases considerably with deposition temperature in this temperature range from 223 ^{0}C to 600 ^{0}C, because particles have a higher surface mobility and more particles can be sticked to the substrate at higher temperatures, for films sputtered without oxygen gas.

6.3.2 FILMS SYNTHESIZED BY PULSE RF SPUTTERING

Although the upper and lower forward power levels of pulse sputtering remains same during each 30 second time intervals, the reflection power and bias voltage change within that 30 seconds. The time variation of bias voltage within 30 s for 350 W upper and 150 W lower forward power levels are given in figures 34 and figure 35. The time average of bias voltage during each pulse can be calculated by using the area between curve and X-axis. If we change the upper and lower forward power levels, then the time average bias voltage also changes. The relationship between deposition rate and time average of bias voltage is given in figure 36. According to this graph, the deposition rate increases drastically up to 1810 V, which corresponds to upper and lower forward power levels of 350 W and 250 W respectively. But the magnetic and structural properties of Ni ferrite films were similar to those of films deposited with steady forward power and, they completely depends on sputtering and annealing conditions.

When the negative bias voltage of target is larger, positive gas ions in the plasma, which bombard on the target, have a higher energy. So those high energy gas ions can knock out more target atoms or molecules from the target, and that will increase the deposition rate of films. Also on the other hand, the deposition rate can be increased only up to a certain level by increasing the bias voltage or rf forward power according to some earlier reports. After that certain value of bias voltage, the deposition rate begins to decrease with bias

voltage as an ion implantation becomes dominant [51]. Also our results agree with the model described by Winters et.al 1976, up to a certain level of bias voltage. But In this range of our bias voltage up to 1810 V, the deposition rate does not start to decrease. The theoretical curve is indicated by the dashed line in figure 36. Because the Ni ferrite targets were brittle and they were broken above this maximum bias voltage of 1810 V due to overheating, it was difficult to study the change of deposition rate above this bias voltage.

The lowest coercivity obtained using pulse sputtering was 200 Oe for films deposited at 263 ^{0}C and 20 mTorr of Ar gas. Similar to films deposited with steady rf sputtering, the coercivity of films increases with deposition temperature, as shown in figure 37. The magnetic properties do not depend on total Ar gas pressure during sputtering according to in plane magnetic hysterisis loops as shown in figure 38. Both theses films were deposited at 315 ^{0}C, and annealed at 330 ^{0}C in 400 Torr of oxygen. But the pressure was varied from 20 mTorr to 80 mTorr of Ar. Also the films deposited in between these two pressures have same coercivity. Also we deposited some films using metal Ni:Fe=1:2 targets, with oxygen during sputtering. The magnetic properties of theses films are similar to films synthesized using stoichiometric Ni ferrite bar targets.

CHAPTER 7

(Li Mn Ti Zn) MIXED FERRITE FILMS SYNTHESIZED WITH SPUTTERING AND LASER ABLATION

7.1 INTRODUCTION AND EXPERIMENT

Similar to other magnetic compounds, Li ferrite with inverse spinel structure is also useful in magnetic recording medium and in microwave application. The Li ferrite is different from general form of spinel ferrite $MO.Fe_2O_3$, in the way Li^{+1} and Fe^{+3} ions occupy tetrahedral and octahedral sites in lattice. In this case, a quarter of octahedral Fe^{+3} ions have been replaced by Li. The size of Li^{+1}, Fe^{+3} are almost same and their radii are about 0.69 Å, and 0.65 Å respectively. The calculated magnetic moment of pure Li ferrite is about 2.55 Bohr magnetons per molecule. By adding some other elements, the net magnetic moment of material can be changed. Sometimes ferrite materials with low magnetic moments are useful

in microwave application, because the domain wall resonance frequency is directly related to the saturation magnetic moment of material. By using materials with low magnetic moments, the domain wall resonance can be avoided in microwave frequency region.

In this case, we have added Mn,Ti,Zn to Li ferrite to decrease the saturation magnetic moment from 310 emu/cc to 272 emu/cc. The change of magnetization can be calculated using a method similar to equation 2.7. The bulk target materials have been sintered using 74.6% of Fe_2O_3, 8.4% of Li_2CO_3, 2% of MnO_2, 0.2% of BiO_3, 7.3% of TiO_2, 7.4% of ZnO. If we neglect the small amount of Bi, then the formula unit of this ferrite can be expressed as $(Li_{0.5}Mn_{0.06}Ti_{0.22}Zn_{0.22})Fe_{4.45}O_X$. In sintering process, some of these material can evaporate easier than others, and the composition will be slightly changed from above formula unit. So the formula unit will be given as (Li Mn Ti Zn)Fe_5O_8 from now on in this chapter. Also the line width ΔH at 3db, Lande' g-factor, resistivity, and dielectric constant of this material can be given as 346 Oe, 2.00, 8410 kOhms-cm, and 14.8 respectively.

We have deposited these ferrite films using rf sputtering with steady input power and using pulsed laser deposition. Again a remarkably higher deposition rate of about 6 Å/s could be obtained with Nd:YAG pulsed laser technique. The films synthesized with rf sputtering give a deposition rate of 0.12 microns per hour. Also it is easier to obtain films of oxide materials with stoichiometric composition using laser ablation. Because the oxygen ions in plasma bombard on the film during sputtering, it is difficult to obtain smooth films with stoichiometric composition. But because oxygen does not ionize during laser deposition

process, we can use enough oxygen to obtain stoichiometric films without disrupting film growth. This plasma free deposition is one big advantage of laser ablation technique as described in most of earlier reports.

These films deposited using sputtering were deposited on Al_2O_3 polycrystalline substrates, and annealed in oxygen to improve the X-ray properties. The films were synthesized in a flow of pure Ar and a mixture of Ar/oxygen. The total rf forward power and the distance from substrate to target were fixed to 150 W and 6 cm respectively, because the properties of films did not depend on these parameters. The rf bias voltage and rf reflected power were in the ranges of 1470 V to 1270 V, and 16 W to 0 W respectively. The magnetic and structural properties have been studied using VSM and Cu-K_α X-ray radiation. Using PLD, we deposited films on polycrystalline Al_2O_3 substrates, on R-plane, A-plane and C-plane sapphire Al_2O_3 substrates, and on fused quartz substrates. Most of the films deposited using both sputtering and PLD did not show any complete orientation of C-axis, except films deposited on C-plane sapphire by PLD..

7.2 FILMS DEPOSITED WITH RF SPUTTERING

The changes of magnetic and structural properties with deposition temperature, total pressure, oxygen partial pressure, and annealing conditions have been studied. The films deposited at deposition temperatures from ambient plasma temperature (70 ^{0}C) to 570 ^{0}C. The total pressure of chamber was varied from 15 mTorr to 70 mTorr. The magnetic

properties of films do not change with annealing at 420 ^{0}C in 400 Torr of oxygen for a short time interval of 30 minutes. The films deposited at lower temperatures could not be crystallized without annealing in oxygen. Also magnetic and structural properties did not depend on total pressure of chamber during sputtering as shown in figure 39, similar to Ni ferrite. These three films were deposited in pressures 50, 60, and 70 mTorr, at same deposition temperature of 420 ^{0}C, and annealed in 400 Torr of oxygen at 470 ^{0}C for 20 minutes. All theses hysterisis loops given in previous figure are measured in the plane of film. However the films deposited with oxygen indicate nonmagnetic properties at 10% oxygen partial pressure, with or without annealing.

The magnetic hysterisis loop of bulk Li ferrite in any arbitrary direction as measured by VSM is given in figure 40. The coercivity and anisotropy of most of films are higher compared to that of bulk. The films directly crystallized at 570 ^{0}C has a higher coercivity of 400 Oe at perpendicular to plane and 200 Oe in plane. Subsequently crystallized films deposited at ambient temperature 70 ^{0}C have small coercivities in plane and perpendicular to the plane of film, which are comparable to those of bulk ferrite. The coercivity increases with deposition temperature as given in figure 41. So again this anisotropy must be induced due to the thermal stress between film and substrate. Also the films deposited at lower temperatures (of 63 ^{0}C) indicate isotropic properties according to in plane and perpendicular magnetic hysterisis loops (similar to polycrystalline Ni ferrite films) as shown in figure 42. The films synthesized at higher deposition temperatures (of 420 ^{0}C) indicate some anisotropy as given in figure 43.

From equation 2.11 and 2.13 in chapter 2, the change of coercivity is directly propotional to the change of temperature. The change of coercivity in the plane of our films versus the change of temperature can be plotted as shown in figure 44. According to graph, the theoretical model well agree with our data in this temperature range. The slope of straight line was found to be 0.38 Oe/^{0}C. Because it was difficult to find required parameters of these feiites such as Young's modulus, thermal expansion coeffiecent, etc., we could not estimate the stress induced anisotropy in this case. Because most of these parameters of all kind of ferrites are approximately in the same range, the stress induced anisotropy of theses feiites may be vary close to estimated stress induced anisotropy of polycrystalline Ni ferrite films (1.25 X 10^4 erg/cc). Still this is comparable to crystal anisotropy constants K_1= -8.6 X 10^4 erg/cc, and K_2= 2 X 10^4 erg/cc of Li-Mn ferrite reported by some other researchers.

The intensity and position of each peak in powder pattern of Li ferrite are given in table 7. X- ray traces of films deposited at 70 ^{0}C, and 570 ^{0}C are given in figure 45 (a) and figure 45(b). At lower temperature, only the (311) is reflected. Here substrate lines are shown with "S". Some different shaped crystallites were observed in SEM micrograph in this case as shown in figure 46. Film was deposited at 570 ^{0}C, and temperature was high enough to crystallize grains of average size 0.6 μm.

7.3 FILMS DEPOSITED WITH LASER ABLATION

Sometimes the oxide films can be crystallized even without a ulrta high vaccum system by using PLD. This is another superior advantage of laser ablation. These ferrite films synthesized on polycrystalline Al_2O_3 films show same magnetic properties as films fabricated using sputtering. The X-ray diffraction pattern changes with deposition temperature in similar manner. Also the films could be crystallized at higher deposition temperatures above 490 ^{0}C without any post deposition annealing. Below 450 ^{0}C, films were not crystallized completely, and they showed weak broad X-ray peaks as deposited, as shown in figure 47. This film was synthesized at 75 mTorr of oxygen flow. Also the X-ray diffraction traces don't change with oxygen partial pressure of chamber as shown in figure 48. Both theses films were fabricated at 550 ^{0}C. These films don't show any proper alignment of easy axis similar to Ni ferrite.

The films deposited on amorphous fused silica substrates also do not show any proper orientation of easy axis. At higher temperatures of 770 ^{0}C, X-ray traces show all the peaks in powder pattern as shown in figure 49(A). It also indicates the formation of secondary impurity phase in addition to Li mixed ferrite only at higher deposition temperatures. As the deposition temperature was decreased, the X-ray patterns shows strong peaks only at (311), (220), (440) reflections as given in figure 49(B). Both these films were deposited at 200 mTorr of oxygen. Below this temperature of 550 ^{0}C, this ferrite could not be crystallized. Also the X-ray properties of films do not change with oxygen partial pressure in a range from 75 mTorr to 500 mTorr. Above 800 ^{0}C, fused silica substrates began to melt.

The X-ray traces of films synthesized on R-plane sapphire even at higher substrate temperature of 950 ^{0}C in 200 mTorr of oxygen do not show any better orientation of easy axis as shown in figure 50. At lower temperatures, it is similar to random pattern. Unlike the Ni ferrite films, it was difficult to obtain textured film of these ferrites even at maximum deposition temperatures which were available in our system. Also the magnetic and structural properties of our films were not sensitive to oxygen pressure during ablation. The well textured films could not be synthesized on A-plane substrates too, in this range of temperature. All these films deposited on polycrystalline Al_2O_3, fused silica, and all three type of substrates have a higher anisotropy and coercivity compared to bulk as measured by VSM.

Some of the films deposited on C-plane sapphire show an strong (111) orientation of C-axis at higher deposition temperatures. At lower deposition temperature of 620 ^{0}C, the X-ray traces of films are similar to the powder pattern as shown in figure 51. But the (222) becomes stronger compared to the powder pattern, as shown in figure 52, at higher deposition temperature of 930 ^{0}C which was the maximum available temperature in our system again. The intensity ratio I(222)/I(311) is equal to 3.88 in this case, which is larger compared to that of powder pattern (0.08). Both these films were synthesized at 500 mTorr of oxygen flow. The texture of film gradually changes in between these temperatures. The resonance line width of these (111) textured Li mixed ferrite films were measured to be 520 Oe, again which is larger compared to that bulk (346 Oe). But this is still smaller compared to the line width of (111) oriented Ni ferrite films. This smaller line width will make these Li mixed ferrite films suitable for microwave applications. $4\pi M_S$ of these films was about 3 kG.

CHAPTER 8

CONCLUSION

We have deposited epitaxial and non-epitaxial films of various kind of ferrites on different type of substrates by using different deposition techniques. According to our results, the magnetic and structural properties of these ferrite films mostly depend on the deposition temperature, and the properties of substrates. The orientation of C-axis is not sensitive to the total pressure of the system, or to the annealing conditions. The Sr ferrite belongs to hard ferrite category, and Ni ferrite and Li ferrite belong to soft ferrite category have been synthesized in thin film form. For a conclusion, all these results can be summarized as following.

We have been able to synthesize Sr ferrite non-epitaxially on polycrystalline Al_2O_3 substrate by rf sputtering with a steady forward power. Films of Sr ferrite with strong (110) texture have been fabricated at deposition temperatures as low as 550 ^{0}C in Ar of 100 mTorr [9]. As the deposition temperature was increased, it becomes similar to the powder pattern of Sr ferrite above 600 ^{0}C. The films could be crystallized as deposited above some minimum crystallization temperature of 500 ^{0}C. Also the magnetic hysterisis loops consolidate the

random orientation of easy axis in the plane of film at 550 ^{0}C, and isotropic properties at 600 ^{0}C. All these films were deposited only in pure Ar gas, because the oxygen content in target was sufficient to crystallize Sr ferrite and too much oxygen causes to form some other non magnetic phases. After annealing in 500 Torr of oxygen at 550 ^{0}C for 30 minutes, the coercivity in the plane of film dramatically increases from about 0.5 kOe to 3.8 kOe.

The epitaxial (or single crystal) Ni ferrite films with complete (111) texture has been synthesized on C-plane sapphire Al_2O_3 substrates by means of Nd:YAG pulsed laser ablation [47]. Again the orientation of C-axis mostly depends on the deposition temperature. At higher deposition temperatures above 900 ^{0}C, and in 200 mTorr oxygen flow, the completely (111) textured Ni films could be crystallized. Because the easy axis of Ni ferrite points along the body diagonal, the easy axis (111) well oriented films are of special interest. Also one of the body diagonal is perpendicular to the plane of film plane in this case. At lower temperatures above some minimum crystallization temperature of 500 ^{0}C, X-ray traces of films deposited on all sapphire substrates resemble the powder pattern of Ni ferrite. The magnetic hysterisis loops performed by VSM well agree with all these X-ray data. We could also synthesize highly textured polycrystalline (400) Ni ferrite films on R-plane sapphire substrates at deposition temperatures of 910 ^{0}C in 200 mTorr oxygen flow using PLD [47]. In this case, one of the cubic edges is perpendicular to the plane of film. The orientation of film C-axis strongly depends on the orientation of sapphire substrate. The films deposited on A-plane sapphire, and fused silica are non oriented in this temperature range up to 950 ^{0}C, according to X-ray diffraction patterns.

In addition to these, non-oriented polycrystalline Ni ferrite films have been deposited on Al_2O_3 polycrystalline substrates by using sputtering with steady forward power and pulse sputtering. At lower deposition temperatures of 223 ^{0}C, the in plane coercivity of theses films are 70 Oe. Using PLD, we could not obtain films with this kind of low coercivity. The films with smaller coercivities and polycrystalline films are important in some applications. As temperature was increased, the coercivity of films also gradually increases. The x-ray diffraction patterns do not show any proper orientation of C-axis in the deposition temperature range up to 750 ^{0}C. Using the pulse sputtering, the deposition rate could be increased by several times. But the magnetic and structural properties of films did not change with deposition rate. However the highest deposition rate could be available only using PLD compared to any sputtering techniques, for these ferrimagnetic materials.

Non-oriented Li ferrite films have been deposited on polycrystalline Al_2O_3 using sputtering and pulsed laser ablation. The lowest obtained in plane coercivity was almost zero for films deposited at ambient plasma temperature of 70 ^{0}C, using sputtering. The films fabricated on C-plane sapphire by PLD provide a strong (111) texture at highest available deposition temperature of our system, 930 ^{0}C. At this higher temperature the intensity of (222) line dominates compared to that of powder pattern. Again at lower temperature, the X-ray traces of films are similar to the powder pattern of Li ferrite. The films deposited on R-plane and A-plane sapphire, and fused silica using PLD does not show any proper orientation of C-axis in this temperature range.

The coercivities and anisotropy of films synthesized at higher deposition temperatures are larger compared that of bulk due to the stress induced anisotropy as shown in previous chapters. The stress induced anisotropy has been estimated using available data of these type of materials only for the comparison. If we want to calculate it exactly, we have to measure the all parameters such as Young's modulus, Poisson ratio, thermal expansion of our synthesized ferrite films in plane and perpendicular to the film plane. The stress induced anisotrpoy increases with deposition temperature. But the highly textured Ni ferrite could be synthesized only at higher deposition temperatures. Using a proper buffer layer, it may be possible to reduce the stress induced anisotropy, and synthesize highly textured films with low coercivity at higher deposition temperatures.

TABLE 1

	Sr FERRITE	Ba FERRITE
SATURATION MAGNETIZATION M_s (emu/cm^3) AT 0 ^{0}K	530	530
SATURATION MAGNETIZATION M_s (emu/cm^3) AT 20 ^{0}C	380	380
CURIE TEMPERATURE T_c (^{0}C)	450	450
REMANENCE B_r (G)	3425	3500
COERCIVITY H_c (Oe)	3000	3000
ANISOTROPY FIELD H_A (kOe)	17	16
ANISOTROPY CONSTANT K_1 (erg/cm^3) X 10^6	3.57	3.25
MAXIMUM ENERGY PRODUCT BH_{max} (MGOe)	2.9	2.9

TABLE 2

FERRITE TYPE	OBSERVED MOMENT	CALCULATED MOMENT
Fe_3O_4	4.1	4
$NiFe_2O_4$	2.3	2
$CoFe_2O_4$	3.7	3
$MnFe_2O_4$	4.6 to 5.0	5
$CuFe_2O_4$	1.3	1
$MgFe_2O_4$	1.1	0
$LiFe_5O_8$	2.5 to 2.6	2.55

TABLE 3

		PULSE ENERGY (mJ) \ PEAK POWER (MW)			
wavelength (nm)	pulsewidth (nsec)	1 pps	10pps	20pps	30pps
1064	7 to 9	900\110	900\110	800\100	700\85
532	5 to 7	360\60	360\60	300\50	250\40
355	4 to 6	160\30	160\30	115\20	90\18
266	4 to 6	125\25	80\16	50\10	35\6
pulse repetition frequency design optimum, pps, range, pps		1 0.2\2	10 2\20	20 3\30	30 4\40
spatial mode		nearly guassian, hole - free, nearly diffraction limited 7 mm diameter (nominal)			
Linewidth at 1064 nm standard with ICE-1 (optional) with ELN-2 (optional)		 <1.0 cm^{-1} <0.2 cm^{-1} <0.02 cm^{-1}			
Beam pointing stability		<0.5 mrad			
Beam divergence		<0.5 mrad, full angle			
Output pulse time jitter		<500 psec rms from Q-switch sync pulse			
Average power stability		5% over 10 hr at 1064nm, also 5%over 10 hr at 532 nm or 355 nm with optional HG-2			
Rated flash lamp life		30 million pulses			
Electrical service current (A)		30	30	50	50
Voltage (V)		208 or 220 (nominal), single phase			

TABLE 4

d-SPACING	Cu-Kα ANGLE 2θ	INTENSITY	MILLER INDICES
4.94	17.958	10	101
4.65	1.088	14	102
3.86	23.044	16	6
2.94	30.407	40	110
2.89	30.946	14	8
2.85	31.391	10	112
2.77	32.322	100	107
2.62	34.228	100	114
2.55	35.198	8	200
2.52	35.631	8	108
2.42	37.156	40	203
2.23	40.454	40	205
2.13	42.443	25	206
1.945	46.707	10	1.0.11
1.814	50.305	16	1.1.10
1.715	53.431	6	210
1.699	53.975	10	126
1.666	55.134	40	127
1.625	56.649	50	304
1.606	57.381	6	128
1.53	60.52	10	129
1.473	63.124	40	220
1.389	67.432	16	310
1.313	71.918	8	1.0.17

TABLE 5

d-SPACING	Cu-K_α ANGLE 2θ	INTENSITY	MILLER INDICES
4.82	18.409	20	111
2.948	30.322	30	220
2.513	35.734	100	311
2.408	37.348	8	222
2.085	43.405	25	400
1.9125	47.549	4	331
1.7025	53.855	8	422
1.6051	57.416	30	511, AND 333
1.476	62.981	40	440
1.41	66.297	2	531
1.3187	71.559	6	620
1.2706	74.717	10	533
1.2573	75.645	4	622
1.2036	79.67	6	444
1.1676	82.65	1	711
1.1145	87.544	6	642
1.0857	90.493	16	731
1.0424	95.401	6	800
0.9827	103.36	2	822
0.963	106.38	10	751
0.9566	107.41	2	662
0.9324	111.56	8	840
0.9152	114.8	2	911

TABLE 6

The oxygen partial pressure in the chamber during sputtering in percentage (%)	The in plane coercivity of film (Oe)
20	349
30	578
50	928
80	1103

TABLE 7

d-SPACING	Cu-Kα ANGLE 2θ	INTENSITY	MILLER INDICES
5.89	15.403	12	110
4.78	18.564	4	111
3.74	23.794	20	210
3.4	26.213	14	211
2.945	30.354	45	220
2.769	32.334	4	221
2.632	34.067	4	310
2.514	35.719	100	311
2.42	37.156	2	222
2.311	38.978	4	320
2.084	43.426	45	400
1.703	53.838	14	422
1.637	56.196	4	510
1.605	57.42	45	511 and 333
1.523	60.827	4	521
1.474	63.076	60	440
1.318	71.603	14	620
1.273	74.552	20	533
1.204	79.638	14	444
1.135	85.577	4	721
1.115	87.495	18	642
1.084	90.674	6	731

TABLE 8

TYPE OF SUBSTRATE	ORIENTATION (PLANE PARALLEL TO SUBSTATE SURFACE)
C-PLANE	0 0 6
R-PLANE	0 1 2
A-PLANE	1 1 0

FIGURE 1

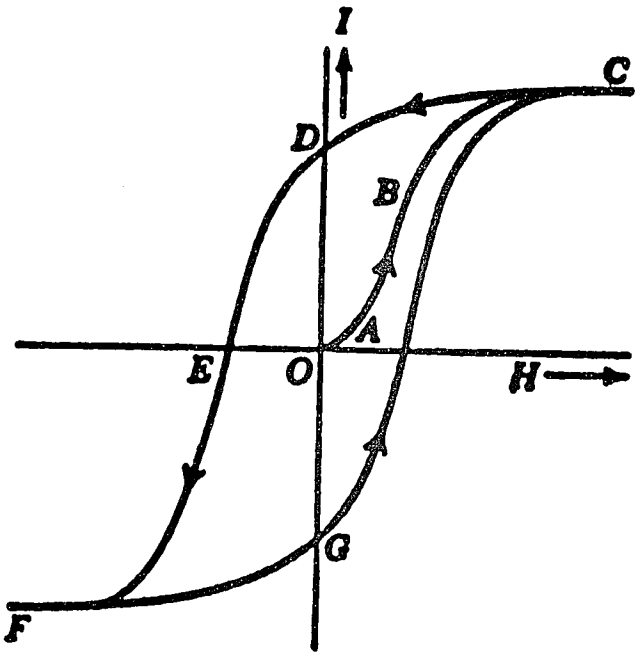

FIGURE 2

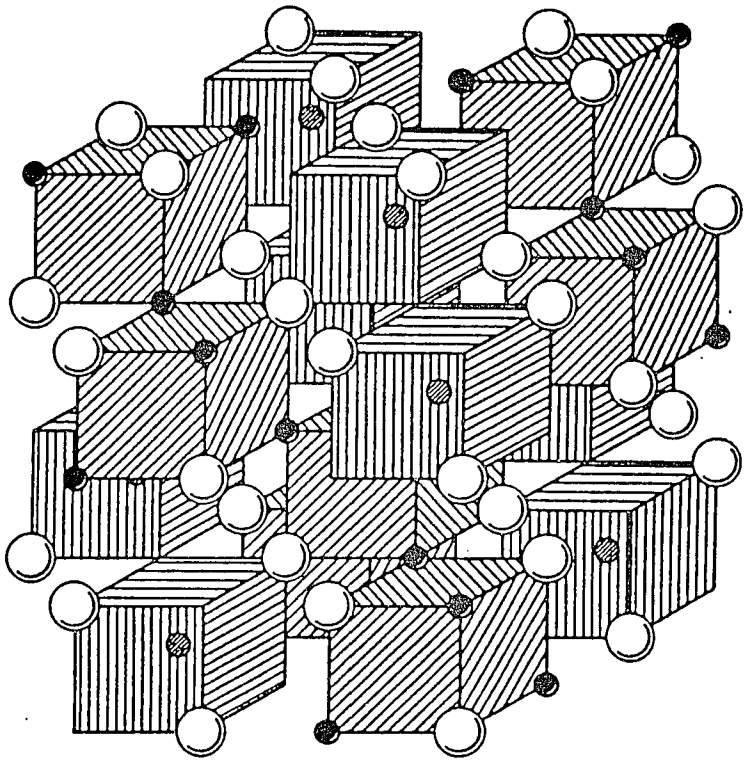

FIGURE 3

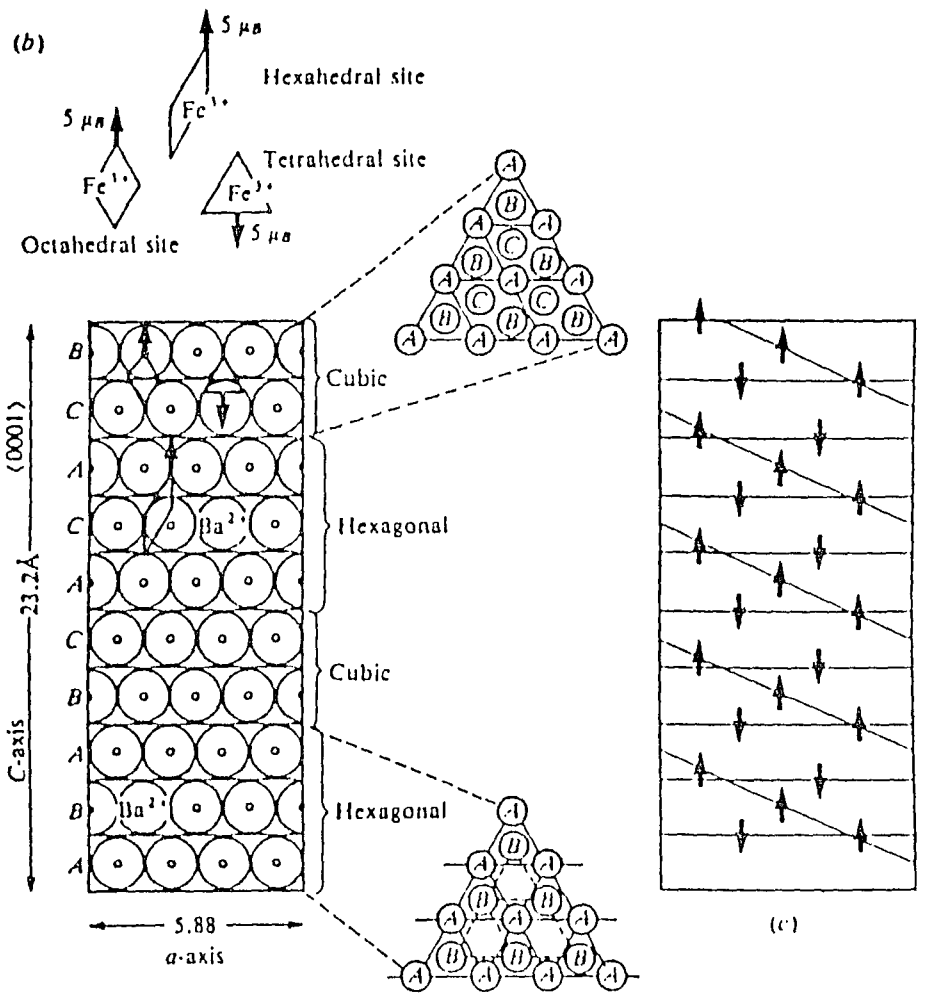
(b)
5 μB
Hexahedral site
Fe3+
5 μB
Fe3+
Tetrahedral site
Fe3+
Octahedral site
5 μB
B
C
A
C
A
C
B
A
B
A
(0001)
23.2Å
C-axis
Ba2+
Ba2+
Cubic
Hexagonal
Cubic
Hexagonal
5.88
a-axis
(c)

FIGURE 4

(a)

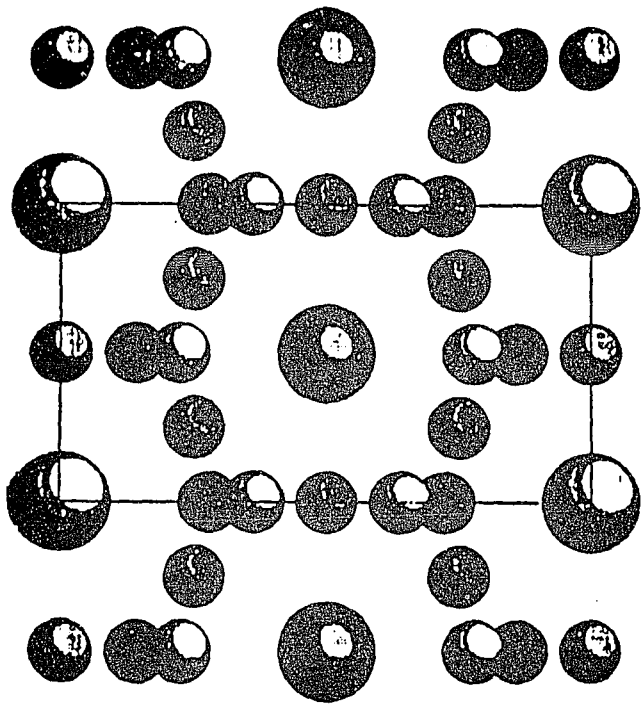

(b)

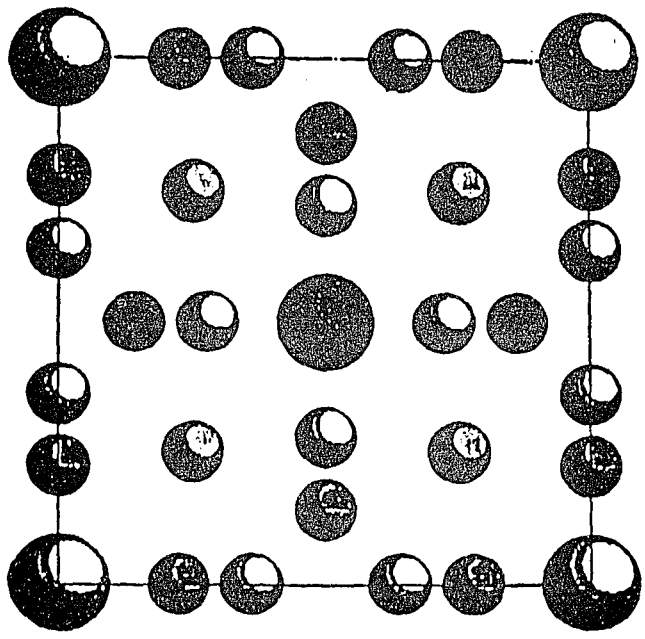

FIGURE 5

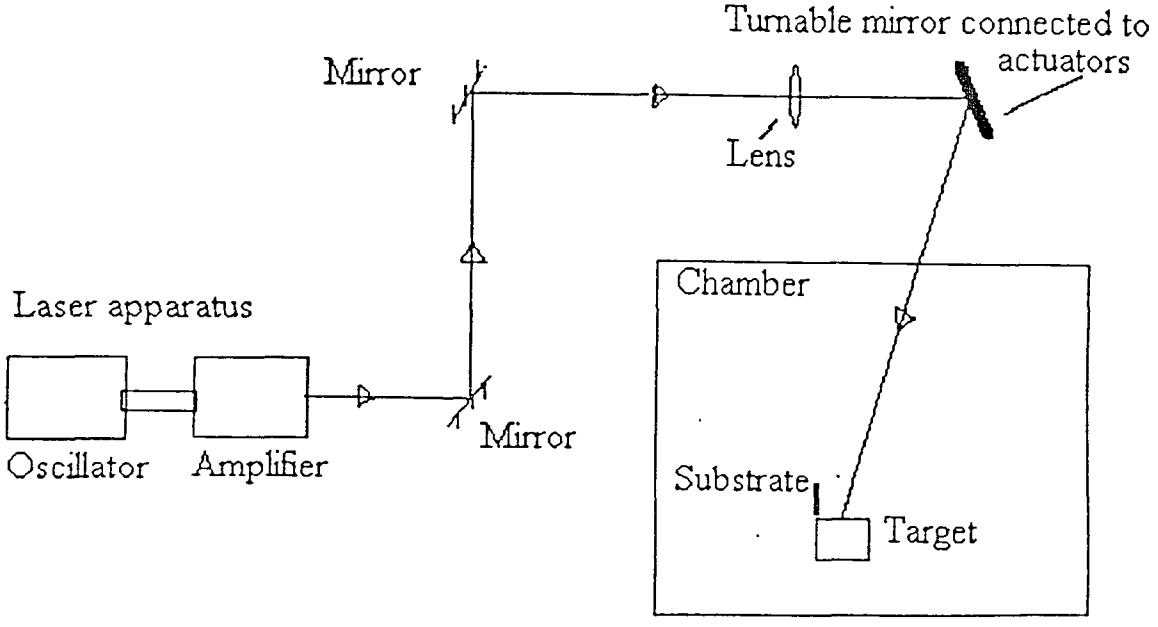
Tunable mirror connected to actuators
Mirror
Lens
Chamber
Laser apparatus
Mirror
Oscillator
Amplifier
Substrate
Target

T0 CURRENT 0 0

T1 VELOCITY 0 0.4

T2 ABSOLUTE 4 10000

T3 STEP 3 0.001

T4 MOVE 4

T5 WAIT 4

T6 INCREMENT 3

T7 WAIT 3

T8 HOME 4

T9 WAIT 4

T10 INCREMENT 3

T11 WAIT 3

T12 JUMP 4 - 470

T13 MOVE 0 0

T14 JUMP 0-6

T15 EXEC MODE

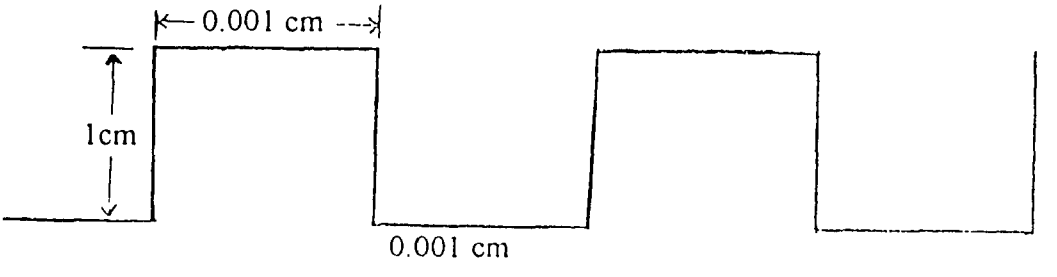

FIGURE 6

FIGURE 7

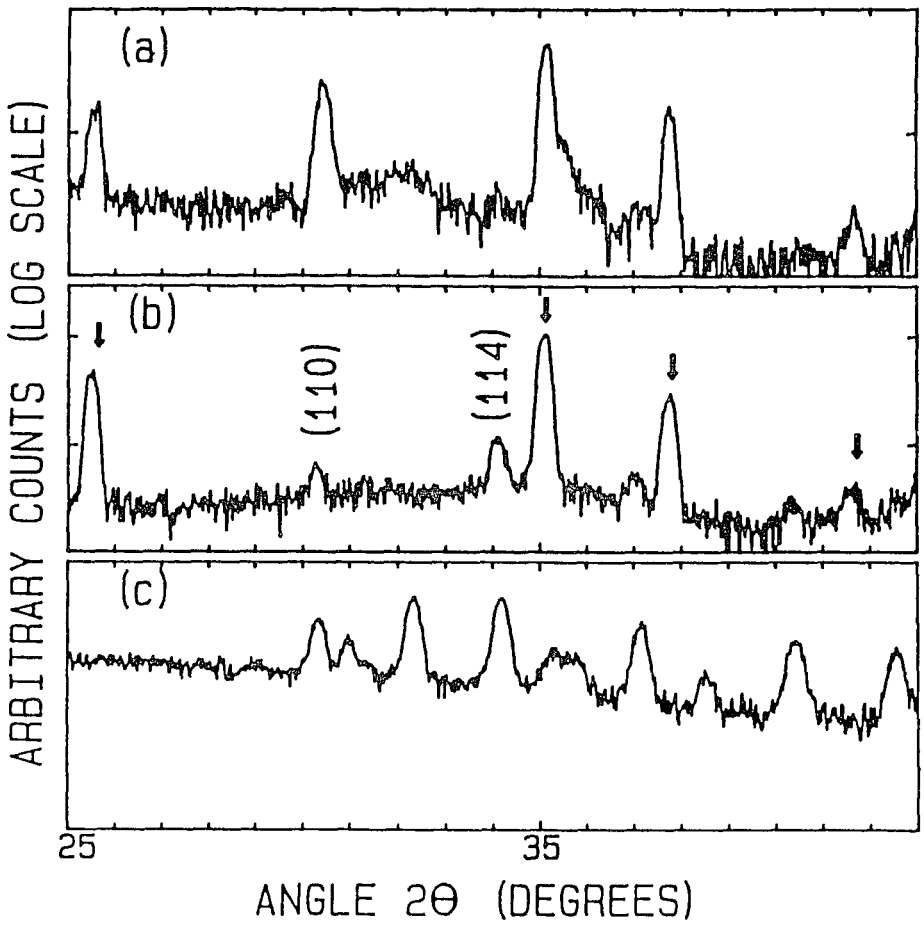
(a)
(b)
(c)
(110)
(114)
ARBITRARY COUNTS (LOG SCALE)
25
35
ANGLE 2Θ (DEGREES)

FIGURE 8

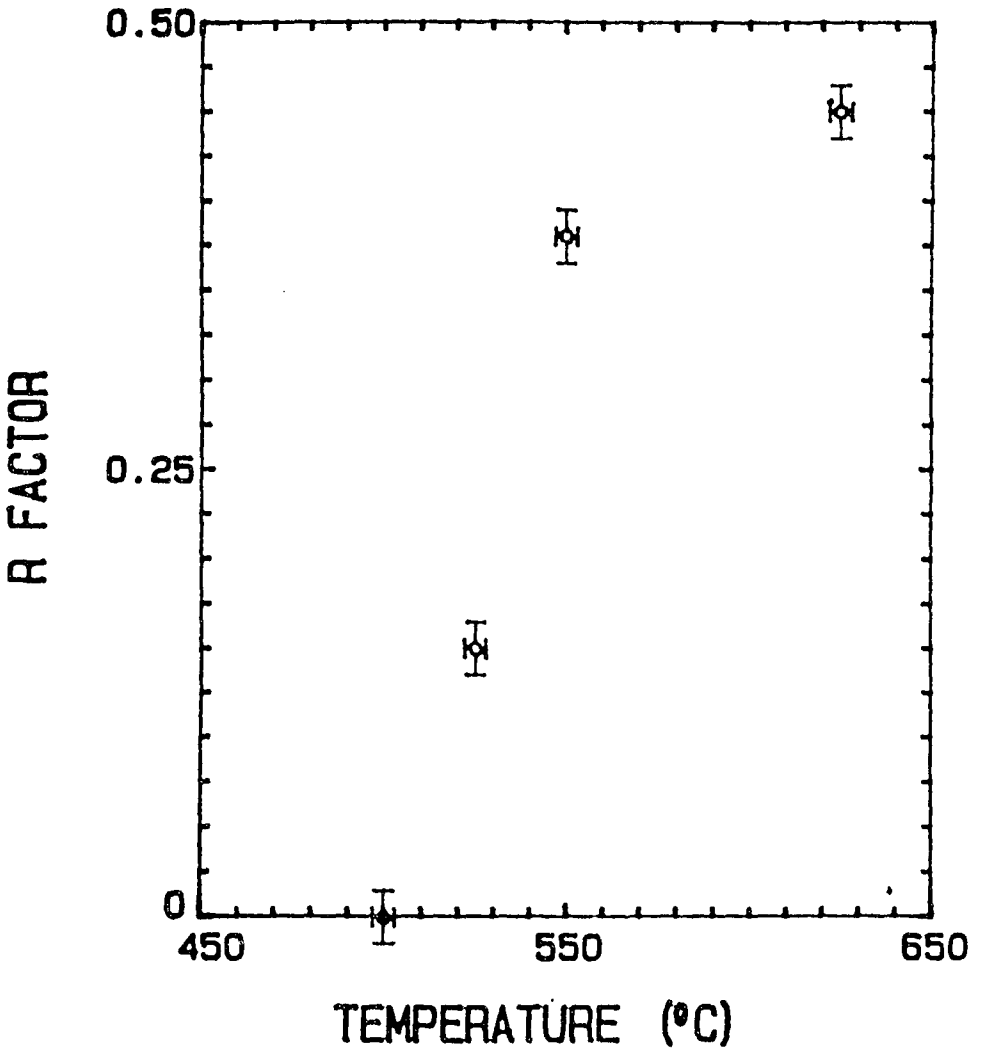

FIGURE 9

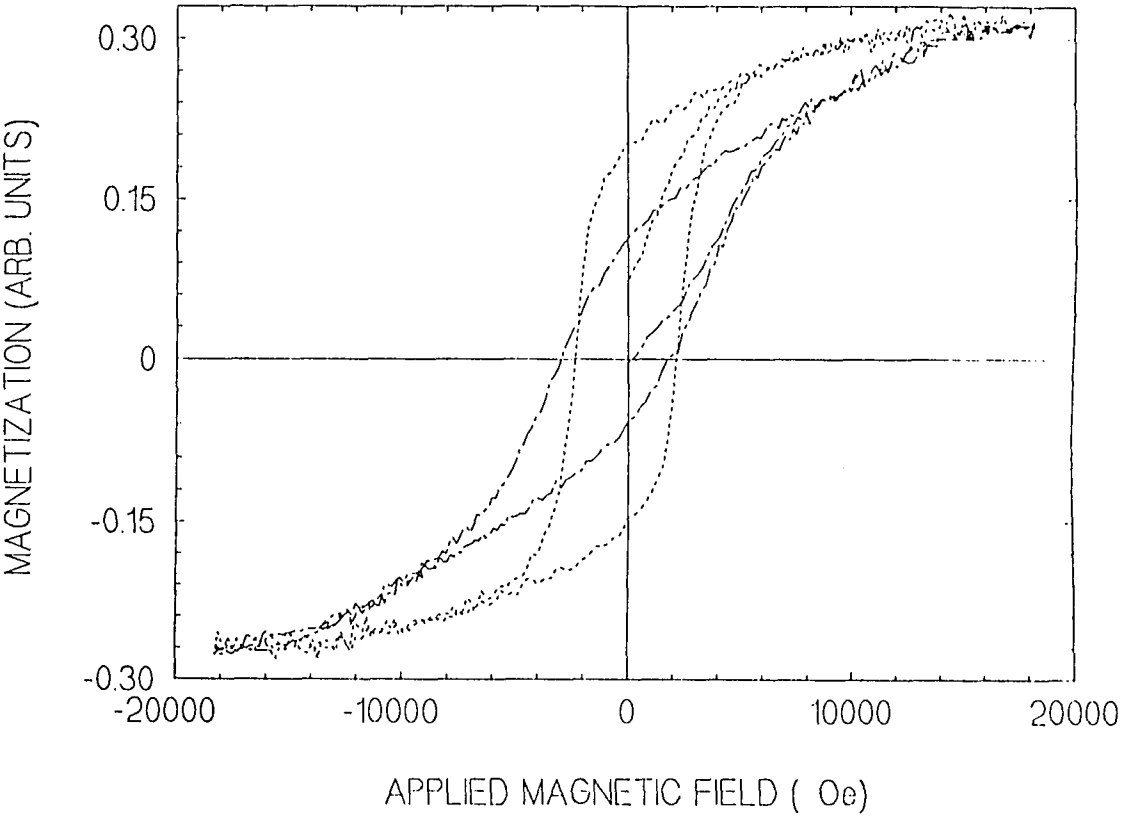
0.30
0.15
0
-0.15
-0.30
MAGNETIZATION (ARB. UNITS)
-20000
-10000
0
10000
20000
APPLIED MAGNETIC FIELD (Oe)

FIGURE 10

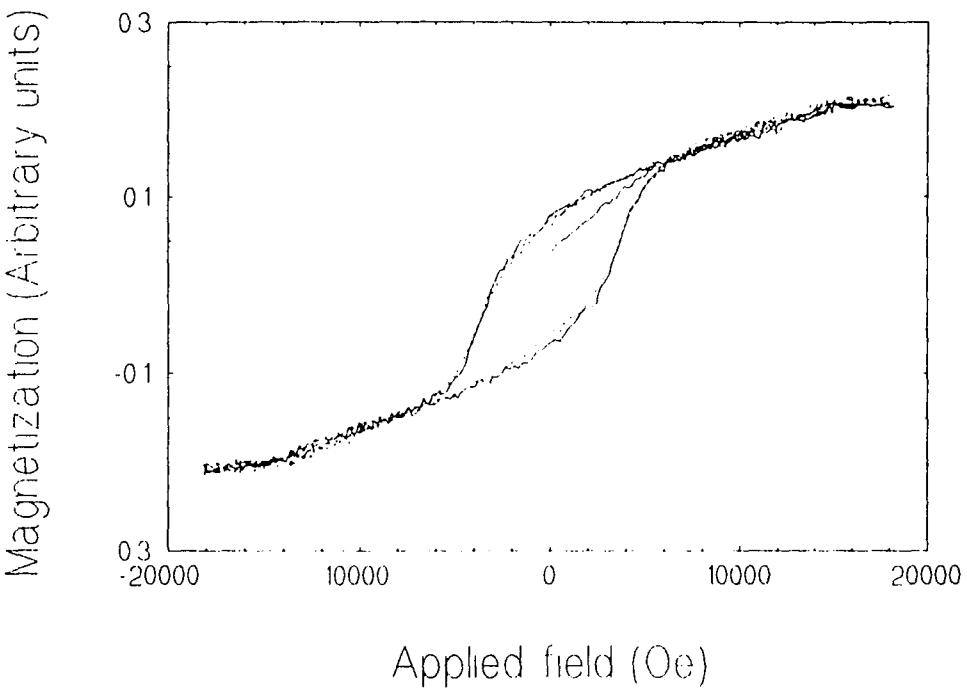
Magnetization (Arbitrary units)
03
01
-01
03
-20000
10000
0
10000
20000
Applied field (Oe)

FIGURE 11

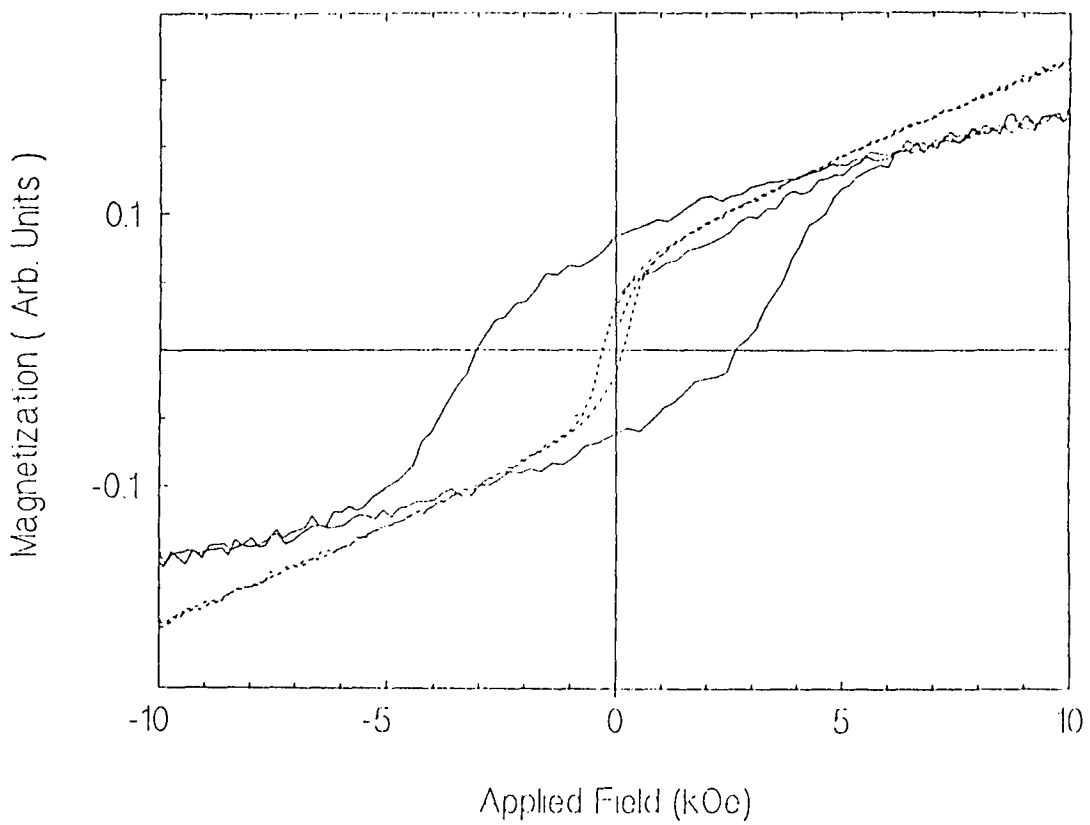

FIGURE 12

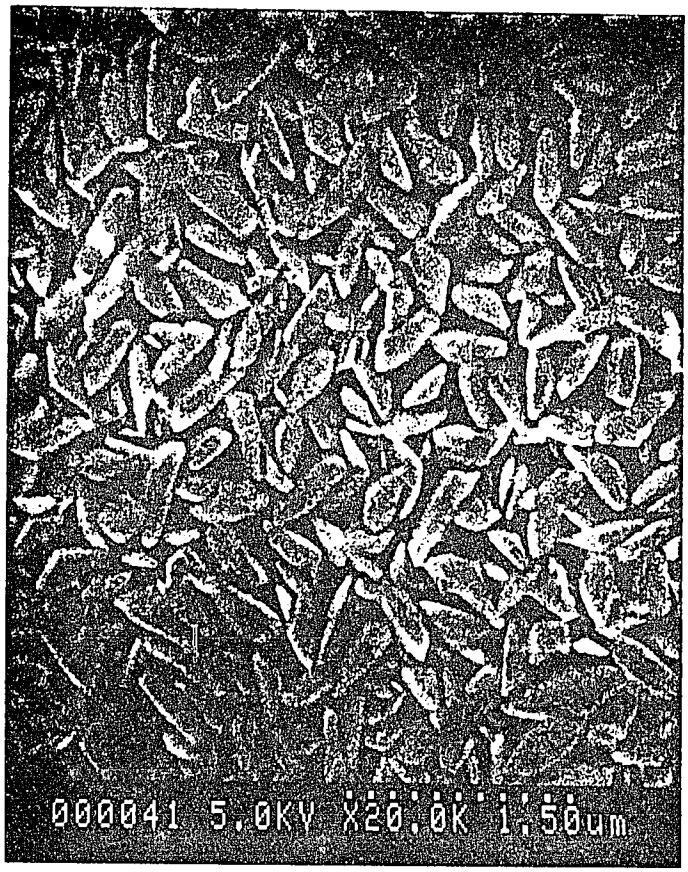

FIGURE 13

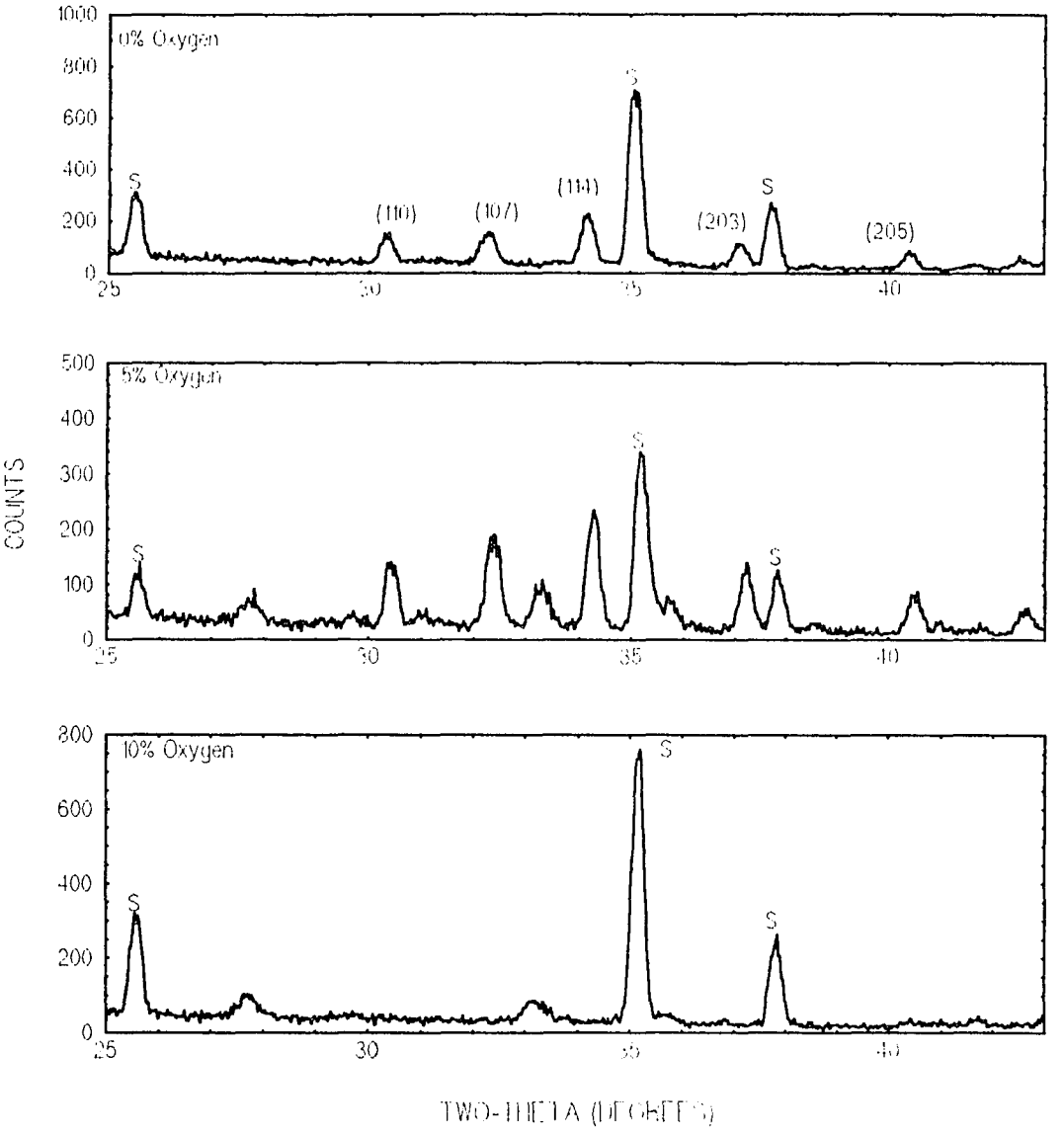
0% Oxygen
5% Oxygen
10% Oxygen
S
(110)
(107)
(114)
(203)
(205)
COUNTS
TWO-THETA (DEGREES)

FIGURE 14

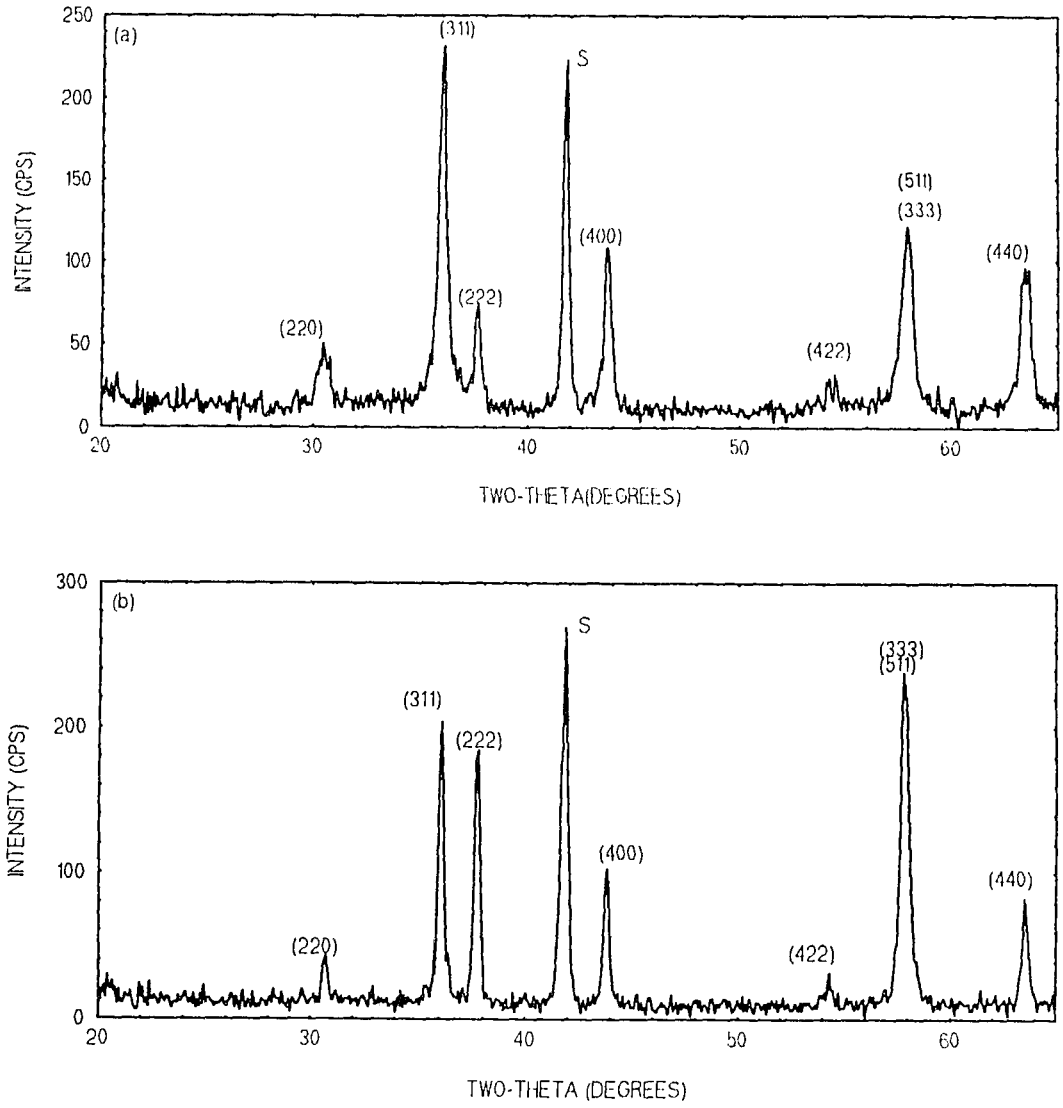
(a)
INTENSITY (CPS)
250
200
150
100
50
0
20
30
40
50
60
TWO-THETA(DEGREES)
(220)
(311)
(222)
S
(400)
(422)
(511)
(333)
(440)
(b)
INTENSITY (CPS)
300
200
100
0
20
30
40
50
60
TWO-THETA (DEGREES)
(220)
(311)
(222)
S
(400)
(422)
(333)
(511)
(440)

FIGURE 15

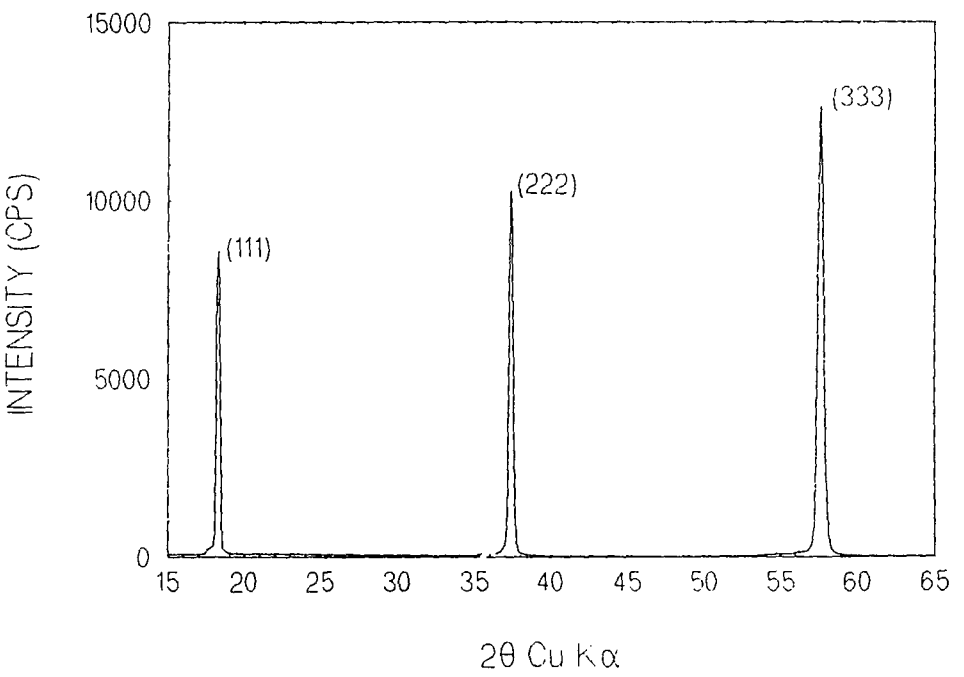
15000
10000
5000
0
INTENSITY (CPS)
(111)
(222)
(333)
15
20
25
30
35
40
45
50
55
60
65
2θ Cu Kα

FIGURE 16

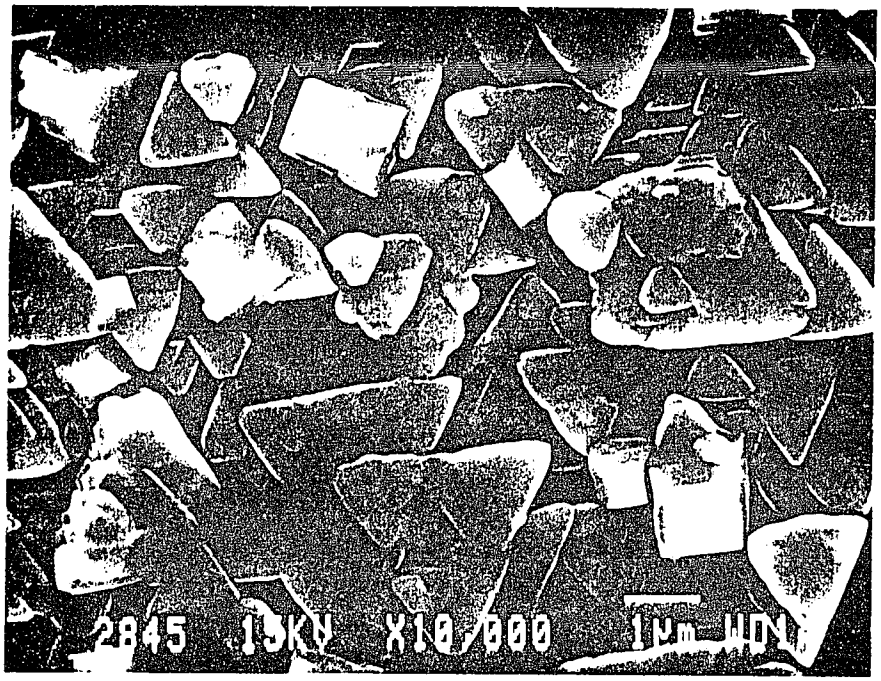

FIGURE 17

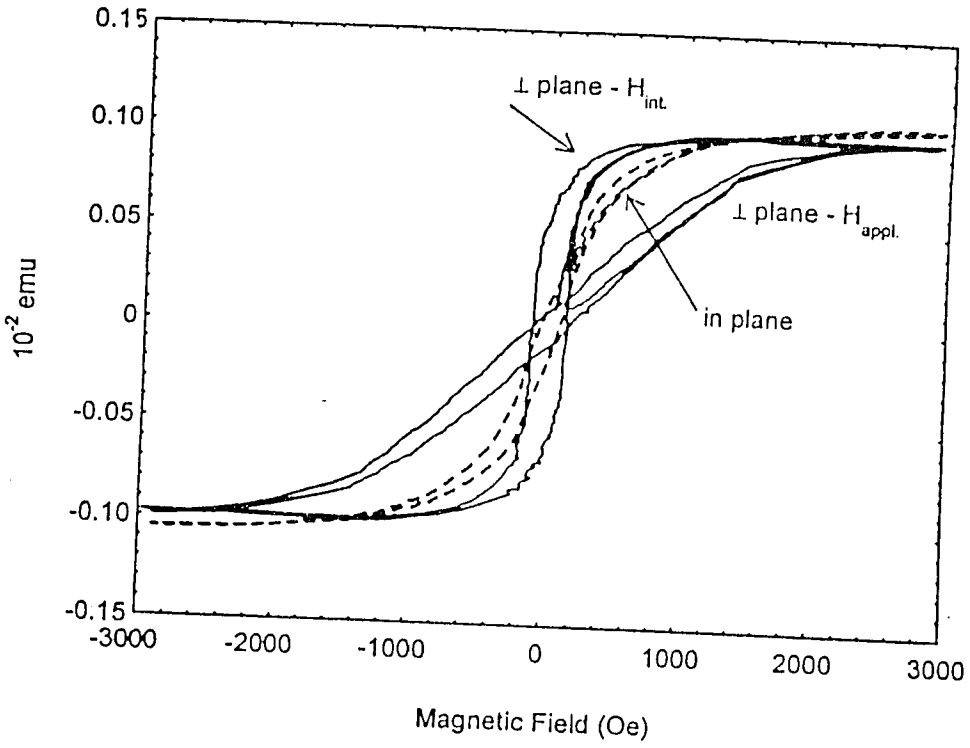
0.15
0.10
0.05
0
-0.05
-0.10
-0.15
10^{-2} emu
-3000
-2000
-1000
0
1000
2000
3000
Magnetic Field (Oe)
⊥ plane - $H_{int.}$
⊥ plane - $H_{appl.}$
in plane

FIGURE 18

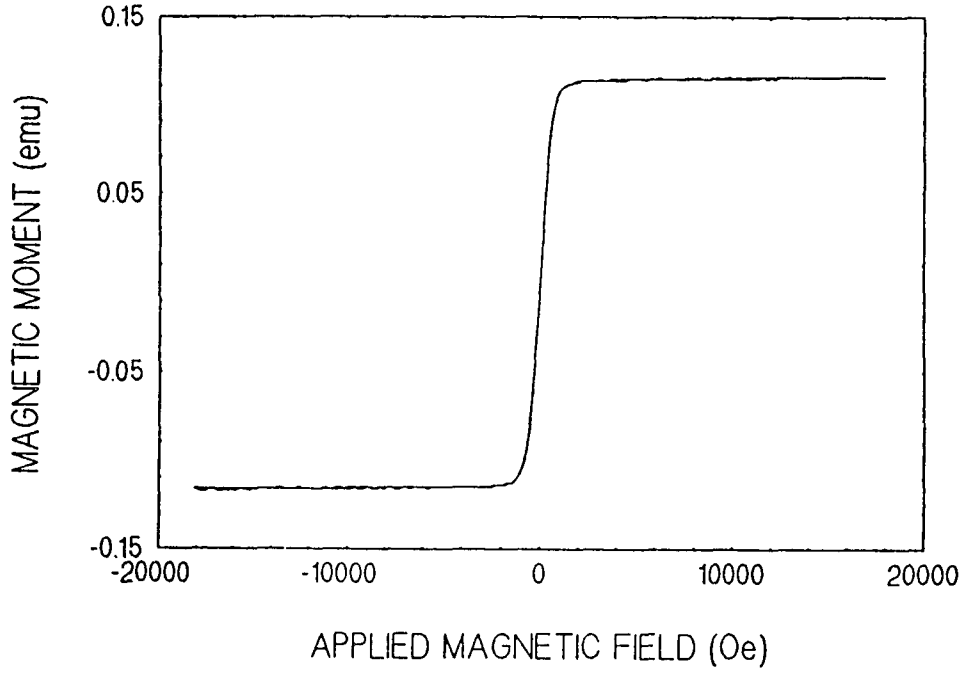
0.15
0.05
-0.05
-0.15
MAGNETIC MOMENT (emu)
-20000
-10000
0
10000
20000
APPLIED MAGNETIC FIELD (Oe)

FIGURE 19

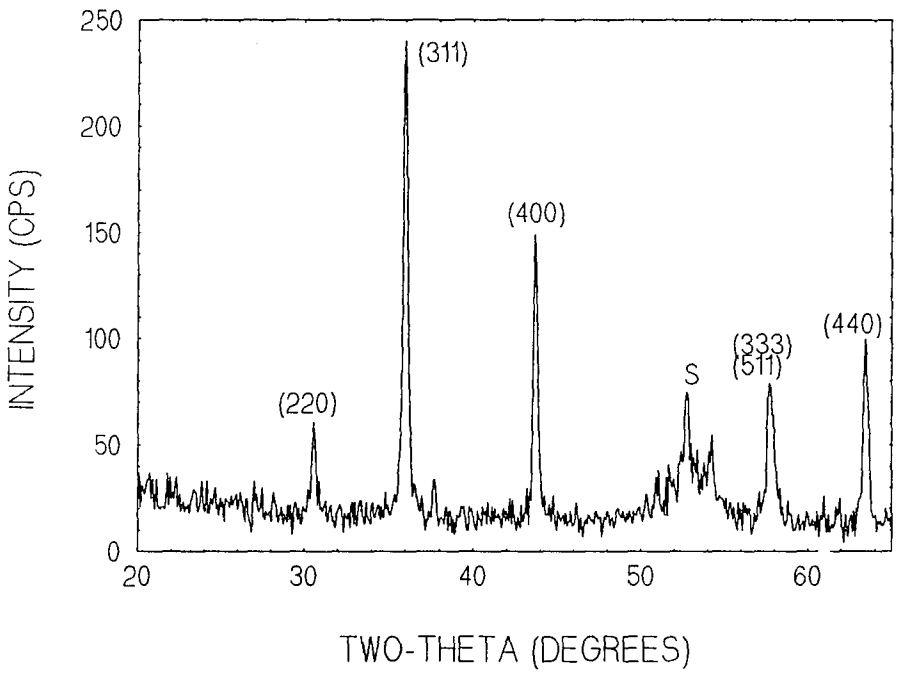
250
200
150
100
50
0
INTENSITY (CPS)
(311)
(400)
(220)
S
(333)
(511)
(440)
20
30
40
50
60
TWO-THETA (DEGREES)

FIGURE 20

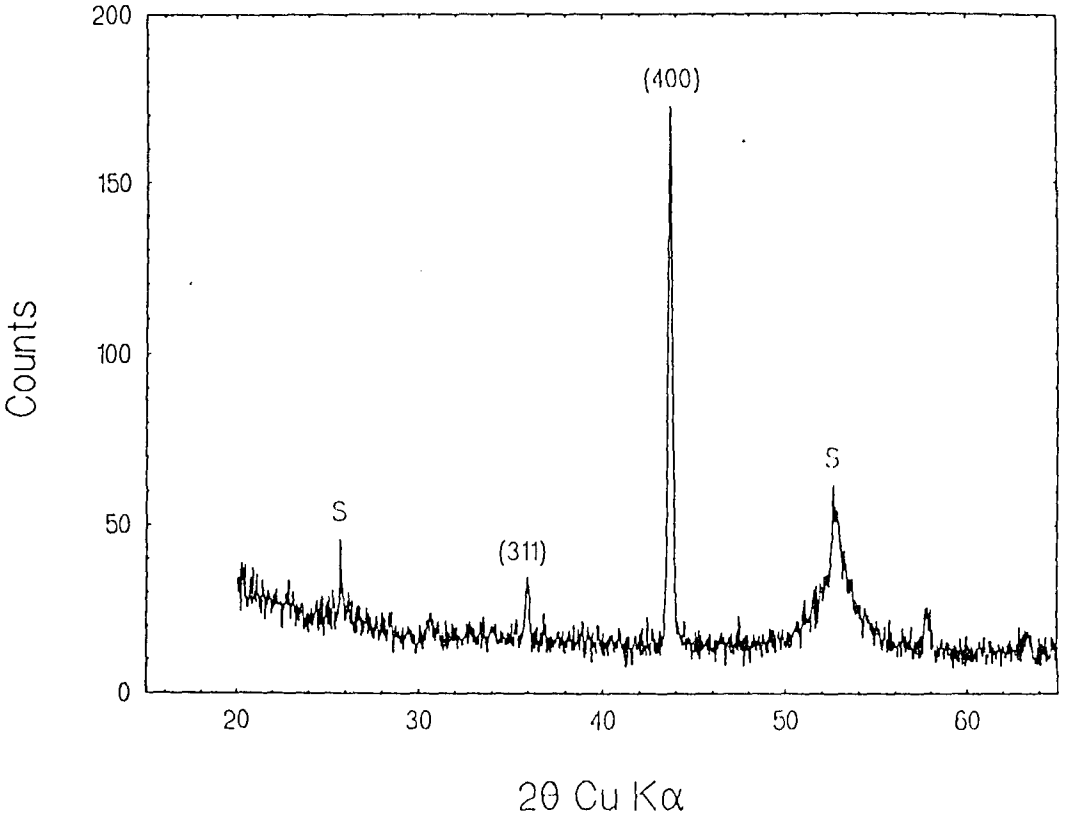

FIGURE 21

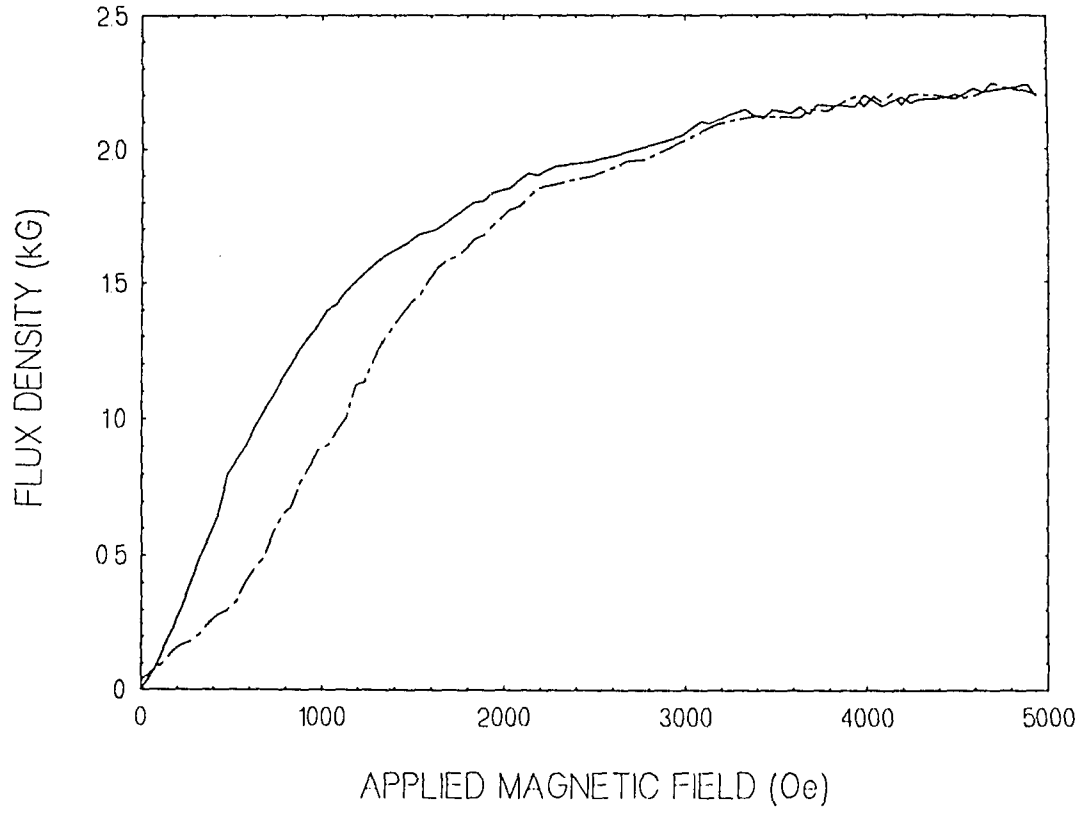
25
20
15
10
05
0
FLUX DENSITY (kG)
0
1000
2000
3000
4000
5000
APPLIED MAGNETIC FIELD (Oe)

FIGURE 22

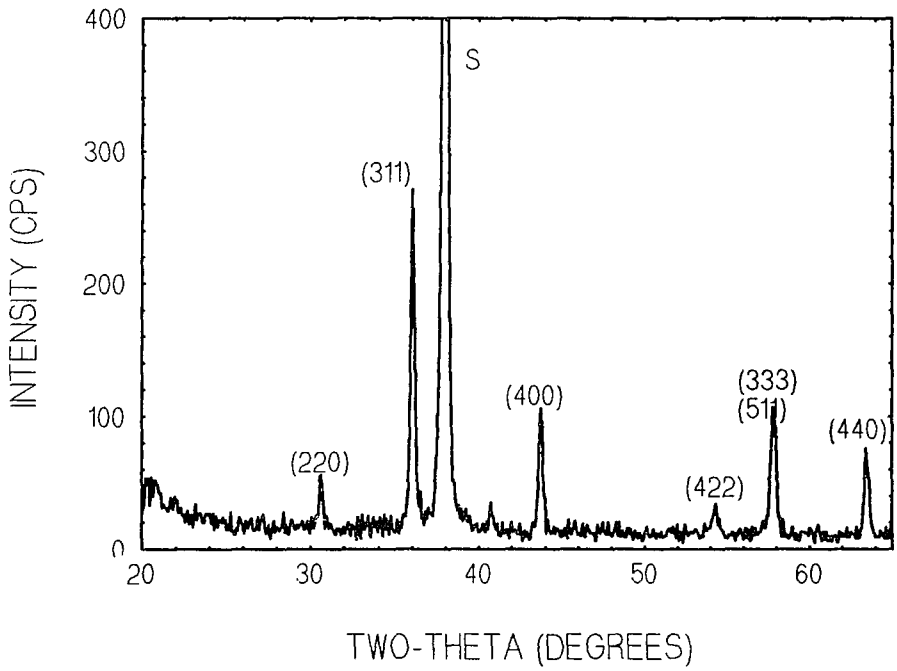
400
300
200
100
0
INTENSITY (CPS)
S
(311)
(400)
(333)
(511)
(440)
(220)
(422)
20
30
40
50
60
TWO-THETA (DEGREES)

FIGURE 23

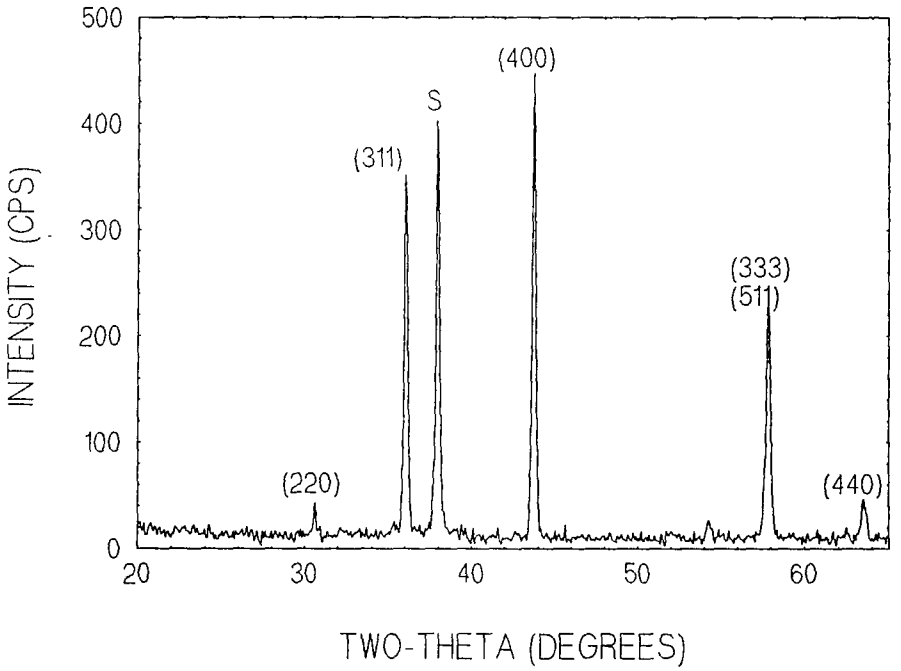
500
400
300
200
100
0
INTENSITY (CPS)
(220)
(311)
S
(400)
(333)
(511)
(440)
20
30
40
50
60
TWO-THETA (DEGREES)

FIGURE 24

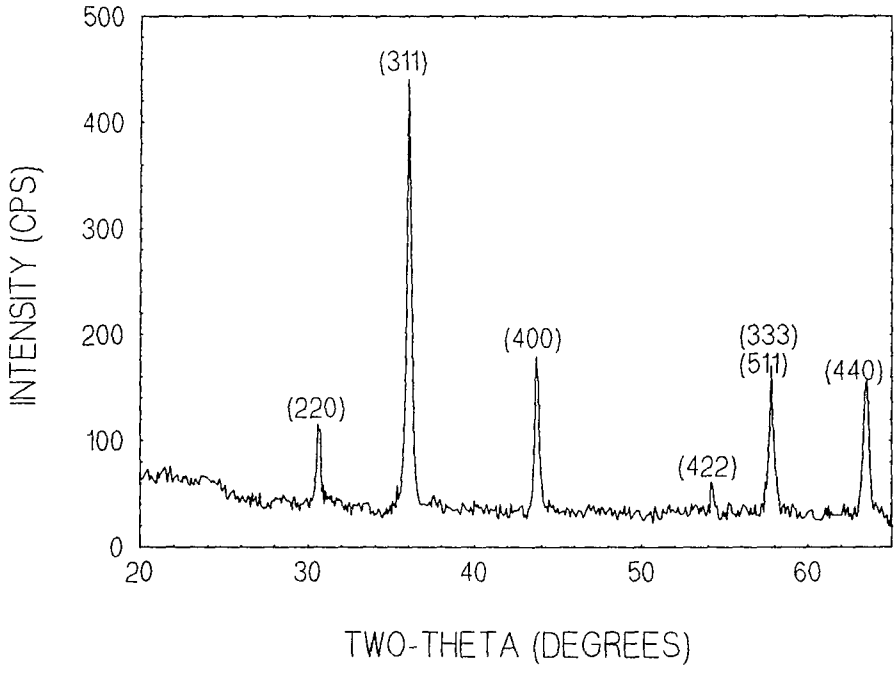
500
400
300
200
100
0
INTENSITY (CPS)
(311)
(400)
(333)
(511)
(440)
(220)
(422)
20
30
40
50
60
TWO-THETA (DEGREES)

FIGURE 25

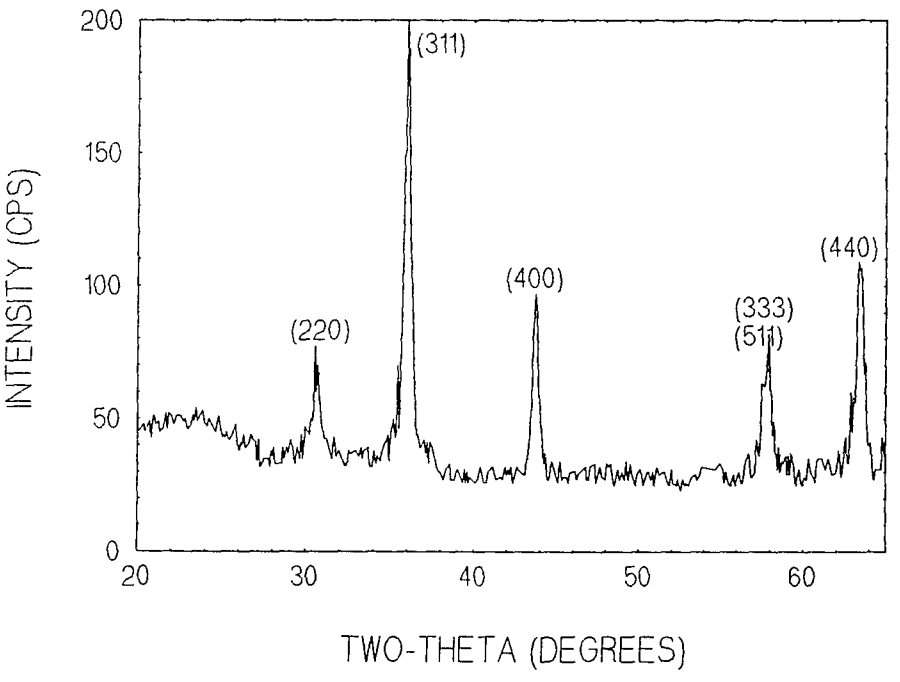
200
150
100
50
0
INTENSITY (CPS)
(311)
(220)
(400)
(333)
(511)
(440)
20
30
40
50
60
TWO-THETA (DEGREES)

FIGURE 26

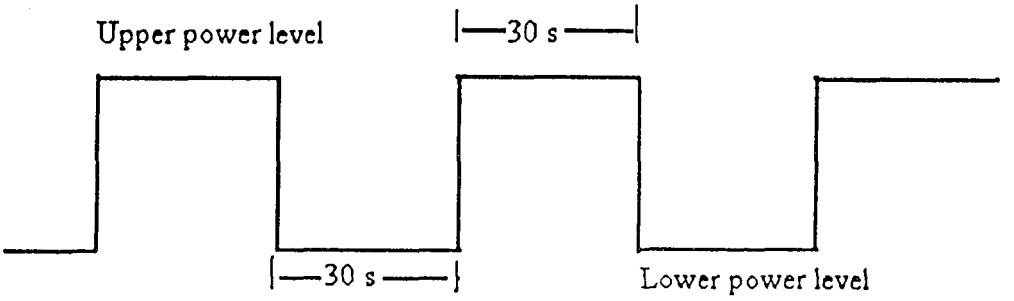

Upper level was changed from 200 to 350 W.

Lower level was changed from 150 to 250 W.

FIGURE 27

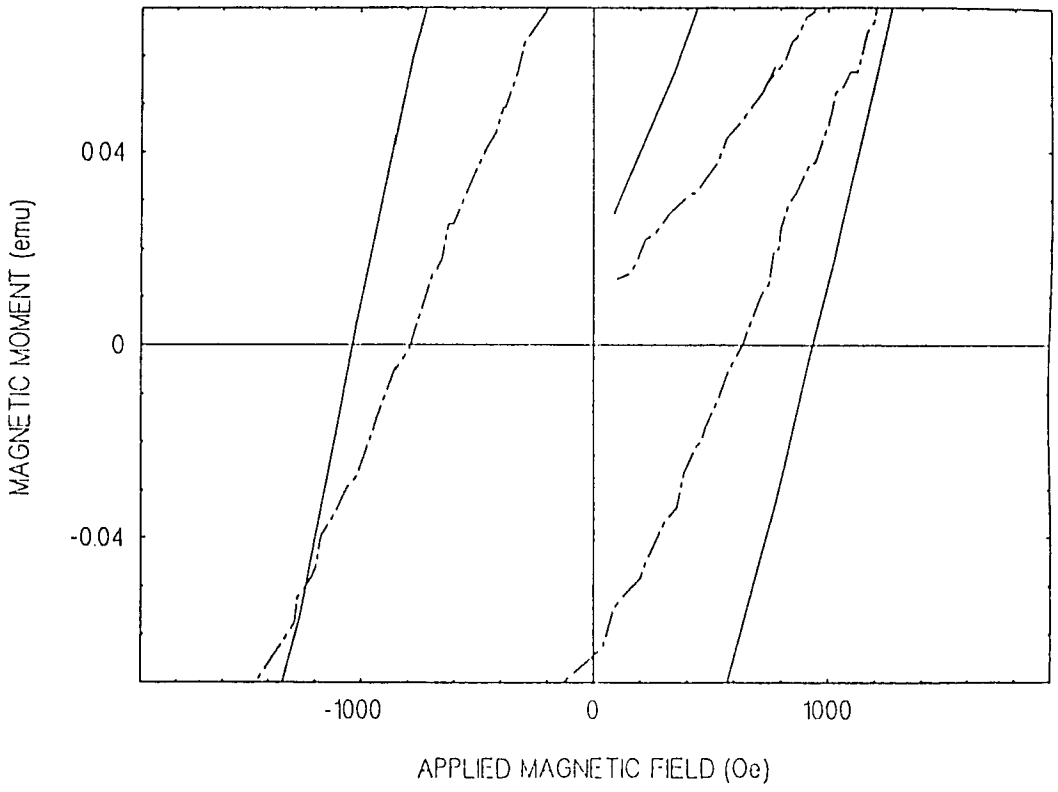
0.04
0
-0.04
MAGNETIC MOMENT (emu)
-1000
0
1000
APPLIED MAGNETIC FIELD (Oe)

FIGURE 28

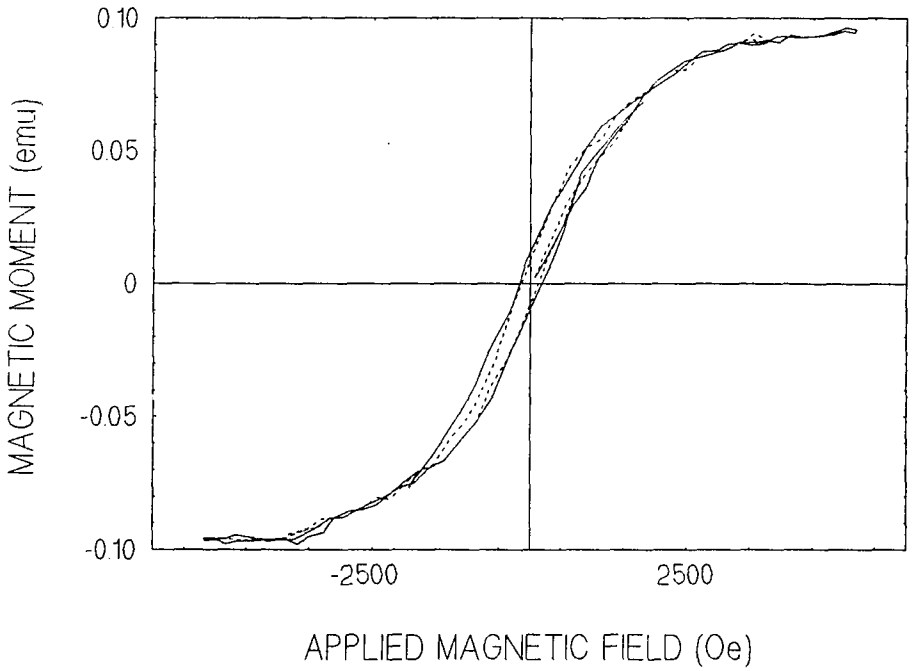
0.10
0.05
0
-0.05
-0.10
MAGNETIC MOMENT (emu)
-2500
2500
APPLIED MAGNETIC FIELD (Oe)

FIGURE 29

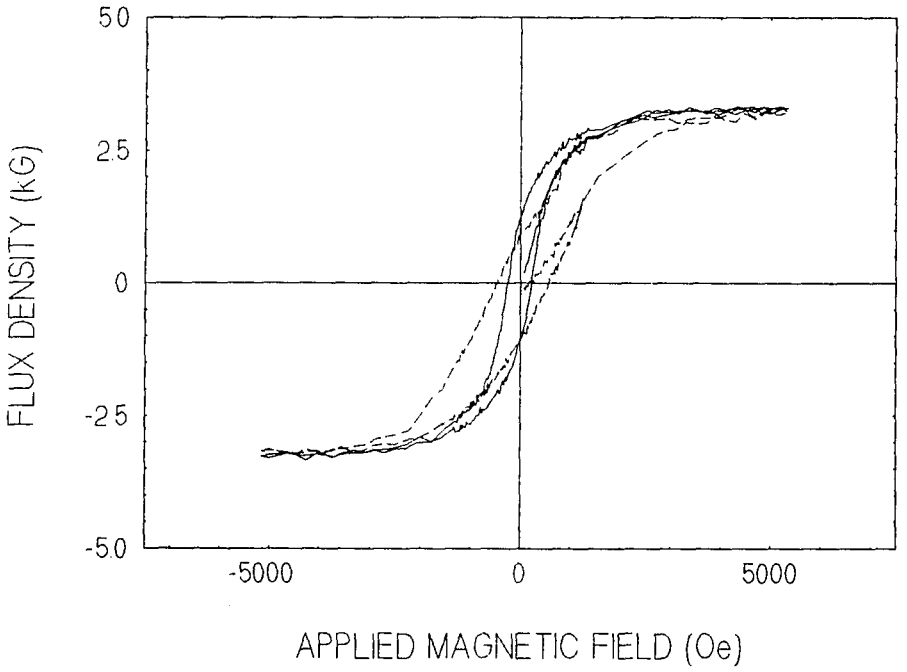
50
2.5
0
-2.5
-5.0
FLUX DENSITY (kG)
-5000
0
5000
APPLIED MAGNETIC FIELD (Oe)

FIGURE 30

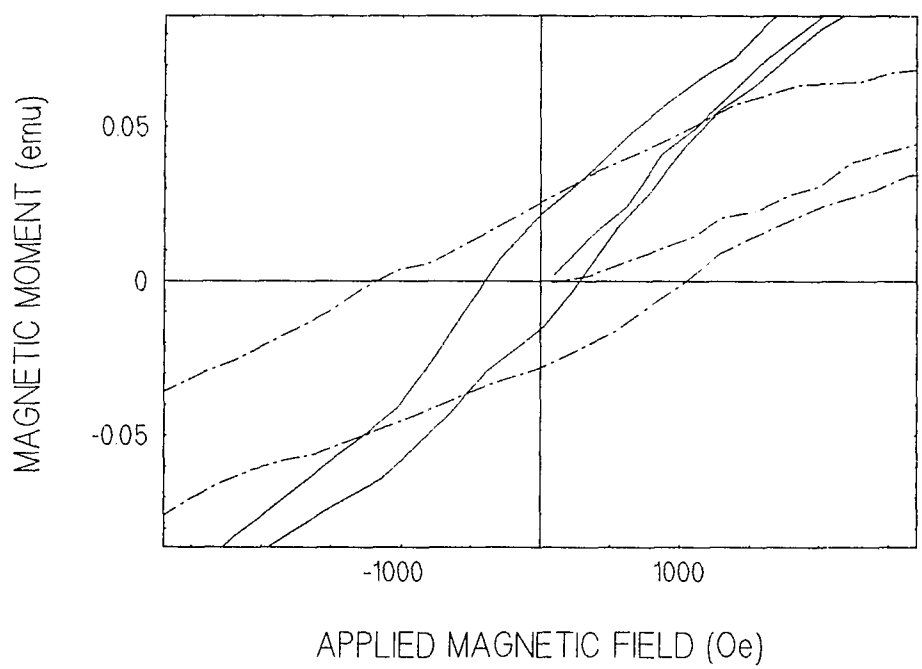
MAGNETIC MOMENT (emu)
0.05
0
-0.05
-1000
1000
APPLIED MAGNETIC FIELD (Oe)

FIGURE 31

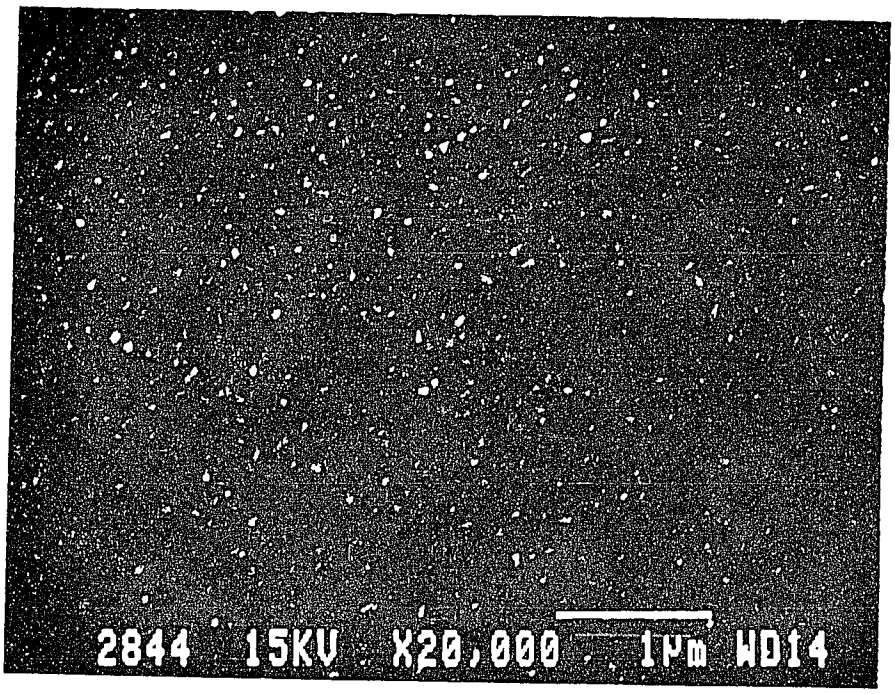

FIGURE 32

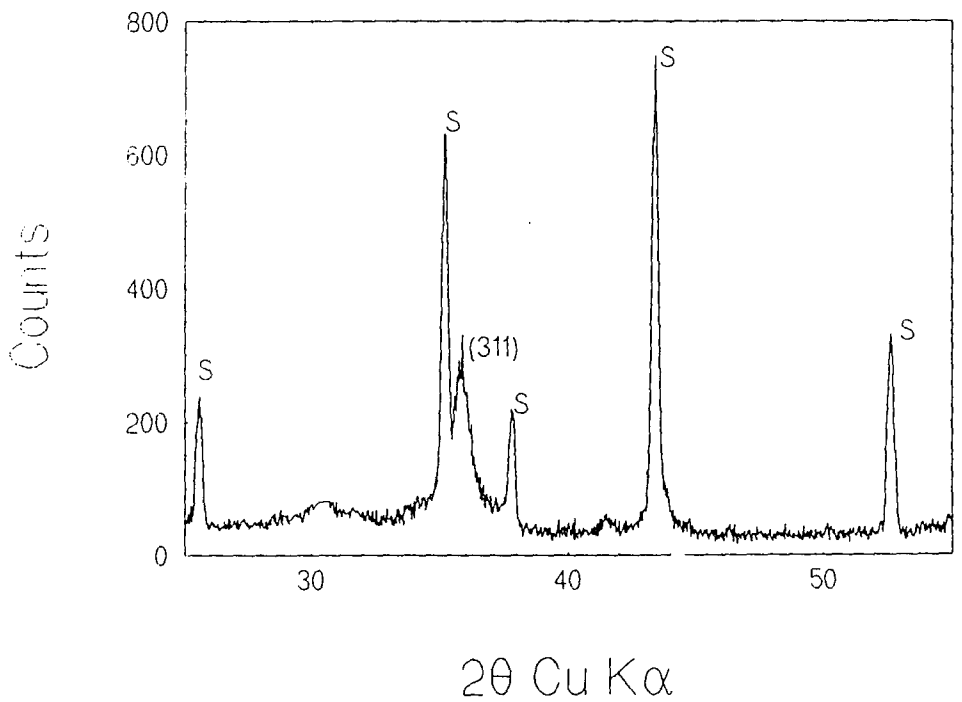

FIGURE 33

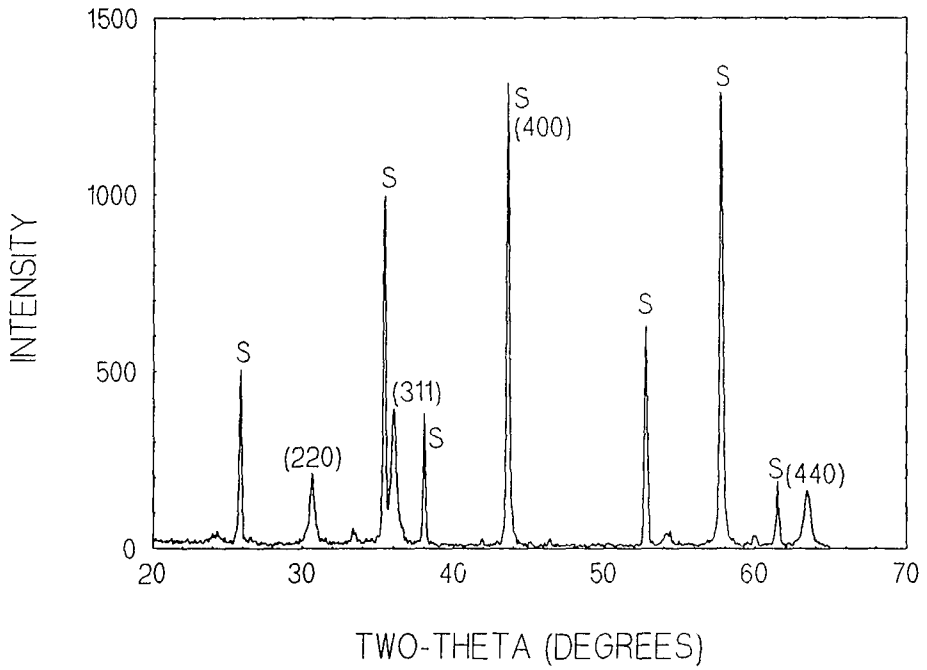
1500
1000
500
0
INTENSITY
S
(220)
S
(311)
S
S
(400)
S
S
S
S(440)
20
30
40
50
60
70
TWO-THETA (DEGREES)

FIGURE 34

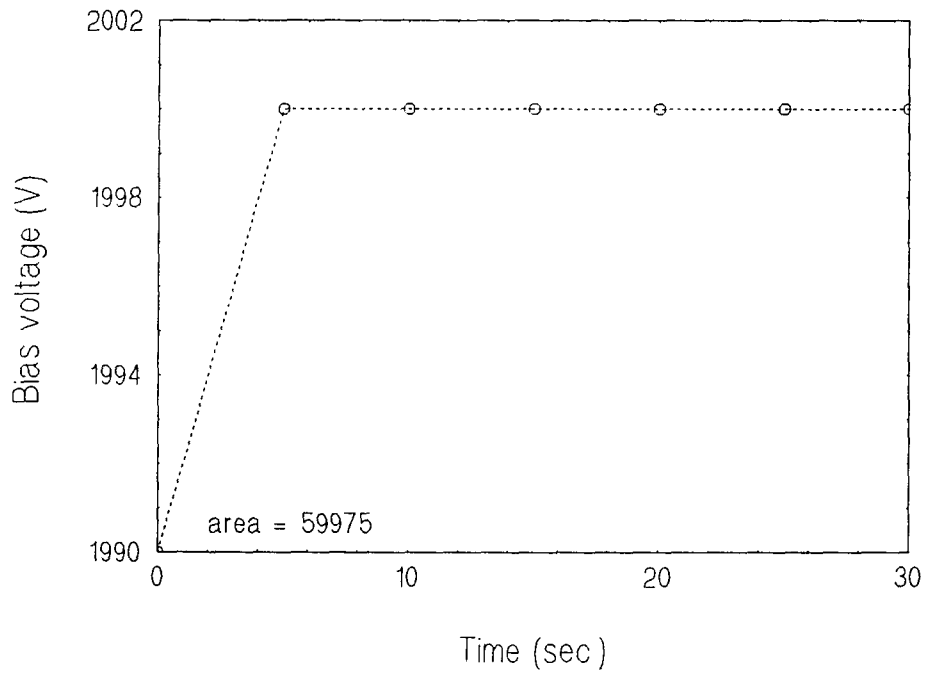
2002
1998
1994
1990
Bias voltage (V)
area = 59975
0
10
20
30
Time (sec)

FIGURE 35

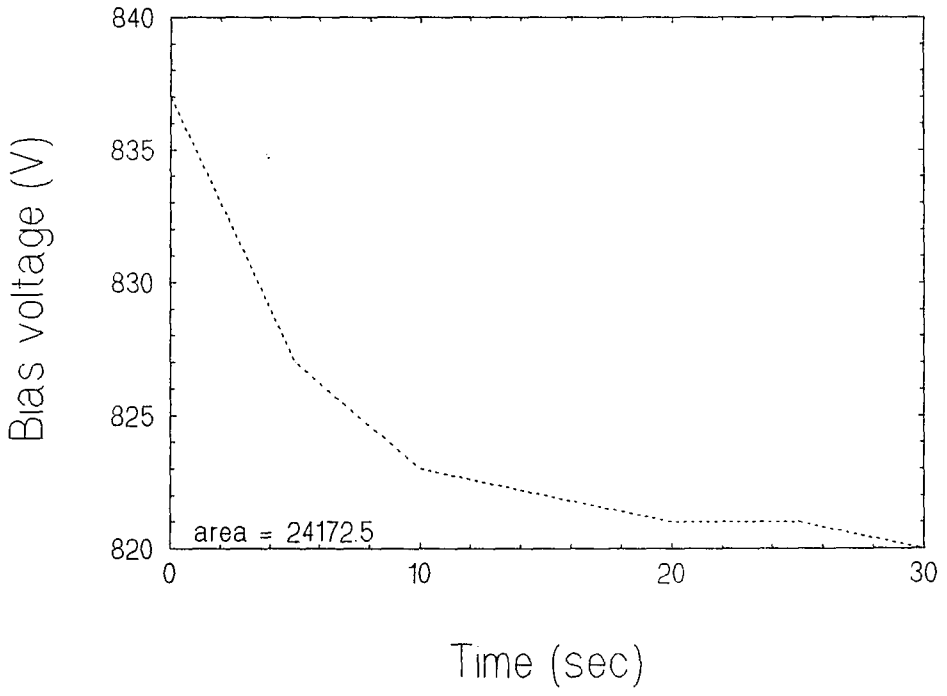
840
835
830
825
820
Bias voltage (V)
area = 24172.5
0
10
20
30
Time (sec)

FIGURE 36

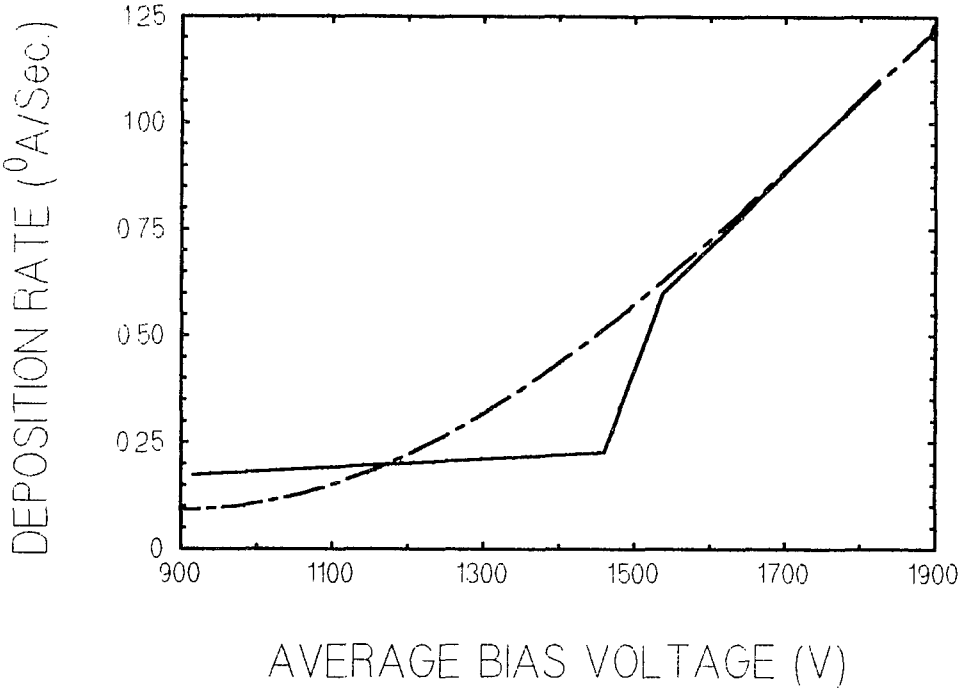
DEPOSITION RATE (^{0}A/Sec.)
125
100
0 75
0 50
0 25
0
900
1100
1300
1500
1700
1900
AVERAGE BIAS VOLTAGE (V)

FIGURE 37

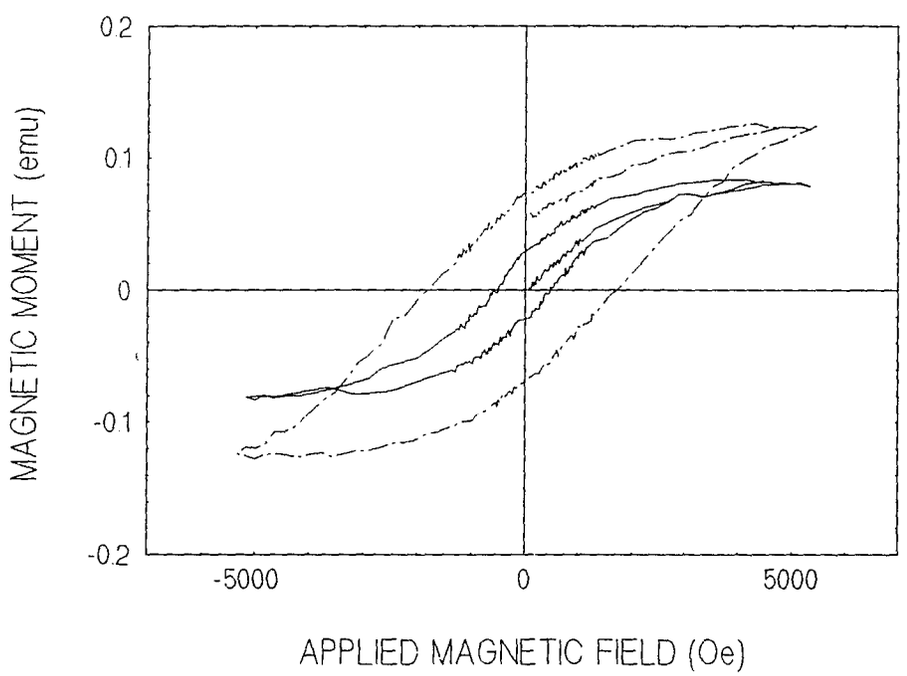
0.2
0.1
0
-0.1
-0.2
MAGNETIC MOMENT (emu)
-5000
0
5000
APPLIED MAGNETIC FIELD (Oe)

FIGURE 38

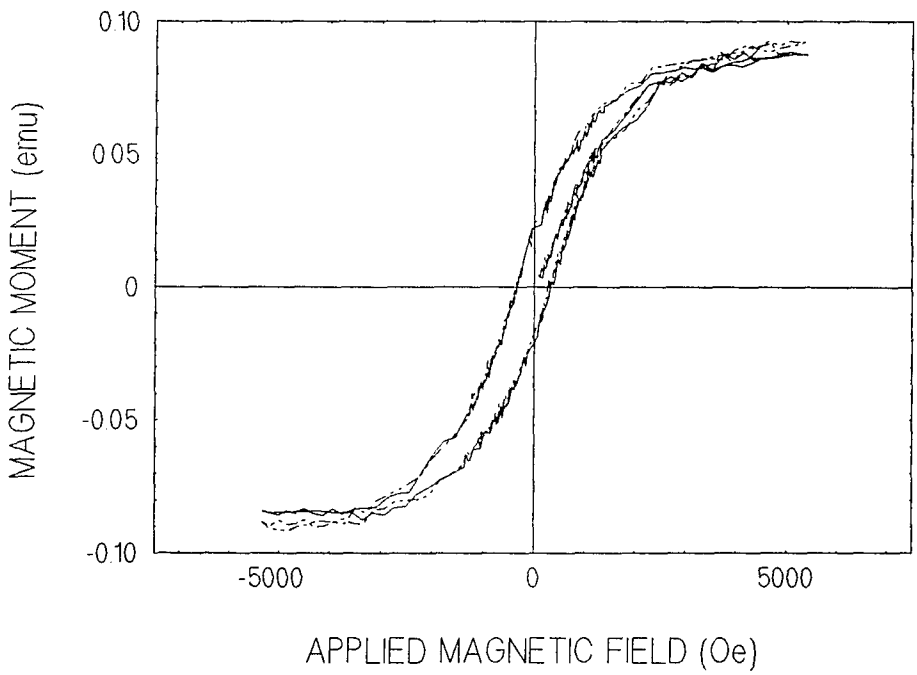
0.10
0.05
0
-0.05
-0.10
MAGNETIC MOMENT (emu)
-5000
0
5000
APPLIED MAGNETIC FIELD (Oe)

FIGURE 39

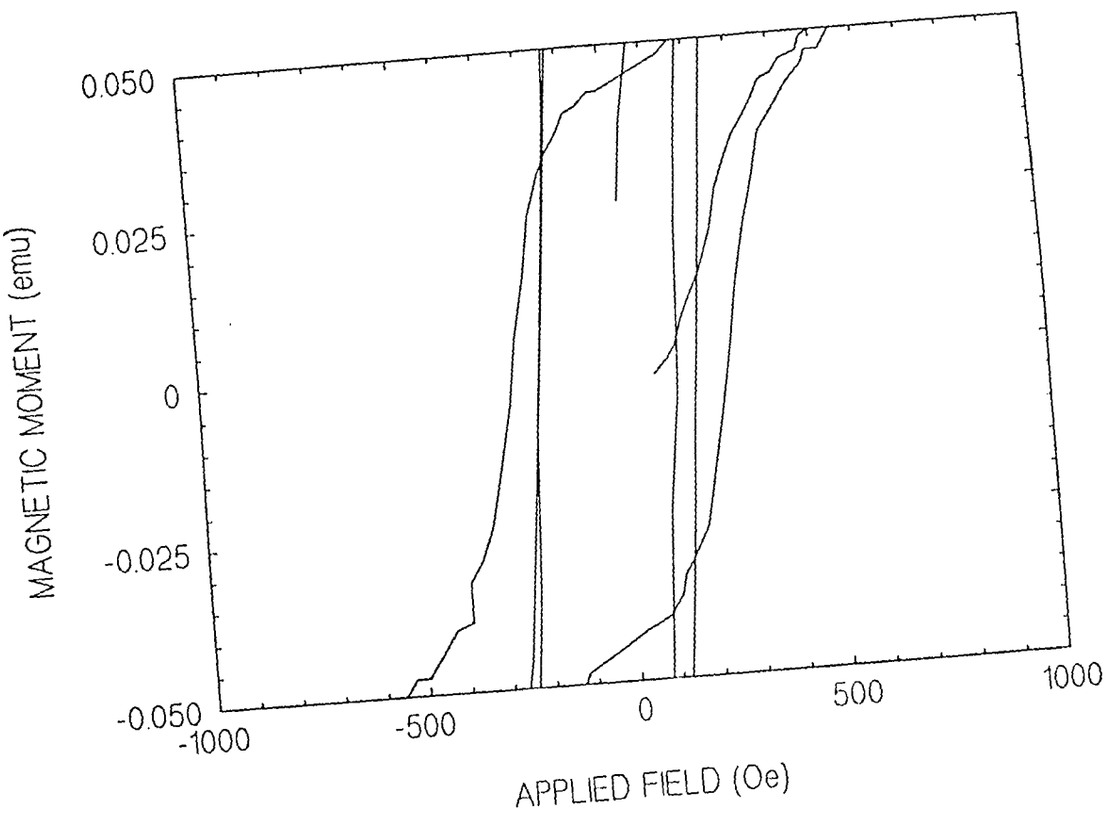
0.050
0.025
0
-0.025
-0.050
MAGNETIC MOMENT (emu)
-1000
-500
0
500
1000
APPLIED FIELD (Oe)

FIGURE 40

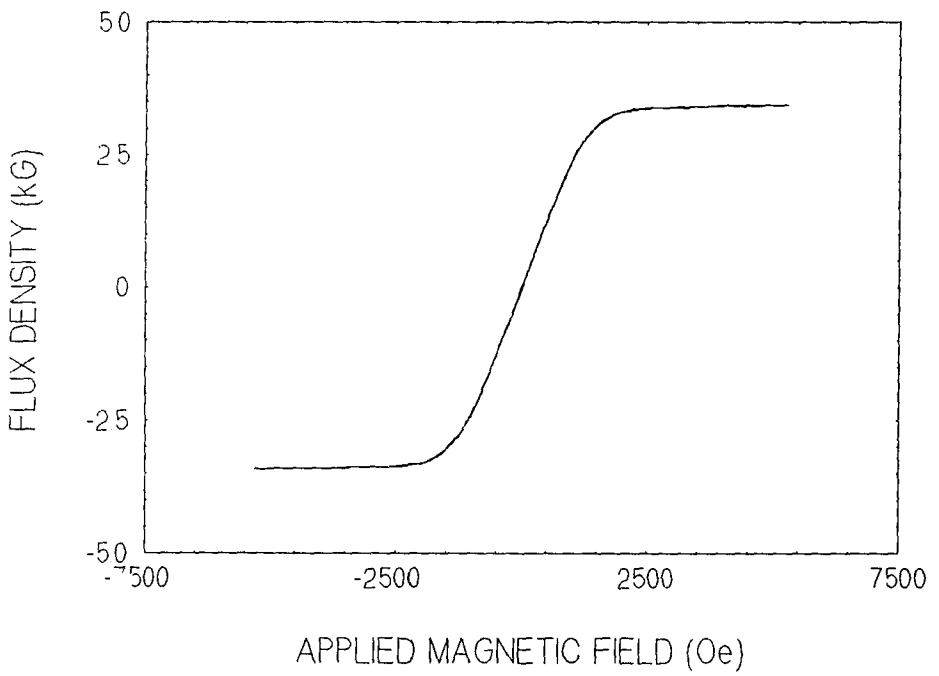
50
25
0
-25
-50
FLUX DENSITY (KG)
-7500
-2500
2500
7500
APPLIED MAGNETIC FIELD (Oe)

FIGURE 41

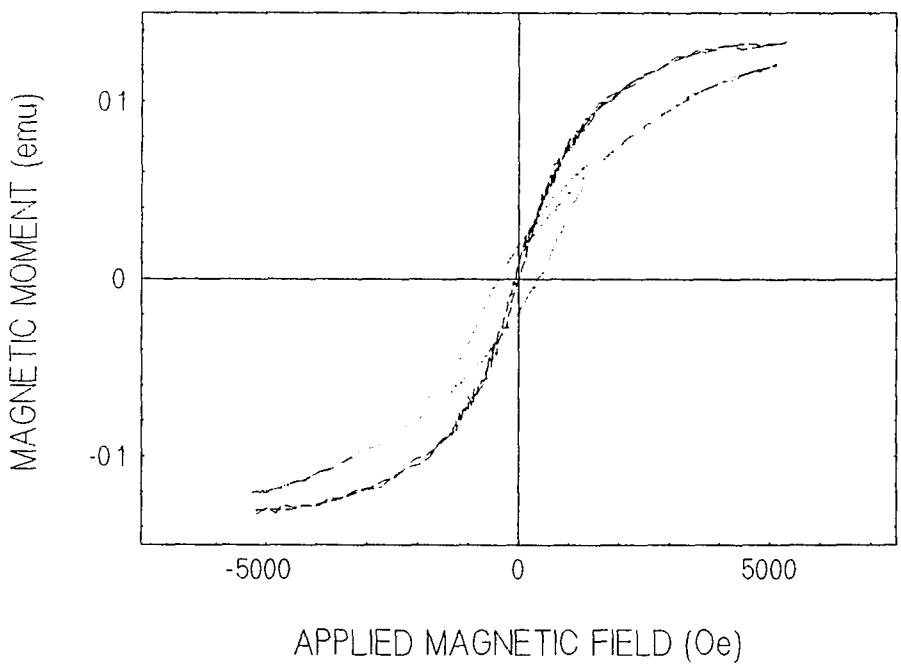
MAGNETIC MOMENT (emu)
01
0
-01
-5000
0
5000
APPLIED MAGNETIC FIELD (Oe)

FIGURE 42

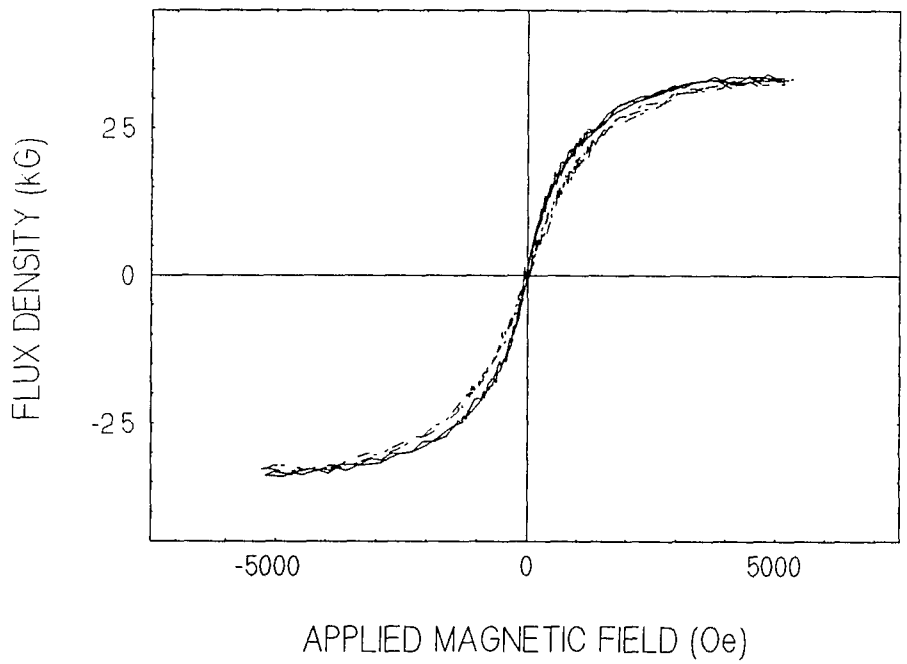

FIGURE 43

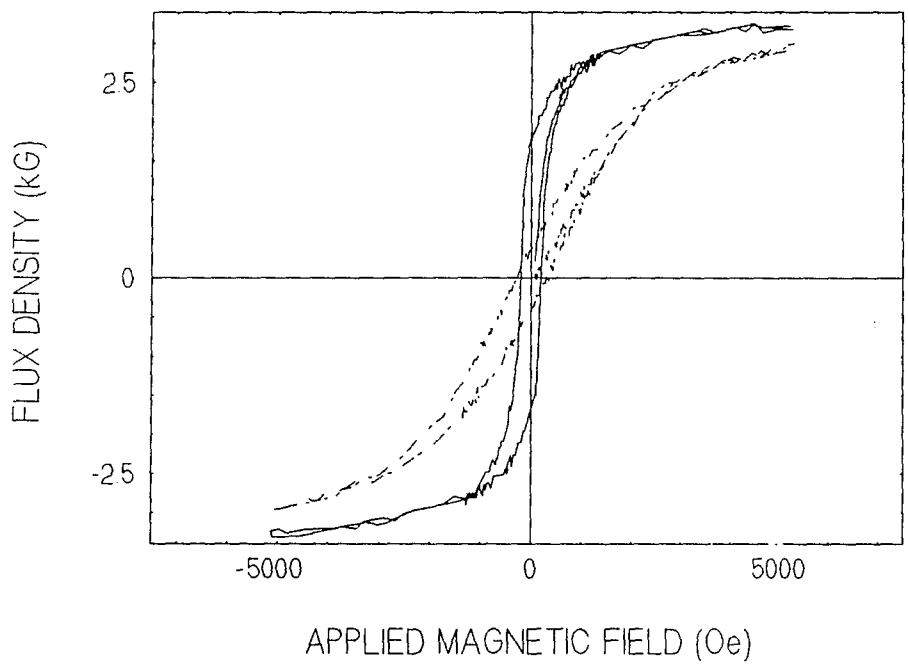

FIGURE 44

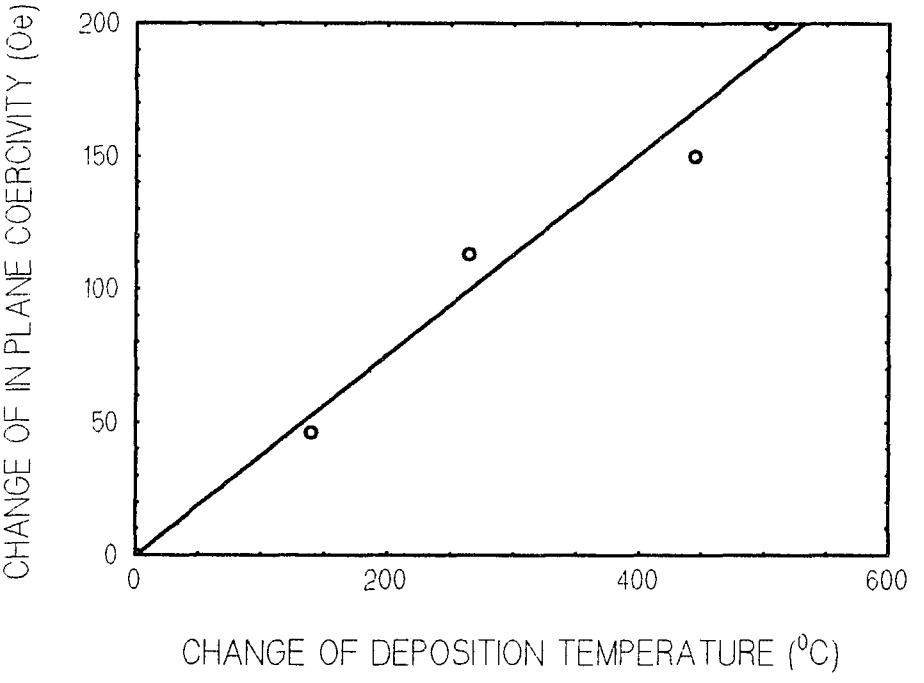
CHANGE OF IN PLANE COERCIVITY (Oe)
200
150
100
50
0
0
200
400
600
CHANGE OF DEPOSITION TEMPERATURE (°C)

FIGURE 45

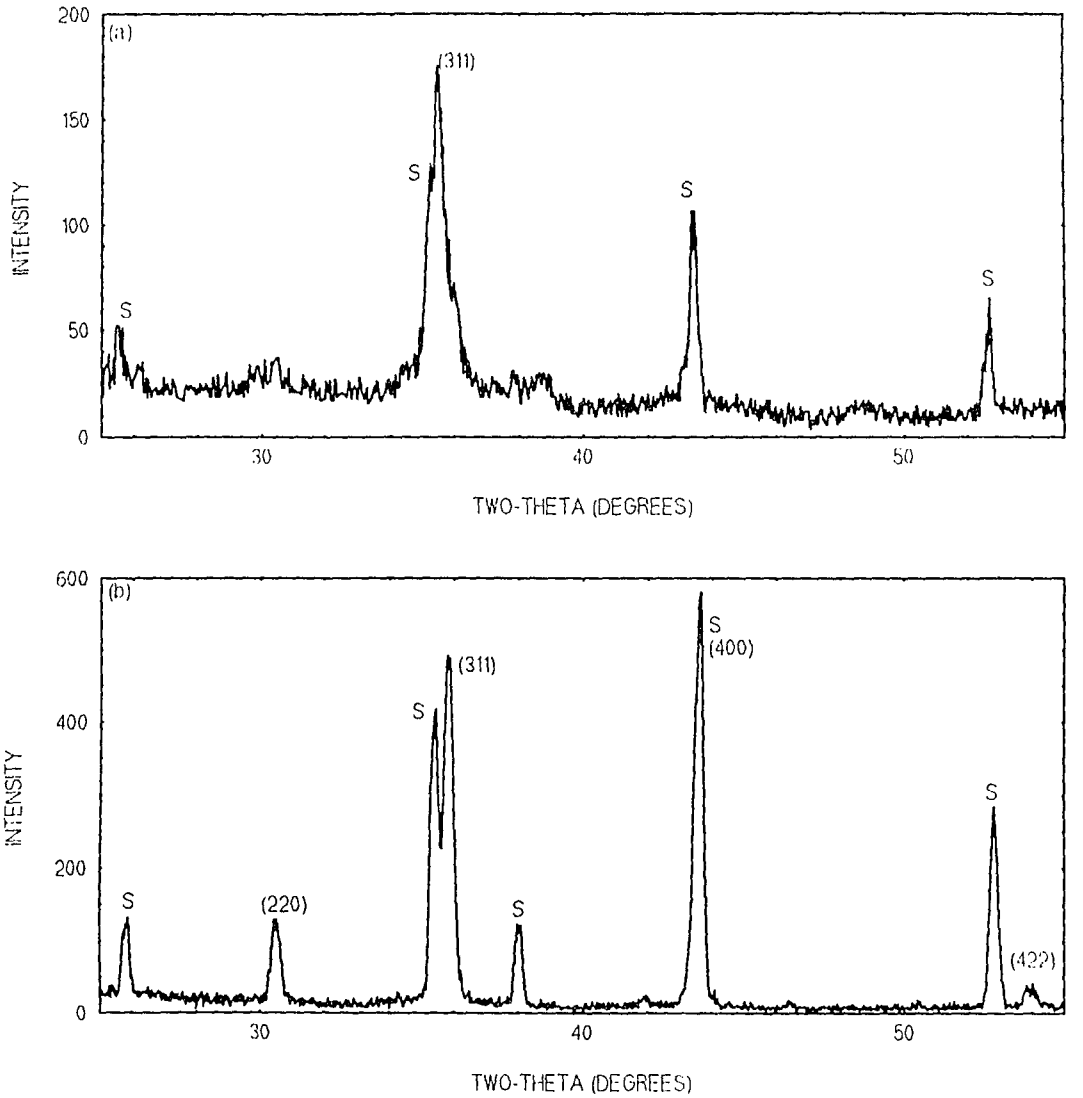
(a)
200
150
100
50
0
INTENSITY
S
S
(311)
S
S
30
40
50
TWO-THETA (DEGREES)
(b)
600
400
200
0
INTENSITY
S
(220)
S
(311)
S
S
(400)
S
(422)
30
40
50
TWO-THETA (DEGREES)

FIGURE 46

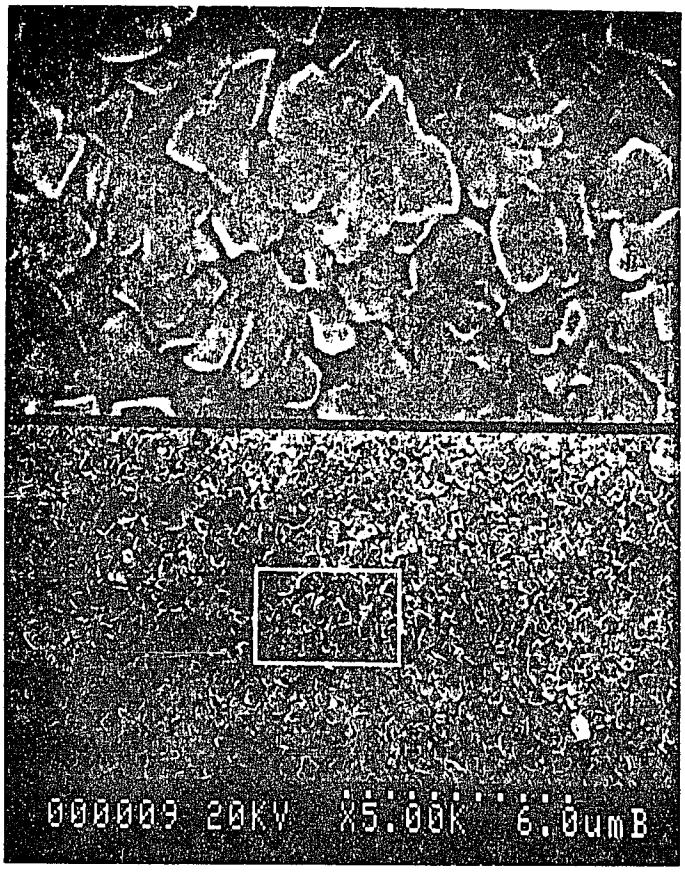

FIGURE 47

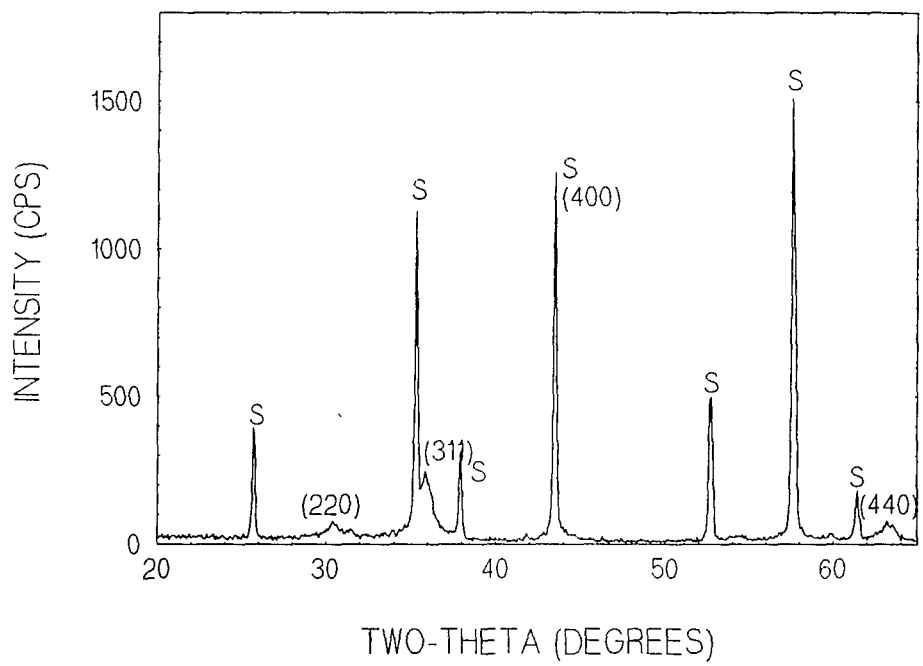
INTENSITY (CPS)
1500
1000
500
0
20
30
40
50
60
TWO-THETA (DEGREES)
S
(220)
S
(311)
S
S
(400)
S
S
S
(440)

FIGURE 48

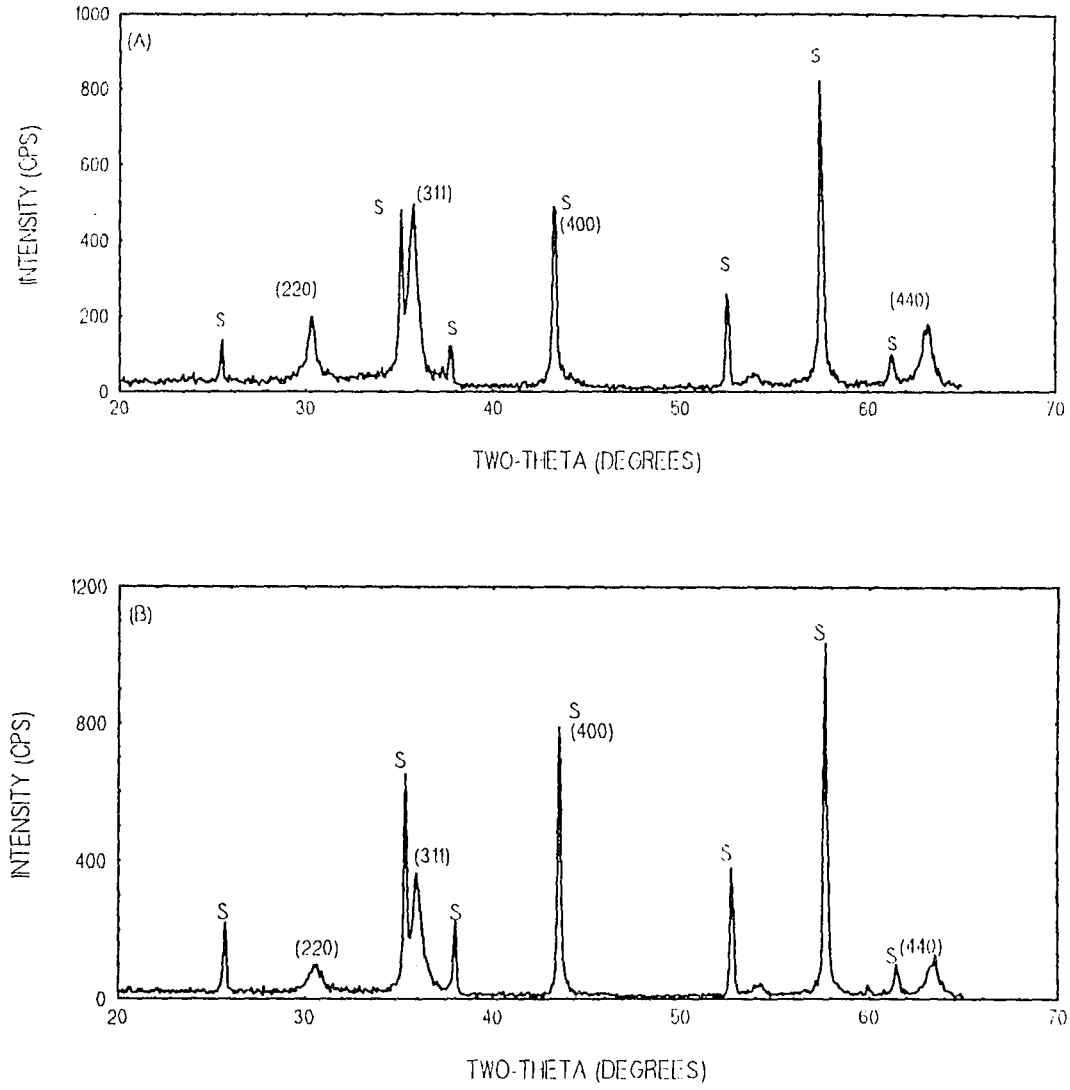
(A)
INTENSITY (CPS)
1000
800
600
400
200
0
20
30
40
50
60
70
TWO-THETA (DEGREES)
S
(220)
(311)
(400)
(440)
(B)
INTENSITY (CPS)
1200
800
400
0
TWO-THETA (DEGREES)

FIGURE 49

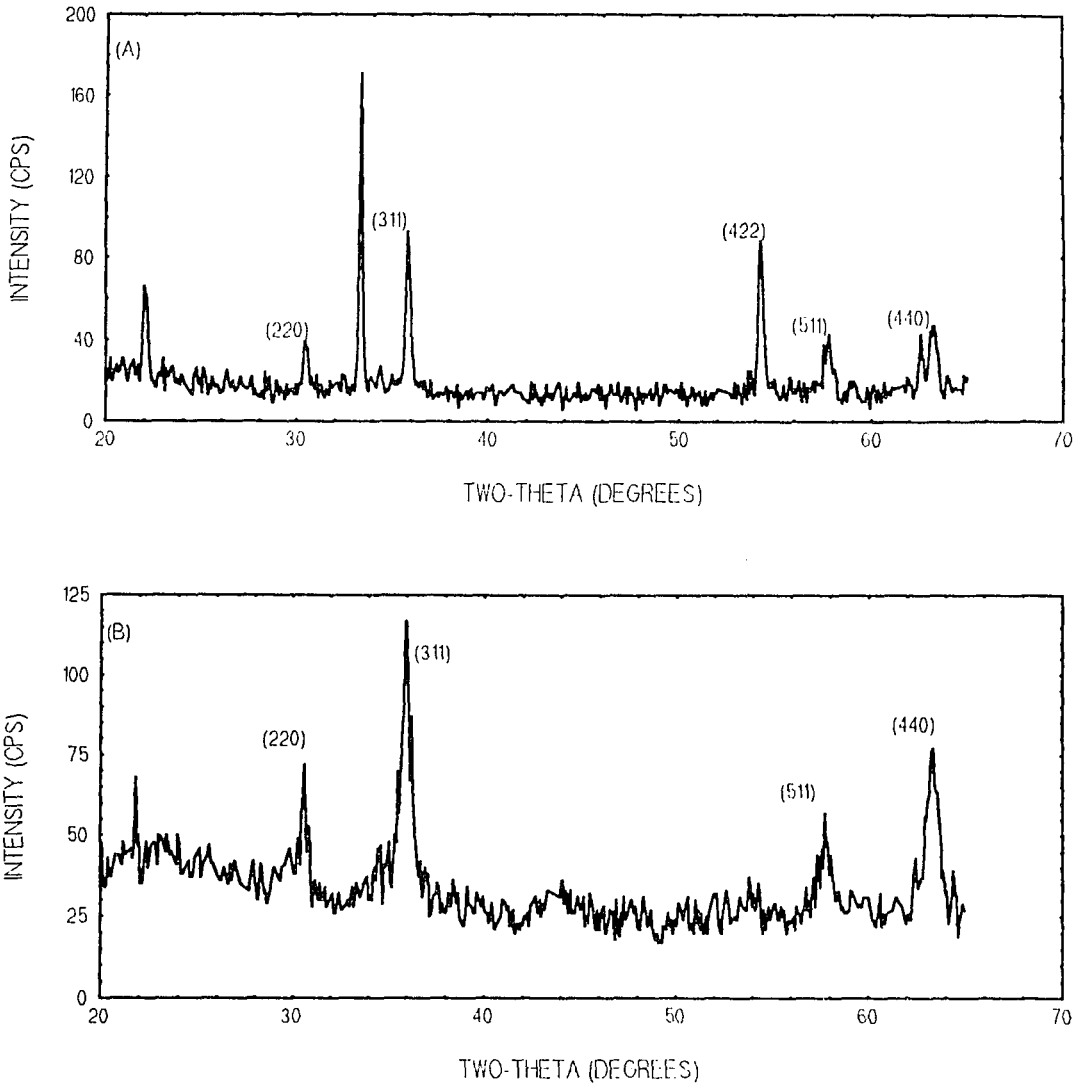
(A)
INTENSITY (CPS)
200
160
120
80
40
0
(220)
(311)
(422)
(511)
(440)
20
30
40
50
60
70
TWO-THETA (DEGREES)
(B)
INTENSITY (CPS)
125
100
75
50
25
0
(220)
(311)
(511)
(440)
20
30
40
50
60
70
TWO-THETA (DEGREES)

FIGURE 50

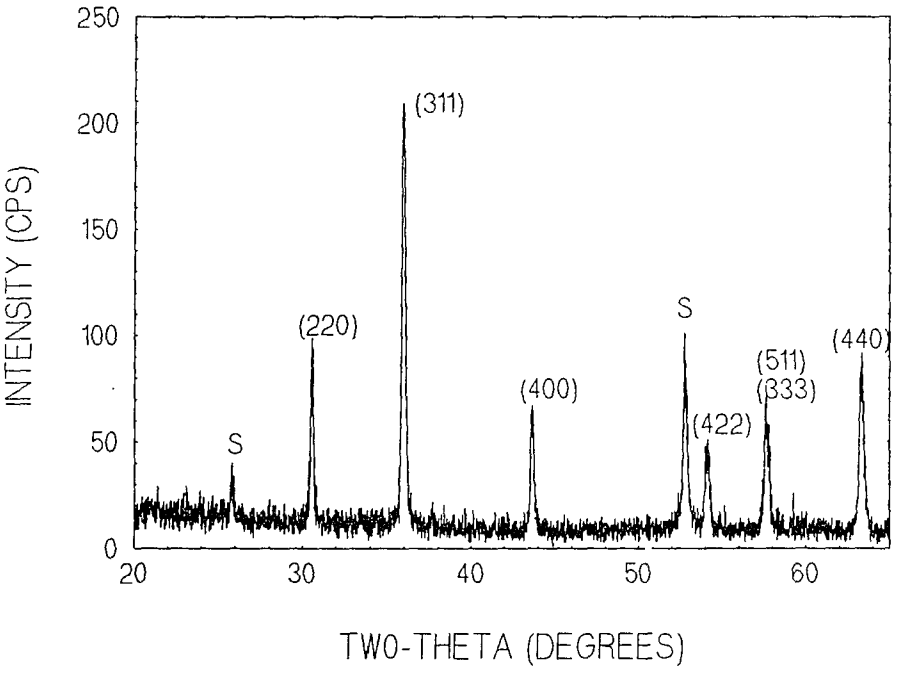
250
200
150
100
50
0
INTENSITY (CPS)
20
30
40
50
60
TWO-THETA (DEGREES)
S
(220)
(311)
(400)
S
(422)
(511)
(333)
(440)

FIGURE 51

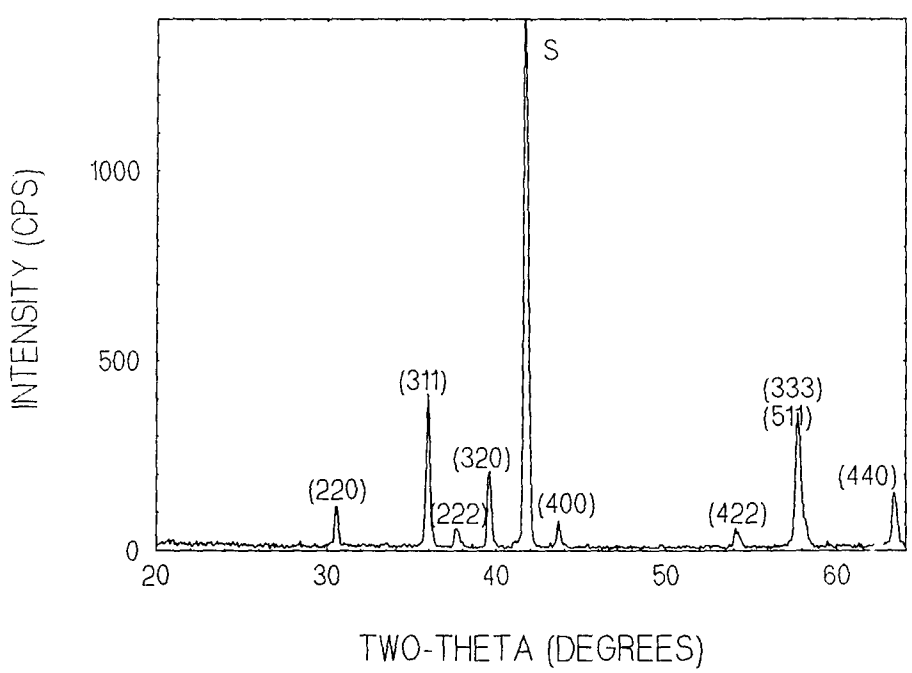
INTENSITY (CPS)
1000
500
0
20
30
40
50
60
TWO-THETA (DEGREES)
S
(311)
(320)
(220)
(222)
(400)
(422)
(333)
(511)
(440)

FIGURE 52

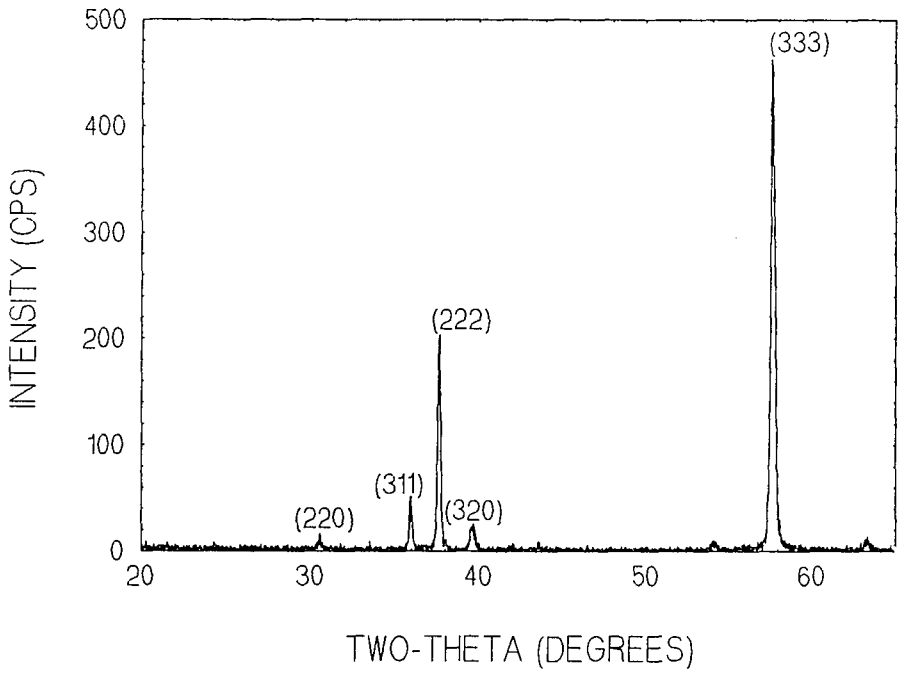
500
400
300
200
100
0
INTENSITY (CPS)
(333)
(222)
(311)
(220)
(320)
20
30
40
50
60
TWO-THETA (DEGREES)

LIST OF REFERENCES

1. T.L. Hylton , M.A. Parker, and J.K. Howard, APPL. PHYS. LETT. 61(7) (1992) 867

2. A. Mrisako, M. Matsumoto, and M. Naoe, IEEE TRANS. MAGN. 23(1) (1987) 56

3. M. Naoe, S. Hasunama, Y. Hoshi, and S. Yamanaka, IEEE TRANS. MAGN. 17 (1981), 3184

4. M. Matsuoka, Y. Hoshi, M. Naoe, and S. Yamanaka, IEEE TRANS. MAGN. 18(6) (1982), 1119

5. N. Matsushita, and M. Naoe, IEEE TRANS. MAGN. 29(6), (1993) 4089

6. Xiaoyu Sui, Mark H. Kryder, Bunsen Y. Wong, and David E. Laughlin IEEE TRANS. MAGN. 29(6), (1993), 3751

7. J.M. Lommel, B.T. Shirk, and W.R. Buessem, J. APPL. PHYS. 40(3), (1969), 1294

8. F.J. Cadieu, PHYSICS OF THIN FILMS, VOL. 16 (ACADEMIC PRESS, SAN DIEGO, 1992)

9. H. Hedge, P. Samarasekara, and F.J. Cadieu, J. APPL. PHYS. 75(10), (1994), 6640

10. A. Morisako, M. Matsumoto, and M. Naoe, IEEE TRANS. MAGN. 24(6), (1988), 3024

11. M. Satou, T. Namikawa, T. Kaneko, and Y.Yamazaki, IEEE TRANS. MAGN. 13(5), (1993), 1400

12. N. Masahiko, and S. Nakagawa, IEEE TRANS. MAGN. 29(6), (1993), 3393

13. Tatso Fujiwara, IEEE TRANS. MAGN. MAG-21, (1985), 1480

14. Toshiyaki Suzuki, IEEE TRANS. MAGN. MAG-28, (1992), 2388

15. B. Ramamurthy, S.N. Piramanayagam, Antony Ajan, S.N. Shringi, S. Prasad, N. Venkataramani, R. Krishnan, S.D Kalkarni, and S.K. Date, J. MAG. MAG. MAT. (1995), 723

16 B. Ramamurthy Acharya, N. Venkataramani, S. Prasad, S.N. Shiringi, R. Krishnan, M. Tessier, and Y. Dumond, IEEE TRANS. MAGN. 29(6), (1993), 3370

17 E. Lacroix, P. Gerard, G. Marest, and M. Dupy, J. APPL. PHYS. 69(8), (1991), 4770

18 M. Matsuoka, M. Naoe, and Y. Hoshi, J. APPL. PHYS. 57(1) (1985), 4040

19 R. Atkinson, I.W. Salter, and P. Papakonastantinou, J. APPL. PHYS. 73(8), (1993), 3917

20 D.S. Speliotis, IEEE TRANS. MAGN. MAG-23, (1987), 3143

21 M. Abe, Y. Tanno, and Y. Tamura, J. APPL. PHYS. 57(1), (1985), 3795

22 N. Matsushita, S. Nakagawa, and M. Naoe, IEEE TRANS. MAGN. 28(5), (1992), 3108

23 H.Y Zhang, B.X. Gu, H.R. Zhoi, M. Lu, and H.B. Huang, J. MAG. MAG. MAT., (1995), 699

24 C.A. Kleint, H.C. Semmelhack, M. Lorenz, and M.K. Krause, J. MAG. MAG. MAT. (1995), 2081

25 H.J. Masterson, J.H. Lunney, D. Ravinder, and J.M.D. Coey, J. MAG. MAG. MAT., (1995), 2081

26 S.H. Talisa, K.C. Yoo, M. Abe, and T. Itoh, J. APPL. PHYS. 64(10), (1988), 5819

27 Hae SeokCho, and Hyeong Joon Kim, APPL. PHYS. LETT. 66(10) (1995), 1282

28 C.M. Williams, M. Abe, T. Itoh, and P. Lubitz, IEEE TRANS. MAGN. 30(6), (1994), 4896

29 Tako Suzuki,Federico Sequeda, Hoa Do, Ting C. Huang, and Grace Gorman, J. APPL. PHYS. 67(9), (1990), 4435

30 N. Watanabe, K. Hayashida, K. Kawano, K. Higucki, M. Ohkoshi, and K. Tsushima, J. MAG. MAG. MAT. (1995), 2131

31 Antonio Azevedo, C. Cinbis, and M.H. Kryder, J. APPL. PHYS. 74(12), (1993), 7450

32 M. Gomi, H. Furuyama, and M. Abe, J. APPL. PHYS. 70(1), (1991), 7065

33 C.J. Yang, S.W. Kim, and Y.S. Kim, IEEE TRANS. MAGN. 30(6), (1994), 4527

34 M. Gomi, T. Tanida, and M. Abe, J. APPL. PHYS. 57(1), (1985), 3888

35 J. Smit, and H.P.J. Wijn, 1959 NEWYORK WILEY JOHN AND SONS, FERRITES

36 H.A. Kramers, PHYSICA 1, (1934), 182

37 P.W. Anderson, PHY. REV. 79, (1950), 350

38 S. Chikazumi, 1964 JOHN WILEY AND SONS, INC.

39 P.J.M. Vander Starten, V.V. Banderanko, and R. Metselaar, J. CRYST. GROWTH 51, (1981), 119

40 Gerald F. Dionne, Rusell G. West, J. APPL. PHYS. 61(8), (1987), 3868

41 Gung-Jian You, D.P. Winters, Zeng-Jun Zhou, Yu Mei, and H.L. Luo, J. APPL. PHYS. 61(8), (1987), 3819

42 W.D. Chang, T.S. Chin, H.S. Wu, S.W. Chou, ang J.H. Jou, J. APPL. PHYS. 77(3), (1995), 1184

43 J.H. Hsu, C.R. Chang, P.C. Kuo, and J.H. Huang, J. MAGN. MAGN. MAT. 89, (1990), 167

44 P.J. Besser, J.E. Mee, P.E. Elkins, and D.M. Hienz, MATER. RES. BULL. 6 (1971), 1111

45 B. Chapman, "Glow Discharge Process", John Wiley and sons Inc., Wiley-Interscience, 1980

46 "Pulsed laser deposition of thin films", by Douglas B. Chrisey and Graham K. Hubler, A Wiley-interscience publications, John Wiley and sons Inc.

47 Xiaoyu Sui, and Mark H. Kryder, APPL. PHYS. LETT. 63(11) (1993), 1582

48 Variable texture Ni ferrite films prepared by pulsed laser deposition, P. Samarasekara, R. Rani, and F.J. Cadieu

49 Sushama Joshi, Rashmi Nawathey, V.N. Koinker, V.P. Godbole, S.M. Chaudhari, S.B. Ogale, and S.K. Date, J. APPL. PHYS. 64, (1988), 5647

50 Hae Seok Cho, Sang Kiha, Min Hong Kim and Hyenong Joon Kim, J. MATER. RES. 10, (1995), 274

51 R.B. Vandover, E.M. Gyorgy, J.M. Phillips, J.H. Marshall R.J. Felder, R.M. Fleming, and H. O'Bryan Jr., (abstract) J. APPL. PHYS. 75 (1994), 6124

52 H.F. Winters, Adv. in Chemistry series No. 158, Radiation effect of solid surfaces, ed. M. Kaminsky, American Chemical society (1976)

53 T. Sheshagiri Rao, B Revathi, M. Purnanandam, IND. J. PURE AND APPL. PHYS. 9(10), (1971), 797